

https://dspace.org/

Synthesis of carbon nanomaterials from carbon dioxide using pre- and post-combustion fly ash as a catalyst

Dlamini, Ndumiso

2022

https://hdl.handle.net/10539/34101

Downloaded from a DSpace repository. https://dspace.org/

Synthesis of Carbon Nanomaterials from Carbon dioxide using Pre- and Post-combustion Fly Ash as a Catalyst

Prepared by

Ndumiso Dlamini (679451)

A dissertation submitted to the Faculty of Engineering and the Built Environment, University of the Witwatersrand, Johannesburg, in fulfillment of the requirements for the degree of Master of Science in Engineering.

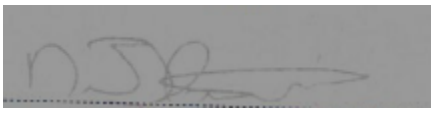
Supervisor: Prof Diakanua Nkazi

Co-supervisor: Dr. Hembe Elie Mukaya

November 2021

Declaration

I declare that this dissertation is my unaided work. It is being submitted for the Degree of Master of Science in Engineering to the University of the Witwatersrand, Johannesburg. It has not been submitted before for any degree or examination to any other university.



(Signature of Candidate)

……23……. day of……November…..……. year……2021..…….
Day *month* *year*

Abstract

Carbon nanomaterials (CNMs) such as carbon nanotubes (CNTs) and carbon nanofibers (CNFs) have become the most prominent fields of study in nanotechnology. This is due to their fascinating and unique features such as their chemical, mechanical, electrical, and optical properties. These characteristics have paved a way for applications in fields of medicine, electronics, and polymers, among others. For their applications, highly reliable synthesis methods that can produce CNMs of high purity in large quantities are desired with less cost. Their synthesis generally requires a catalyst, carbon source, and heat. The carbon sources and catalysts used are toxic and expensive. Furthermore, the catalysts must be prepared which is time-consuming and incurs more costs. This has acted as a major motivating factor to find and compare alternative reagents that are available in abundance, cheap, non-toxic, and can be used as received with no pre-treatments. Such materials, fly ash and carbon dioxide, were used in this investigation to develop a synthesis method for the production of CNMs.

Pre-combustion (Sasol) and post-combustion (Eskom) fly ash are characterized and compared based on their catalytic ability to produce pure, good crystalline CNMs in high yields. Carbon dioxide (CO_2) and acetylene were used as carbon sources. Chemical vapour deposition (CVD) is used for their synthesis which allows the tuning of certain parameters. The growth of CNMs is influenced by several process parameters such as catalyst mass, temperature, and flow rates of the carbon source gas, and carrier gas. The fly ash catalysts and CNMs were characterized using FESEM coupled with EDS, XRD, XRF, particle size, and Zeta Potential Analyzer, TEM, and TGA.

SEM analysis revealed that Sasol fly ash (S-FA) contains a significant number of spheres that are poorly rounded, containing coarser, chipped, and uneven surfaces. While the SEM analysis of Eskom fly ash (E-FA) showed finer and well-rounded spheres. The particle size distribution (PSD) was similar (2.8-88 μm) in both catalysts. However, the proportion of small and large particles were higher in S-FA. Furthermore, S-FA contained significant amounts of irregular fragments and E-FA contained more spherical particles. The sizes and shapes of catalysts influenced the morphology and structure of CNMs. XRF analysis showed a higher Loss on Ignition (LOI) and

Fe content in S-FA (LOI=8.5 wt% and Fe=4.51 wt%) than E-FA (LOI=0.9 wt% and Fe=3.33 wt%). It was found by EDS that high Fe content is mostly concentrated on the irregularly shaped fragments than the sphere particles in S-FA. Whereas E-FA spheres showed higher Fe content.

Using CO_2 as a carbon source, S-FA had better yields, purity, and crystallinity than E-FA. SEM analysis of E-FA showed crystallization of the minerals present in it with no identifiable CNMs. Raman spectroscopy of E-FA did show nanomaterials containing poor graphitization. TGA showed that synthesized CNMs had a high level of impurities. Optimum yields and crystallinity for S-FA catalyst were obtained at 750 ℃, a CO_2 flow rate of 962 sccm and argon (Ar) flow rate of 1202 sccm, and a mass catalyst of 1000 mg. The morphologies of CNMs found on the spheres were different from morphologies of CNMs on the irregular fragments. The pressure was found to be more influential on the yield and quality of the carbonaceous products than the flow rate.

When C_2H_2 was the carbon source, the results were consistent with CO_2. CNFs in good yield and good quality were formed in S-FA than in E-FA. CNFs with uniform large diameters were formed in S-FA from the large catalyst size. For E-FA, TEM analysis and DTG revealed growth of CNFs, CNTs, and carbon microspheres (CMS).

These results show that CO_2 and fly ash can be converted to commodity products, which can contribute towards mitigating their negative impact on the environment and generate monetary value from them. Sasol fly ash was also found to be superior to Eskom fly ash for the production of CNMs under all conditions.

Dedication

This work is dedicated to all 7 of my siblings and more especially to my parents. They have held me up high and been with me through this tough journey.

Thank you for your support boNkosi, Dlamini, Hlub'lomuhle.

Acknowledgments

It has been a tough journey to reach this point and I would not have made it if it were not for the following people:

- God, you have been my main source of strength and comfort. I wanted to give up many times, but you sustained me in various ways. Always making a way, giving me money to study, ideas, a strong support system, and a place to stay.
- My supervisor, Prof Diakanua Nkazi you exceeded my expectations and went beyond the call of duty. Your kindness and financial support have been immense and thank you for seeing to the completion of this project.
- Dr. Mukaya for your advice, corrections, and contribution
- The guys at the workshop, Rodney, Hopewell, and Phatho, helped a lot in setting up for my experiments and were patient.
- Funding from Feenix and the postgraduate merit award.
- Mrs. Petra Dinham for helping me with SEM, the knowledge you imparted and your connections helped make sense of my work.
- Janet Smith and Motlatso Phali for helping with TGA and chemicals.
- Staff at MMU for helping with coating, XRD, and TEM
- Dr. Rudolph Erasmus for helping with Raman analysis.
- Thapelo from chemistry for helping me with the synthesis
- The guy from Lafarge who helped with getting the fly ash
- Kgaogelo for your prayers and for being there.
- Importantly, my family (Sizwe, Zweli, Phindile, my Father, and my Mother) you guys played a very important role in my life. Live long and prosper.

Publications

- Dlamini, N. J., Mukaya, H. E., Nkazi, D. B., Carbon-based nanomaterials production from environmental pollutant byproducts: A Review - Sent for publication to *Journal of CO_2 utilization*.
- Dlamini, N. J., Mukaya, H. E., Nkazi, D. B., A comparative study of Fischer-Tropsch, and energy generation processes for the growth of carbon nanomaterials - Sent for publication to *Journal of CO_2 utilization.*

Table of Contents

Declaration i

1. Abstract ii
2. Dedication iv
3. Acknowledgments v
4. Publications vi
5. List of Figures x
6. List of Tables xiii
7. List of Abbreviations xiv
1. Chapter 1: Overview and Scope 1
   - 1.1 Introduction 1
   - 1.2 Problem Statement 3
   - 1.3 Research Questions 4
   - 1.4 Research Aim and Objectives 4
   - 1.5 Hypothesis 4
   - 1.6 Structure of the Dissertation 4
   - 1.7 References 7
2. Chapter 2: Literature Review 12
   - 2.1 Carbon Dioxide 12
   - 2.2 Formation and Source of CO_2 13
     - **2.2.1 Natural Formation** 13
     - **2.2.2 Anthropogenic** 13
   - 2.3 CO_2 Capture and Storage 14
   - 2.4 Application of Carbon Dioxide 15
     - **2.4.1 Physical/Direct Utilization** 15
     - **2.4.2 Chemical Utilization** 16
   - 2.5 Carbon nanotubes 21
     - **2.5.1 Synthesis Methods of CNMs (CNTs)** 24
     - **2.5.2 Growth of CNMs from carbon dioxide** 28
     - **2.5.3 Growth Mechanism** 37
     - **2.5.4 Carbon nanomaterials Synthesis parameters** 39

2.6 Coal 41
2.6.1 Coal Rank/Classification 42
2.6.2 Composition and mineralogy of coal 43
2.6.3 Coal Consumption 44
2.7 Coal Combustion in South Africa 45
2.8 Fly ash 46
2.8.1 Fly ash physical properties 47
2.8.2 Mineralogy and chemical properties 47
2.9 Fly ash classification 48
2.10 Applications of fly ash 48
2.10.1 Agriculture 48
2.10.2 Environmental protection/adsorbent 50
2.10.3 Construction 51
2.10.4 Fly ash as a catalyst 52
2.11 Carbon Dioxide as a carbon source and fly ash as a catalyst for CNMs production 57
2.12 Fly ash disposal 58
2.13 Conclusion and Summary of CNMs production from fly ash and CO_2 59
2.14 References 60
3. Chapter 3: Methodology 83
3.1 Introduction 83
3.2 Materials 83
3.3 Synthesis of CNMs 83
3.4 Characterization Methods for fly ash and CNMs 84
3.4.1 Scanning Electron Microscopy (SEM) 84
3.4.2 Energy Dispersive Spectroscopy (EDS) 85
3.4.3 Thermogravimetric Analysis (TGA) 85
3.4.4 Transmission Electron Microscopy (TEM) 85
3.4.5 Raman Spectroscopy 86

3.4.6 X-ray fluorescence (XRF) 86

3.4.7 X-ray diffraction (XRD) 86

3.4.8 Particle Size Analyser 87

4. Chapter 4: Fly Ash Characterization 88

4.1 Introduction 88

4.2 Results and Discussion 89

4.3 Conclusion 94

4.4 References 95

5. Chapter 5: Synthesis of CNMs from CO_2 using Sasol and Eskom Fly ash as catalyst 97

5.1 Introduction 97

5.2 Experimental and Characterization Methods 98

5.3 Results and Discussion 99

5.3.1 CNMs synthesis from Sasol Fly Ash 100

5.3.2 CNMs synthesis from Eskom fly ash 110

5.4 Conclusion 115

5.5 References 117

6. Chapter 6: Synthesis of CNMs from C_2H_2 using Sasol and Eskom Fly Ash 122

6.1 Introduction 122

6.2 Experimental Method 123

6.3 Results and Discussion 123

6.4 Conclusion 130

6.5 References 132

7. Chapter 7: Conclusion and Recommendations 137

Recommendations 138

List of Figures

Figure 2.1: Phase Diagram of CO_2 showing different phases of CO_2 under different temperature and pressure conditions [224] 12
Figure 2.2: Anthropogenic CO_2 sources according to sectors [5] 14
Figure 2.3: Simplification of various CO_2 utilization pathways 15
Figure 2.4: Different forms of carbon and carbon nanomaterials [225] 22
Figure 2.5: Graphene sheet rolled up in various ways to form (a) zigzag, (b) chiral and (c) armchair SWCNTs 23
Figure 2.6: A schematic representation of the arc discharge method [84] 25
Figure 2.7: A typical laser ablation instrument for CNT synthesis [87] 26
Figure 2.8 : Electron Microscopy CNTs images by (a) Motiei using Mg metal, (b) Lou using Li and (c) Na, (d) Zhang using Mg metal and (e) by Lou using NaBH4 [110], [114], [116], [117] 29
Figure 2.9: TEM micrographs of CNTs obtained from different studies of CO_2 as a precursor (a) Straight CNTs, (b) purified CNTs, (c) CNTs structures synthesized at optimum temperatures of 800℃ and (d) 1100℃ [120], [121], [122], [125] 34
Figure 2.10: CNTs broadly accepted growth mechanism: (a) tip growth and (b) base/root growth mechanism [108] 38
Figure 2.11: Global consumption of coal [173] 44
Figure 2.12: A typical pulverized fuel combustion process [161] 45
Figure 2.13: Fly ash production and utilization rates from different countries [180] 46
Figure 2.14: Various types of morphologies of fly ash [179] [181][182] 47
Figure 2.15: Electron microscopy images of (a) CNFs entwined with MWCNTs from 5 wt% Fe and fly ash, (b) CNTs from ethanol and carrier gas (3:10) and fly ash, (c) CNT ribbons from PVA and 25 wt% fly ash, (d) CNTs obtained at the optimum conditions of 650 ℃, 300 torr [217]–[219], [221], [222] 54
Figure 3.1: Chemical vapour deposition setup used in this study 84
Figure 4.1: SEM micrographs of (a) Eskom and (b) Sasol fly ashes. A closer inspection of the fly ash particles showing (c) smaller spheres, broken granular fragments in E-FA and (d) course surface of S-FA spheres mixed with higher fraction of irregular 89

Figure 4.2: Comparison of the particle size distributions of raw (a) Sasol and (b) Eskom fly ash 90
Figure 4.3: EDS analysis of raw Sasol fly ash showing elemental composition of a spherical particle (spectrum 1) and an irregularly fragment (spectrum 2) 92
Figure 4.4: EDS analysis of raw Eskom fly ash of selected individual particles (spherical and irregular fragment) 92
Figure 4.5: XRD patterns of Eskom and Sasol fly ashes showing phases that are present. U-Mullite, Q-quartz, Ca-calcite, M-magnetite 93
Figure 5.1: Thermal analysis of the as-synthesized CNMs at various temperatures (a) TGA curve showing decomposition temperatures and (b) derivative thermogravimetric curve showing oxidation temperature 101
Figure 5.2: SEM images of CNMs grown at 750℃ showing (a) mixture of CNMs with fly ash and (b) net-like CNMs 101
Figure 5.3: Raman Spectra obtained from CNMs synthesized using Sasol fly ash at different temperatures 102
Figure 5.4: CNMs synthesized from Sasol fly ash at 850℃ showing (a) a splashed like liquid-substance on the surface of fly ash resembling CNMs and (b) an irregular and deformed fly ash structure 103
Figure 5.5: CNMs from Sasol fly ash obtained at a temperature of 950℃ showing (a) deformed fly ash particle and (b) short-length rod-like structures 104
Figure 5.6: Thermograms of Sasol CNMs at various flow rates of CO_2/Ar, (a) TGA and (b) DTG 105
Figure 5.7: Products grown from Sasol fly ash at CO_2/Ar flow rate of 600.1/1202 sccm with a decreased pressure showing (a) a dried chunk of fly ash material and (b) a flat-like structure.. 106
Figure 5.8: Raman Spectroscopy of carbonaceous products synthesized from Sasol fly ash at various CO_2 and argon flow rates 106
Figure 5.9: SEM micrographs of CNMs grown at CO_2/Ar flowrates of 962/1202 sccm showing (a) short-length CNMs mixed fly ash particles and (b) CNMs covering fly ash sphere 107
Figure 5.10: Effect of catalyst mass (S-FA) on the growth of CNMs determined using (a) TGA and (b) DTG 108

Figure 5.11: SEM micrographs showing CNMs grown from Sasol fly ash masses of (a) 600 mg, (b) 800 mg and (c) 1000 mg 109
Figure 5.12: Raman spectra showing the effect of catalyst mass on the crystalinity of the CNMs 110
Figure 5.13: SEM micrographs of products obtained from Eskom fly ash at a temperature of 750℃ showing (a) small twigs or rod-like structures in the fly ash sphere (b) hematite minerals 111
Figure 5.14: Products obtained from Eskom fly ash grown at 850℃ showing (a) pores in fly ash with spheres occupying them and (b) twigs and rod-like structures..... 112
Figure 5.15: Products obtained at 950℃ during CNMs synthesis showing (a) a fly ash sphere covered with patterned and growth of magnetite and silica minerals and (b) twigs or rod-like structures of mullite 112
Figure 5.16: Raman Spectra of products synthesized from Eskom fly ash at temperatures of 750℃, 850℃, and 950℃..... 113
Figure 5.17: SEM images of products obtained from Eskom fly ash at CO_2/Ar flowrates of (a) 300.1/601 sccm, (b) 600.1/1202 sccm and (c) 901.5/1202 sccm..... 114
Figure 5.18: Raman Spectra of products synthesized from Eskom fly ash at CO_2/Ar flow rates of 300.5/601 sccm, 600.1/1202 sccm and 901.5/1202sccm..... 115
Figure 6.1: TGA data of CNMs synthesized from acetylene using raw Sasol and Eskom fly ash 124
Figure 6.2: Derivative Weight curves of Sasol and Eskom carbon nanomaterials..... 125
Figure 6.3: SEM images of CNMs grown on fly ash (a) Eskom CNMs (b) Sasol CNMs (c) morphology of E-CNMs (d) morphology of S-CNMs (e) small rod-like CNMs precipitating from E-FA..... 126
Figure 6.4: TEM micrographs showing morphology of (a) Sasol CNMs from S-FA and (b) Eskom CNMs from E-FA 128
Figure 6.5: Carbon microspheres covered with amorphous material observed in Eskom carbon nanomaterials 128
Figure 6.6: XRD patterns of (a) Raw Sasol and Eskom fly ashes and (b) synthesized CNMs from Sasol and Eskom. U-Mullite, Q-quartz, Ca-calcite, M-magnetite 129
Figure 6.7: Raman Spectra of CNMs synthesized from Eskom and Sasol fly ash as catalyst ... 130

List of Tables

Table 2.1: Summary of synthesis parameters and results of CNMs structures obtained by chemical reaction 28
Table 2.2: Synthesis conditions of CNTs from CO_2 using the CVD and the optimized parameters 32
Table 2.3: Types of coal based on their heating value and carbon content 43
Table 2.4: Minerals found in coal 43
Table 2.5: Summary of synthesis conditions used in the growth of CNMs from fly ash catalysts 53
Table 4.1: Chemical composition of Sasol and Eskom fly ash obtained from XRF 91
Table 4.2: Quantitative elemental analysis of Eskom and Sasol fly ash from EDS 93
Table 5.1: Reaction parameters varied for the synthesis of CNMs from Sasol and Eskom fly ash 99
Table 5.2: Summary of the best synthesis conditions obtained from each of the parameters investigated in Sasol fly ash 100
Table 6.1: Summary of DTG and TGA temperature values of Eskom and Sasol CNMs 125

List of Abbreviations

CNTs/CNFs:	Carbon nanotubes and Carbon nanofibers
CNMs:	Carbon nanomaterials
CMSs:	Carbon microspheres
CO_2:	Carbon dioxide
CCS:	Carbon capture and storage
CCSU:	Carbon capture, storage and utilization
CO:	Carbon monoxide
Ar:	Argon
H_2:	Hydrogen
N_2:	Nitrogen
C_2H_2:	Acetylene
C_2H_4:	Ethylene
Fe:	Iron
Ni:	Nickel
Co:	Cobalt
Al_2O_3:	Alumina
SiO_2:	Silica
Sasol:	South African Synthetic Oil Limited
Eskom:	Electricity Supply Commission
S-FA:	Sasol fly ash
E-FA:	Eskom fly ash
MWCNTs:	Multi walled carbon nanotubes
SWCNTs:	Single walled carbon nanotubes
DWCNTs:	Double walled carbon nanotubes
CVD:	Chemical vapour deposition

FESEM:	Field Emission Scanning Electron Microscopy
EDS:	Energy Dispersive Spectroscopy
XRD:	X-Ray Diffraction
XRF:	X-Ray Fluorescence
TEM:	Transmission Electron Microscopy
TGA:	Thermogravimetric Analysis
DTG:	Derivative Thermogravimetry
LOI:	Loss on Ignition
PSD:	Particle Size Distribution
EOR:	Enhanced Oil Recovery
SCCM:	Standard cubic centimetres per minute
mg:	Milligrams
min:	Minutes
atm:	Atmosphere
a.u:	Arbitrary unit
I_D:	Intensity of the D-band
I_G:	Intensity of the G-band
Wt%:	Weight percentage
PBL:	Planbureau voor de Leefomgeving
GHG:	Greenhouse gas

Chapter 1: Overview and Scope

1.1 Introduction

Carbon nanomaterials (CNMs) such as CNFs and CNTs are cylindrical structures that are filled and hollow, respectively. They are composed of only the carbon atom with diameters in the nanometer range and contain lengths that extend from a few to several microns [1]–[4]. The interest in these materials can be attributed to their unique and tremendous properties such as high electrical and thermal conductivity and good mechanical strength [5]–[7]. These properties created opportunities for CNMs to be applied in flat panel displays, batteries, water purification, and catalysis to mention a few [8]–[13]. A variety of techniques have been reported and used in literature to produce different CNMs structures. These methods include arc-discharge, laser ablation, chemical vapour deposition (CVD) [14]–[16]. The arc-discharge method involves the vaporization of two high pure graphite electrodes by an electric current [14]. The laser ablation method is like the arc-discharge method. However, instead of a current, a laser is used to vaporize a carbon target doped with metals such as Ni, Fe, and Co [15]. In CVD, a carbon-containing compound (ethylene, methane, acetylene, CO, etc.) mixed with a carrier gas (H_2, Ar, N_2) is reacted over transition metal catalysts to form CNMs [17]. All three of these techniques have disadvantages and advantages. However, the most promising and widely used technique is the CVD. This is because the CVD method is cheap, easy to set up, and can be scaled up for industrial production [16]. The CVD method generally uses transition metals (Ni, Fe, Co, and alloys) as catalysts upon which the CNMs nucleate. However, these catalysts and carbon sources are expensive and toxic. Thus, inexpensive and readily available industrial waste products such as fly ash and carbon dioxide (CO_2) are the respectively desired catalysts and carbon sources for the production of nanomaterials.

Carbon dioxide (CO_2) is one of the major waste gases produced in the world because of the great reliance on fossil fuel energy. A report published by PBL (Planbureau voor de Leefomgeving) Netherlands Environmental Assessment on global trends of CO_2 and total GHG (greenhouse gas) emissions, showed that in the past decade global GHGs emissions have increased by 1.2% [18]. The main GHGs are carbon dioxide, methane, nitrous oxide, and fluorinated gases which contribute 82% 10%, 6%, and 3%, respectively [19]–[21]. These gases are responsible for trapping heat in the atmosphere causing a rise in the temperature of the planet. This phenomenon is normally

referred to as global warming. The effects of global warming on the planet are quite severe and are well documented [21]–[24]. Currently, the countries with the highest GHG emissions globally are China (26%), the United States (13%), European Union (8%), India (7%), The Russian Federation (5%), and Japan (3%). These countries contribute 62% worldwide to GHG emissions and they also have the highest CO_2 emission levels [18], [25].

CO_2 can be captured in a process called carbon capture and storage (CCS), whereby it is captured from the atmosphere or production plants and stored underground [26]–[28]. However, after decades of research this technology has been hit by high operational costs, concerns with the period of the CO_2 storage underground unit [29]–[33]. As such, research interests in carbon capture, storage, and utilization (CCSU) seemed to be gaining momentum and more favoured. The utilization of CO_2 not only contributes to the reduction of GHGs but also provides economic relief. It has also been a goal for scientists to find uses of carbon dioxide to produce value-added products. It has found its use in carbonated drinks, dry ice, solvent, refrigerant, welding medium, and Enhanced Oil Recovery (EOR) [29], [34]. These are relevant but not significant enough to the abatement of CO_2 concentrations in the atmosphere[35].

The main barrier to the usage of CO_2 as a chemical feedstock is its high stability (ΔG_f = -396 kJ/mol). It is both a kinetically and thermodynamically stable molecule and difficult to reduce, therefore, converting it requires a significant of energy [36]. Among the research areas of CO_2 utilization is in the synthesis of CNMs such as CNTs and CNFs as a carbon source [37]. The studies conducted on CO_2 as a carbon source for CNMs are still lacking and need further research including using different catalysts.

Fly ash, also known as pulverized ash, is a solid waste product produced in coal-fired power plants when generating electricity. Fly ash mostly consists of silicon dioxide (SiO_2), aluminium oxide (Al_2O_3), and iron oxide (Fe_3O_2). It also has minor constituents of calcium, magnesium, silica, potassium, manganese, lead, nickel, cobalt, zinc, arsenic, selenium, and boron [38], [39]. Its composition depends upon the coal bed composition and combustion method [40].

The management and disposal of fly ash have raised some environmental and economic concerns. Since fly ash is waste, the common practice is to dump it in the sea or into landfills [41]–[43]. This is not good because, although they exist in small amounts, fly ash contains some toxic metals [38]. When fly ash is dumped, there is a possibility of the metals leaching into groundwater or surface

water nearby [44]. Furthermore, it could cause air pollution by being blown away by air and could also affect human health through direct inhalation [45]. More importantly, there exists a long-term financial burden associated with land use and maintenance with ash dumps [39], [46]. Thus, this led researchers around the world to try and find the uses of fly ash as a value-added commodity.

The research into the uses of fly ash has received a great deal of attention. It has found use in the construction industry, agriculture, geopolymers, soil amendment, ceramic materials, and catalysis to name a few [47]. Researchers around the world have also attempted to use fly ash as a catalyst in the synthesis of CNMs [48]–[51]. One of its advantages is its low cost and availability which also provides an incentive to use this material. Furthermore, it contains a small portion of the catalysts that are used in the production of CNM such as iron.

In this study, carbon dioxide was used as a sole and main source of carbon along with pre– and post-combustion fly ash to synthesize carbon nanomaterials. Pre-combustion fly ash is generated at South African Synthetic Oil Limited (Sasol) during coal combustion, which implies the coal is partially combusted resulting in unburnt carbon. The coal from the Electricity Supply Commission (ESKOM) is post-combusted, meaning it is completely combusted and leaves low unburnt carbon content. For the rest of the chapters, pre-combustion fly ash will be addressed as Sasol fly ash and post-combustion will be referring to a Eskom fly ash. The two fly ashes were characterized using EDS and XRF analysis to determine their compositions. Two comparative studies were conducted, one using CO_2 as a carbon source under various parameters and the other using acetylene (C_2H_2). These studies were conducted to determine which fly ash forms purer CNMs with good crystallinity in high terms of their ability to synthesize CNMs using the CVD method. The fly ashes were used untreated, and argon (Ar) was used as a carrier gas used.

1.2 Problem Statement

Currently, waste such as fly ash and carbon dioxide poses an environmental problem. Fly ash can cause air pollution by being blown away by air and affect human health through direct inhalation. It also contains some toxic metals that can leach into underground water. While carbon dioxide is a well-known greenhouse gas and a major contributor to global warming. Both these waste products have been studied for their applications. This study aims toward contributing to the currently existing technology and research on mitigating the environmental effects of these waste

products. This will be done by investigating them as a carbon source (CO_2) and catalyst (fly ash) on the synthesis of carbon nanomaterials.

1.3 Research Questions

- Which fly ash catalyst produces good quality and good yield of CNMs between Sasol and Eskom fly ash?
- Can the variation of CO_2 and carrier gas flow rate, reactor temperature, type, and mass of catalyst result in optimum quality and quantity of CNMs production?
- How do the composition and particle size of fly ash influence the structure and morphology of CNMs?

1.4 Research Aim and Objectives

In South Africa, only one type of fly ash has been investigated to produce carbon nanomaterials, this is post-combustion fly ash from Eskom. This research aims to investigate the effect of Sasol (pre-combustion) and Eskom (post-combustion) fly ash as a catalyst to produce CNTs from CO_2 via the CVD.

The aim can be achieved through the following objectives:

- To determine the best-operating conditions such as reactor temperature, catalyst amount, and gas flowrate on the production of CNMs;
- To investigate the effect of carbon sources (CO_2 and C_2H_2) on the production of CNMs;
- To compare the production of CNMs using pre-combustion and post-combustion fly ashes.

1.5 Hypothesis

Since the coal from Sasol is pre-combusted resulting in fly ash with higher levels of unburnt carbon than Eskom fly ash. Therefore, good quality and yield of CNMs will be obtained with Sasol fly ash.

1.6 Structure of the Dissertation

This dissertation is divided into seven chapters including this one. It is organized as follows:

Chapter 1: Overview and Scope

This chapter gives an overview and summary of the work done and justifies the use of CO_2 and fly ash for carbon nanomaterial synthesis. It also highlights the challenges faced by using both

waste materials as feedstock (CO_2) and catalyst (fly ash). Lastly, the benefits of using these by-products are mentioned.

Chapter 2: Literature Review

A comprehensive overview and background on the properties, applications, challenges, and environmental impact of fly ash and CO_2 are given. Studies of fly ash as a catalyst and CO_2 as a carbon precursor for CNMs synthesis are deliberated separately. They are subsequently discussed as a carbon source and catalyst combination. A literature review on CNMs is given, with a focus on CNTs. Factors and synthesis conditions that influence the formation of CNMs from CO_2 are mentioned.

Chapter 3: Methodology

The materials, methods, and characterization techniques used in this study are presented in this chapter.

Chapter 4: Fly ash Characterization

A comparative study on the properties of the two fly ash catalysts was conducted and the results are presented. The characterization methods used to compare their properties are SEM, EDS, XRF, and XRD and a particle size analyser.

Chapter 5: Synthesis of CNMs from CO_2 using Sasol and Eskom fly ash

The catalytic abilities of the fly ash catalyst are compared to determine which catalyst produces better CNMs when CO_2 is a precursor gas. The parameters: reactor temperature, the flow rate of precursor gas carrier gas, and catalyst mass were varied to examine their effect on the yield and quality of the CNMs. The products were studied using TGA and DTG, SEM, and Raman spectroscopy.

Chapter 6: Synthesis of CNMs from C_2H_2 using Sasol and Eskom and fly ash

This chapter presents detailed results of the CNMs produced from C_2H_2 as a precursor gas and argon as a carrier gas. The products are compared by using SEM, TEM, TGA and DTG, XRD, and Raman spectroscopy.

Chapter 7: Conclusion and Recommendations

Here, a summary of the findings in this study is given and their implications for the future production of CNMs from fly ash and CO_2. Areas that require further investigation are discussed.

1.7 References

[1] J. Ren, M. Johnson, R. Singhal, and J. Licht, “Transformation of the greenhouse gas CO2 by molten electrolysis into a wide controlled selection of carbon nanotubes,” *J. CO2 Util.*, vol. 18, pp. 335–344, 2017.

[2] V. J. Pillewan, D. N. Raut, K. N. Patil, and D. K. Shinde, “Carbon to Carbon Nanotubes Synthesis Process: An Experimental and Numerical Study,” in *Materials Today: Proceedings*, 2018, vol. 5, no. 2, pp. 6444–6452.

[3] L. Feng, N. Xie, and J. Zhong, “Carbon nanofibers and their composites: A review of synthesizing, properties and applications,” *Materials (Basel).*, vol. 7, no. 5, pp. 3919–3945, 2014.

[4] P. Serp, M. Corrias, and P. Kalck, “Carbon nanotubes and nanofibers in catalysis,” *Appl. Catal. A Gen.*, vol. 253, no. 2, pp. 337–358, 2003.

[5] R. S. at al. Ruoff and D. C. Lorents, “Mechanical and thermal properties of carbon nanotubes,” *Carbon N. Y.*, vol. 33, no. 7, pp. 925–930, 1995.

[6] P. Saxena and S. P. Sanyal, “Phonon and thermal properties of achiral single-wall carbon nanotubes,” vol. 67, no. 2, pp. 305–317, 2006.

[7] M. S. D. Ado Jorio, Gene Dresselhaus, *Carbon Nanotubes Advanced Topics in the Synthesis, Structure, Properties and Applications*, vol. 111. 2007.

[8] S. Frank, P. Poncharal, Z. L. Wang, and W. A. de Heer, “Carbon nanotube quantum resistors,” *Sci. (Washington, D. C.)*, vol. 280, no. 5370, pp. 1744–1746, 1998.

[9] K. Balasubramanian and M. Burghard, “Biosensors based on carbon nanotubes,” *Anal. Bioanal. Chem.*, vol. 385, no. 3, pp. 452–468, 2006.

[10] J. Doh and J. Lee, “Prediction of the mechanical behavior of double-walled CNTs using a molecular mechanics-based finite element method: Effects of chirality,” *Comput. Struct.*, vol. 169, pp. 91–100, Jun. 2016.

[11] W. Han, “Synthesis of Gallium Nitride Nanorods Through a Carbon Nanotube-Confined Reaction,” *Science (80-.).*, vol. 277, no. 5330, pp. 1287–1289, 1997.

[12] F. Cheng, Z. Tao, J. Liang, and J. Chen, “Template-Directed Materials for Rechargeable Lithium-Ion Batteries,” *Chem. Mater.*, vol. 20, no. 3, pp. 667–681, 2008.

[13] P. Simon and Y. Gogotsi, “Materials for electrochemical capacitors,” *Nat. Mater.*, vol. 7, no. 11, pp. 845–854, 2008.

[14] N. Arora and N. N. Sharma, “Arc discharge synthesis of carbon nanotubes: Comprehensive review,” *Diamond and Related Materials*, vol. 50. Elsevier B.V., pp. 135–150, 2014.

[15] F. Kokai, † K Takahashi, M. Yudasaka, R. Yamada, T. Ichihashi, and S. Iijima, “Growth Dynamics of Single-Wall Carbon Nanotubes Synthesized by CO2 Laser Vaporization,” *J. Phys. Chem. B*, vol. 103, no. 21, pp. 4346–4351, 1999.

[16] N. M. Mubarak, E. C. Abdullah, N. S. Jayakumar, and J. N. Sahu, “An overview on methods for the production of carbon nanotubes,” *Journal of Industrial and Engineering Chemistry*, vol. 20, no. 4. The Korean Society of Industrial and Engineering Chemistry, pp. 1186–1197, 2014.

[17] X.-D. Wang, K. Vinodgopal, and G.-P. Dai, “Synthesis of Carbon Nanotubes by Catalytic Chemical Vapor Deposition,” *Intech*. 2019.

[18] J. G. J. Olivier and J. A. H. W. Peters, “TRENDS IN GLOBAL CO2 AND TOTAL GREENHOUSE GAS Summary of the 2019 Report,” 2019.

[19] E. I. Administration, “BP Statistical Review of World Energy,” 2017.

[20] World Resources Institutes, “World Greenhouse Gas Emissions: 2016,” *wri.org*, 2020. [Online]. Available: https://www.wri.org/resources/data-visualizations/world-greenhouse-gas-emissions-2016. [Accessed: 30-Mar-2021].

[21] Center for Climate and Energy Solutions, “Global Emissions: Center for climate and energy solutions,” 2016. [Online]. Available: https://www.c2es.org/content/international-emissions/. [Accessed: 22-Dec-2019].

[22] A. Bradford and S. Pappas, “Effects of Global Warming | Live Science,” *Live Science*, 12-Aug-2017. [Online]. Available: https://www.livescience.com/37057-global-warming-effects.html. [Accessed: 13-Oct-2020].

[23] Hannah Ritchie and M. Roser, "CO2 and Greenhouse Gas Emissions," *OurWorldInData.org*, 2020. [Online]. Available: https://ourworldindata.org/co2-and-other-greenhouse-gas-emissions#citation. [Accessed: 30-Mar-2021].

[24] "Effects | Facts – Climate Change: Vital Signs of the Planet." [Online]. Available: https://climate.nasa.gov/effects/. [Accessed: 13-Oct-2020].

[25] D. Spencer, "BP Statistical Review of World Energy Statistical Review of World," 2019.

[26] B. P. Spigarelli and S. K. Kawatra, "Opportunities and challenges in carbon dioxide capture," *J. CO2 Util.*, vol. 1, pp. 69–87, 2013.

[27] D. Y. C. Leung, G. Caramanna, and M. M. Maroto-Valer, "An overview of current status of carbon dioxide capture and storage technologies," *Renew. Sustain. Energy Rev.*, vol. 39, pp. 426–443, 2014.

[28] S. D. Kenarsari *et al.*, "Review of recent advances in carbon dioxide separation and capture," *RSC Adv.*, vol. 3, no. 45, pp. 22739–22773, 2013.

[29] A. Rafiee, K. Rajab Khalilpour, D. Milani, and M. Panahi, "Trends in CO2 conversion and utilization: A review from process systems perspective," *J. Environ. Chem. Eng.*, vol. 6, no. 5, pp. 5771–5794, 2018.

[30] S. M. Benson and D. R. Cole, "CO2 sequestration in deep sedimentary formations," *Elements*, vol. 4, no. 5, pp. 325–331, 2008.

[31] G. T. Rochelle, "Amine Scrubbing for CO2 Capture," *Science (80-.).*, vol. 325, no. 5948, pp. 1652–1654, 2009.

[32] H. Vidas, B. Hugman, A. Chikkatur, and B. Venkatesh, "Analysis of the costs and benefits of CO2 sequestration on the US outer continental shelf," 2012.

[33] K. Z. House, C. F. Harvey, M. J. Aziz, and D. P. Schrag, "The energy penalty of post-combustion CO2 capture & storage and its implications for retrofitting the U.S. installed base," *Energy Environ. Sci.*, vol. 2, no. 2, pp. 193–205, 2009.

[34] K. Dodds, L. J. Pekot, and S. Whittaker, "Carbon Dioxide — Challenges and Opportunities," *Oilf. Rev.*, vol. 27, no. 2, pp. 36–50, 2015.

[35] P. B. Joshi, “Carbon dioxide utilization: A comprehensive review,” *Int. J. Chem. Sci.*, vol. 12, no. 4, pp. 1208–1220, 2014.

[36] E. T. Kho, T. H. Tan, E. Lovell, R. J. Wong, J. Scott, and R. Amal, “A review on photo-thermal catalytic conversion of carbon dioxide,” *Green Energy Environ.*, vol. 2, no. 3, pp. 204–217, 2017.

[37] G. S. Simate, S. E. Iyuke, S. Ndlovu, C. S. Yah, and L. F. Walubita, “The production of carbon nanotubes from carbon dioxide: Challenges and opportunities,” *Journal of Natural Gas Chemistry*, vol. 19, no. 5. pp. 453–460, 2010.

[38] D. Paswan, S. M. A, M. Shaikh, A. Nadar, and S. D. Maniyar, “Heavy Metals in Fly Ash ; Its Impact on Human Health and Environment,” in *NICMAR 2nd International Conference On Construction, Real Estate, Infrastructure and Project (CRIP) Managemen*, 2017.

[39] A. Bhatt, S. Priyadarshini, A. Acharath Mohanakrishnan, A. Abri, M. Sattler, and S. Techapaphawit, “Physical, chemical, and geotechnical properties of coal fly ash: A global review,” *Case Stud. Constr. Mater.*, vol. 11, Dec. 2019.

[40] K. Nizar, H. Kamarudin, and M. S. Idris, “Pysical, Chemical & Mineralogical Properties of Fly-ash,” no. January 2015.

[41] A. Dwivedi and M. K. Jain, “Fly ash – waste management and overview : A Review Fly ash – waste management and overview : A Review,” *Recent Res. Sci. Technol. 2014*, vol. 6, no. 1, pp. 30–35, 2014.

[42] B. Lokeshappa, “Disposal and Management of Flyash,” *2011 Int. Conf. Life Sci. Technol.*, vol. 3, no. 2011, pp. 11–14, 2012.

[43] I. Nawaz, “Disposal and Utilization of Fly Ash to Protect the Environment,” *Int. J. Innov. Res. Sci. Eng. Technol.*, vol. 2, no. 10, pp. 5259–5266, 2013.

[44] A. Kumar, S. R. Samadder, and V. Kumar, “Assessment of groundwater contamination risk due to fly ash leaching using column study,” *Environ. Earth Sci.*, vol. 78, no. 1, pp. 1–12, 2019.

[45] S. Wang, “Application of solid ash-based catalysts in heterogeneous catalysis,” *Environ.*

Sci. Technol., vol. 42, no. 19, pp. 7055–7063, 2008.

[46] J. Li, X. Zhuang, X. Querol, O. Font, and N. Moreno, "A review on the applications of coal combustion products in China," *International Geology Review*, vol. 60, no. 5–6. Taylor and Francis Inc., pp. 671–716, 26-Apr-2018.

[47] S. Mostafa, H. Asl, A. Ghadi, M. Sharifzadeh, and H. Javadian, "Porous catalysts fabricated from coal fly ash as cost-effective alternatives for industrial applications : A review," *Fuel*, vol. 217. Elsevier, pp. 320–342, 2018.

[48] N. Hintsho *et al.*, "Direct synthesis of carbon nanofibers from South African coal fly ash," *Nanoscale Res. Lett.*, vol. 9, no. 387, 2014.

[49] O. M. Dunens, K. J. Mackenzie, and A. T. Harris, "Synthesis of Multiwalled Carbon Nanotubes on Fly Ash Derived Catalysts," *Environ. Sci. Technol*, vol. 43, pp. 7889–7894, 2009.

[50] N. Hintsho, A. Shaikjee, P. K. Tripathi, P. Franklyn, and S. Durbach, "The effect of CO2 on the CVD synthesis of carbon nanomaterials using fly ash as a catalyst," *RSC Adv.*, vol. 5, no. 66, pp. 53776–53781, 2015.

[51] D. C. D. Nath and V. Sahajwalla, "Application of fly ash as a catalyst for the synthesis of carbon nanotube ribbons," *J. Hazard. Mater.*, vol. 192, pp. 691–697, 2011.

Chapter 2: Literature Review

2.1 Carbon Dioxide

Carbon dioxide (CO_2) is a colourless, odourless, nontoxic [1] and stable molecule usually in gaseous form at standard pressure and temperature conditions (1 atm and 25 ℃). It can also exist as a liquid or solid (dry ice) under certain conditions. At 1 atm, solid CO_2 directly sublimes to a gas. Below a pressure of 5.11 atm, it does not exist as a liquid. Its structure consists of two oxygen atoms that are covalently bonded to a single carbon atom forming a double bond. It is a non-polar and chemically unreactive molecule under standard conditions that exists predominantly in the earth's atmosphere. Its stability makes it difficult to react with other molecules. Most reactions of CO_2 occur at the C-atom by a nucleophilic attack using electron-donating agents or electrophilic attack at the O-atom [2]. It can dissolve in water to reversibly form carbonic acid (H_2CO_3). CO_2 is a supercritical fluid ($scCO_2$) at temperatures and pressures at or above the critical point (30.98 ℃, 72.79 atm) as shown in Figure 2.1. This enables it to have some properties of both gas and liquid. This uniform phase gives CO_2 the property to mix with other fluids.

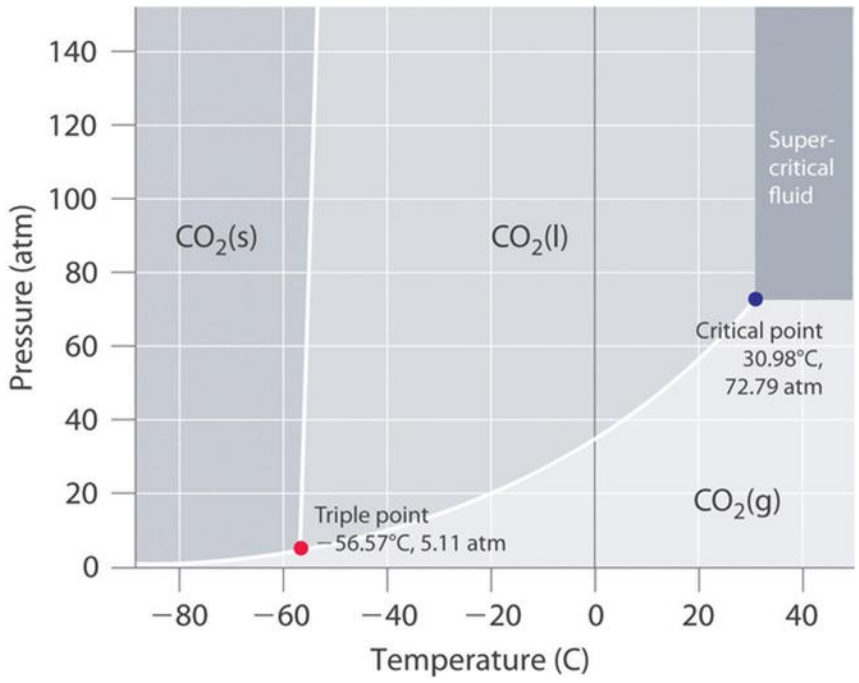


Figure 2.1: Phase Diagram of CO_2 showing different phases of CO_2 under different temperature and pressure conditions [224]

2.2 Formation and Source of CO_2

Carbon dioxide is an essential molecule for plants for their survival. Its concentration in the atmosphere depends on the processes that consume or release it. Plants, algae, and certain bacterium types use light energy to convert CO_2 and water to O_2, carbohydrates, and water. CO_2 may be produced through natural and anthropogenic processes [3].

2.2.1 Natural Formation

The natural formation of CO_2 is associated with indigenous gases and the carbon cycle. This mainly includes plant and animal respiration and decay, volcanic eruptions, hot springs, and geysers. These natural sources of CO_2 contribute very little to the Green House Gas (GHG) effect, most of the contributions come from anthropogenic activity.

2.2.2 Anthropogenic

These are human activities or industrial processes that produce large amounts of CO_2. The heavy reliance on carbon fossils is driven by the global energy demands for modernization, a better quality of life, and the need for economic growth [4]. Notwithstanding the measures that have been put in place such as alternative energy sources, environmental awareness campaigns, and policies, the burning of fossil fuels continues to be the preferred source of energy. The main sources of man-made CO_2 emissions can be divided into sectors as shown in Figure 2.2. The energy sector is the leading source of CO_2 emissions and contributes around 72% globally and includes electricity and heat, transportation, manufacturing, and construction fugitive emissions, and other fuel combustion. In the energy sector, the combustion of coal electricity, and heat is the leading emitter of CO_2 at 31%, followed by transportation (15%) and, manufacturing and construction (12.4%). Transportation includes but is not limited to the movement of people and using cars, buses, ships, airplanes, and trucks. The energy sector is followed by agriculture (11%). Industrial emissions contribute 6% and mostly include the production of cement, hydrogen, ethylene oxide, and limestone [5],[6].

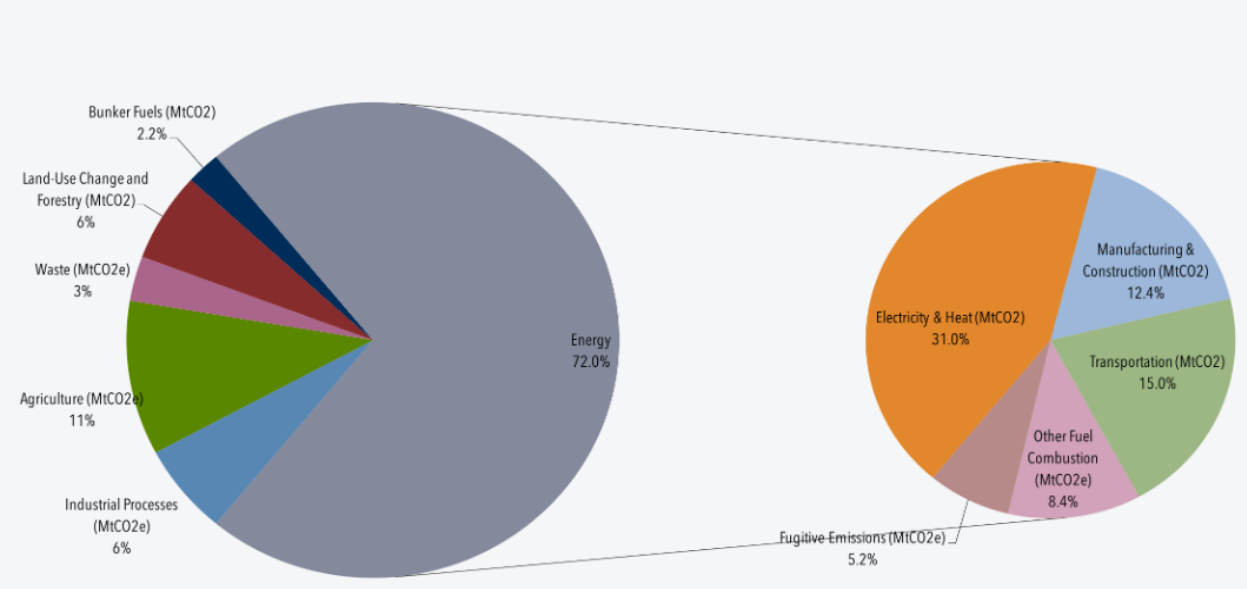


Figure 2.2: Anthropogenic CO_2 sources according to sectors [5]

2.3 CO_2 Capture and Storage

Carbon capture and storage (CCS) is one of the leading and early developed technologies used in the abatement of CO_2 concentration. Although expensive [7],[8], this method has been extensively studied. It is an area that is not short of literature and it is available at a commercial scale [3]. The CCS technology mainly targets CO_2 emissions from large point sources such as fossil fuel power plants, refineries, iron and steel factories, oil and gas production sites, cement, and other chemical plants. This is where most CO_2 emissions emanate from[9], as seen in Figure 2.2. The steps involved in capturing CO_2 include capture and compression from flue gas, transportation via pipelines, utilization, and storage. The technologies that are currently available for capturing CO_2 are pre-combustion[10]–[13], post-combustion [14]–[17] and oxyfuel combustion capture [18], [19]. The captured CO_2 is stored in the underground formation, deep sedimentary formations, saline aquifers, depleted oil and gas reservoirs, and in the ocean [3], [20]–[22]. An alternative approach to carbon management is to utilize the captured carbon dioxide instead of storing it underground.

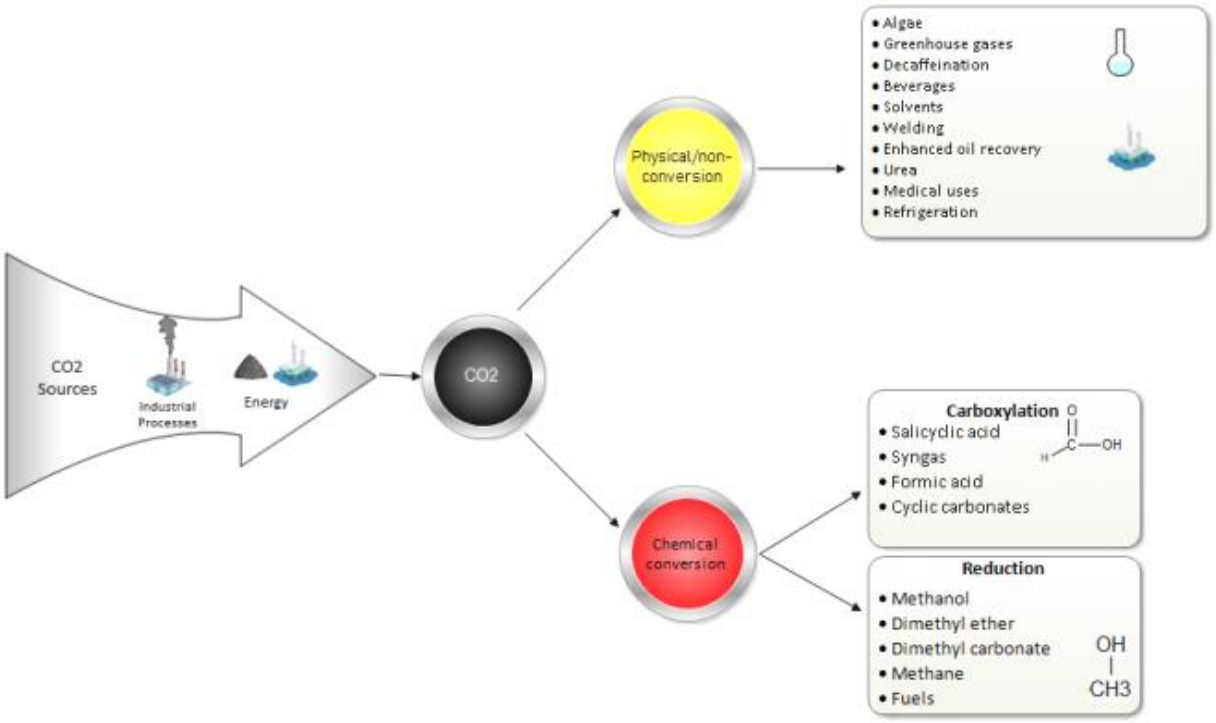


Figure 2.3: Simplification of various CO_2 utilization pathways

2.4 Application of Carbon Dioxide

Carbon dioxide has found several applications in chemical industrial processes and research is still ongoing to find efficient and economic routes of its utilization. Its conversion to chemicals and fuels can be traced back to the late 1800s where it was used in the synthesis of salicylic acid [23], $NaHCO_3$ [24], $NaCO_3$ [25], and in the early 1900s for its conversion to urea [26]. From then it has grown to a vast number of applications. Huang and Tan [27] categorized the application of CO_2 into two parts: chemical and physical utilization Figure 2.3.

2.4.1 Physical/Direct Utilization

In the physical or direct utilization, CO_2 remains in its purest form without any conversion and can also be suspended in a solution. One of its most common applications is in beverages. It is dissolved in cold drinks and other beverages to assist in sharpening the taste and flavour when the reaction of CO_2 gas with water forms carbonic acid [28]. It is chosen for beverages because of its solubility in water, stability, cost, preservation, and it is safer when compared with other gases. In the oil and gas industry, it is used to enhance the production and recovery of oil after primary recovery by injecting it into the reservoir. The oil containing dissolved CO_2 is brought to the surface, and CO_2 is separated for reinjection. The recovery of oil and gas can be increased up to

15% by CO_2 flooding. In fire extinguishers, CO_2 gas is used as a fire suppressant. The fire extinguisher is filled with CO_2 under extremely high pressures. During a fire, CO_2 can remove oxygen from the triangle of fire, thereby stopping the flames [30]. CO_2 is used in welding as a shielding gas to prevent the molten weld from meeting oxygen, nitrogen, and hydrogen gases in the air atmosphere. Meeting these gases results in porosity in the welded area [31], [32].

In its solid form, which is referred to as dry ice, it is used to preserve food as a refrigerant since it is much colder than ice water causing it to have a greater effect. Doctors use it to freeze and remove skin infections. It can be used in many other fields in different ways [29]. Supercritical carbon dioxide ($scCO_2$) can be used as a solvent to replace volatile organic compounds. It is an attractive solvent especially for a majority of nonpolar, limited polar, and low molecular weight organic compounds. Additionally, it is used in the synthesis of nanoparticles or composites and polymer modification [33], [34]. These physical applications are mostly on a small scale and have a minimal effect or contribution towards reducing CO_2 concentration. However, the advantage in most of its direct applications is the limited amount of energy required.

2.4.2 Chemical Utilization

This classification of CO_2 utilization stems from the conversion of CO_2 to fuels and chemicals. It can serve as a carbon source and feedstock to form a chemically different compound. Under suitable conditions, CO_2 bonds are broken down into their pure carbon or CO molecules form in exothermic or endothermic reactions. Furthermore, it can react with other compounds to create long hydrocarbon chains. The amount of energy required to convert CO_2 depends on the type of conversion it undergoes.

Generally, CO_2 can undergo carboxylation and reduction transformations. Where in the former transformation, the whole CO_2 moiety is incorporated into a polymeric or molecular compound and requires less energy whereas the latter produces reduced forms of CO_2 and requires a significant amount of energy.

Carboxylation Reactions

Urea

Urea (carbamide) production from carbon dioxide and ammonia is one of the matured technologies for the conversion of CO_2 and has been in existence for nearly a century. The reaction takes place

at 185-190 ℃ and 180-200 atm and occurs in two steps at equilibrium. In the first step (Equation 2.1), which is fast and exothermic, the whole CO_2 molecule is attached to liquid ammonia to form ammonium carbamate. The second step (Equation 2.2) is slow and endothermic, ammonium carbamate is decomposed into water and urea [35].

Equation 2.1

$$2NH_3 + CO_2 \leftrightarrow H_2N - COONH_4$$

Equation 2.2

$$H_2NCOONH_4 \leftrightarrow (NH_2)_2CO + H_2O$$

The most notable application of urea is in fertilizers due to its high nitrogen content (46%), when it reacts with water it releases ammonia and CO_2 to the soil. Therefore, using CO_2 for urea synthesis is not considered as a measure to reduce CO_2 concentrations.

Salicylic Acid

Salicylic acid is a precursor to aspirin. It is obtained when CO_2 is brought into contact with sodium phenoxide under high pressure and temperature (100 atm and 125 ℃) [36]. The product obtained is treated with sulphuric acid. Iijima and Yamaguchi [37] obtained salicylic acid from phenol and supercritical CO_2 in good yields in the presence of a Lewis acid catalyst at moderate temperatures. Among the catalysts they studied, aluminium bromide ($AlBr_3$) was found to be the most active.

Cyclic carbonates

Cyclic carbonates containing five-membered rings can be produced through cycloaddition of CO_2 to epoxides. These have reached industrial-scale production and have since found applications in lithium batteries, reagents, polar solvents, and diluents [38]. Cyclic carbonates can be used as components of oils and paints and can also undergo ring-opening polymerization to synthesize polycarbonates [39] and polyurethanes [40]. Their reaction usually requires a Lewis acid or base catalysts which require harsh synthesis conditions, thus limiting the formation. North et al. [41] reviewed major developments of catalyst systems used in the synthesis of cyclic carbonates and alternative routes that allow synthesis to be carried out under milder conditions. Yu et al. [42] studied the free-solvent conversion of CO_2 and epoxides to cyclic carbonates under atmospheric and room temperature conditions. A new Cu_6 cluster $[Cu_6(\mu_4\text{-}O)_2(SO_4)_4(DMA)_6]$ with a high density of active Lewis acid sites were synthesized and found to be a suitable catalyst for this process. CO_2 can undergo copolymerization to form polymers. A copolymer is a molecule that

contains two different repeating units. It is formed by polymerizing the two monomers (CO_2 and epoxide) at the same time to form a single chain [43].

Formic acid

Formic acid is the simplest form of carboxylic acid. It is used in the leather and textile industry, silage preservation, and synthesis of other organic chemicals [44]. Formic acid is produced commercially using four different methods:

- Oxidation of hydrocarbons
- Methyl formate hydrolysis
- Hydrolysis of formamide
- Preparation from formats

However, the most common production method used is methyl formate hydrolysis [45]. In this process, the carbonylation of methanol with CO takes place in the presence of a base catalyst (2.5 wt%) such as sodium methoxide (NaOMe) at 80 ℃ and 45 bar. The resulting methyl formate is subsequently hydrolysed to give formic acid [46]. Some of the available processes that exist to convert CO_2 into formic acid are homogenous catalysts, heterogeneous catalysts, and photocatalytic reduction. Direct hydrogenation of CO_2 to formic acid using a heterogeneous catalyst is the preferred method of synthesis since they have a high selectivity [47].

Reduction Reactions

Methane

Methane or natural gas can be consumed as feedstock in dry reforming with CO_2 to afford synthesis gas (Equation 2.3). It can also be formed as a product in the hydrogenation of CO_2 (Sabatier process) in the presence of a metal catalyst (Equation 2.4). Dry reforming of methane with CO_2 is an endothermic reaction and requires high temperatures. Synthesis gas (also called syngas) resulting from this process primarily constitutes carbon monoxide (CO), hydrogen (H_2) and often contains CO_2. It can be used in the matured Fischer-Tropsch process to produce a range of valuable liquid hydrocarbons such as methanol. This process is also found to be beneficial since both feedstocks are cheap and are greenhouse gases as opposed to using steam. Normally, hydrogen is the targeted product when steam is used. However, with CO_2 more CO is produced [40].

Equation 2.3: Dry reforming

$$CO_2 + CH_4 \leftrightarrow CO + 2H_2$$

Equation 2.4: Methanation/Sabatier process

$$CO_2 + 4H_2 \leftrightarrow CH_4 + 2H_2O$$

The Sabatier process or methanation of CO_2, unlike the consumption of methane, is exothermic. The reaction between CO_2 and H_2 usually takes place in the temperature range of 300-500 ℃, at pressures from atmospheric to 100 bar in the presence of a ruthenium-based catalyst. Currently, it is used to purify syngas in ammonia plants, reduce carbon oxide in hydrogen-rich syngas, and polymer electrolytes in fuel cell anodes [48]. Particle size, catalyst support, and operating temperature play an important role in methanation reactions [45]. However, the industrial application of this process has been halted by the carbon deposition which deactivates the catalyst [49].

Methanol

Methanol has found applications in fuels as a raw material, dyes, paints, rubbers, pharmaceuticals, and medicine [27], [50]. Thus, it is an important commodity in the chemical industry. Nearly all the methanol today is produced from synthesis gas obtained via gasification of carbon feedstocks (Equation 2.5). As also shown above (Equation 2.3), natural gas or methane can be industrially used for syngas generation. The commercial conversion of syngas to methanol is carried out over metal catalysts ($Cu/Zn/Al_2O_3$ system) at 5-10 MPa and 200-300 ℃ and is also very exothermic [51].

Equation 2.5

$$CO + 2H_2 = CH_3OH$$

Equation 2.6

$$CO_2 + 3H_2 = CH_3OH + H_2O$$

Equation 2.7

$$CO_2 + H_2 \rightarrow CO + H_2O$$

Research efforts are concentrated on the catalytic hydrogenation of CO_2 to synthesize methanol (Equation 2.6). Unfortunately, this is accompanied by an undesirable side reaction, the reverse-water-gas shift reaction (RWGS) as shown in (Equation 2.7). The RWGS reaction consumes hydrogen, decreasing the yield of methanol. The large amount of water produced from both reactions inhibits the catalyst active sites. Other by-products such as alcohols and hydrocarbons are also formed. A highly effective catalyst is considered a key factor in synthesizing methanol successfully in high selectivity [52], [53].

Dimethyl carbonate (DMC)

The direct synthesis of DMC from CO is an attractive process for the use of CO_2 [54]. DMC is an environmentally friendly chemical with potential applications in the electronics and chemical industry [55]. Initially, it was produced from phosgene with methanol. However, the process had to be abandoned due to the toxicity of phosgene and other synthesis routes were developed [56].

Equation 2.8

$$CO_2 + CH_2OH \leftrightarrow DMC + H_2O$$

Furthermore, the direct synthesis from CO_2 and methanol (Equation 2.8) is considered a green chemical process [57]. De Groot et al. [58] discussed the design of a DMC production plant using methanol and CO_2 as feed materials. They proposed 3 routes:

1. Direct synthesis from methanol and CO_2.
2. Conversion of DMC with methanol from CO_2 and ammonia and forming a cyclic carbonate from CO_2.
3. Ethylene oxide which can be converted to DMC via transesterification with methanol.

Dimethyl ether (DME)

Dimethyl ether (DME) is the simplest form of an ether that is environmentally friendly, non-toxic nor carcinogenic and it is used as an alternative to Liquified petroleum gas (LPG) [59]. Methanol produced from the hydrogenation of CO_2 is dehydrated to DME in the presence of acidic catalysts like zeolite (Equation 2.9).

Equation 2.9

$$CH_3OH \leftrightarrow CH_3OCH_3 + H_2O$$

Another alternative route is by considering the reverse water-gas shift reaction (Equation 2.10) This route is considered to break the equilibrium barrier and results in a synergistic effect. In using CO_2, hydrogenation takes place using a bifunctional catalyst in a single step to methanol (Equation 2.11).

Equation 2.10

$$2CO + 4H_2 \leftrightarrow CH_3OCH_3 + H_2O$$

Equation 2.11

$$2CO_2 + 6H_2 \leftrightarrow CH_3OCH_3 + 3H_2O$$

The stability of CO_2 is high (-394.3 kJ/mol), and its conversion as a single reactant is energy intensive. One way to overcome this is by using a CO_2 as co-reactant with another reactant that has a higher Gibbs free energy like methane or hydrogen.

Carbon dioxide can be converted to methanol and water with hydrogen. This is one of the simplest and straightforward methods for methanol synthesis and DME. Other techniques for methanol synthesis from CO_2 such as electrochemical reduction, photochemical reduction, plasma (cold& thermal).

Most of the CO_2 that is targeted for utilization is from industrial processes such as the production of cement and the burning of fossil fuels. This emitted CO_2 is usually contaminated and contains other waste materials other than CO_2 and would require purification for its utilization.

The volume of CO_2 that is emitted is significantly larger compared to the amount of carbon dioxide used. Currently, only 200 Mt/yr is used from the anthropogenic CO_2 that is emitted (3200 Mt/yr) [25], and this calls for an improvement on the current technology and processes that use CO_2. An emerging application of CO_2 that is gaining the attention of researchers is its use as a sole carbon source for the synthesis of carbon nanomaterials.

2.5 Carbon nanotubes

Due to the number of studies produced in carbon nanotubes and their popularity, this section will solely focus on them and no other carbonaceous products. A CNT is a rolled-up sheet of graphene material, forming a cylindrical shape or tube with a diameter in the nanometre scale and length in microns. CNTs were 1st observed by Iijima in 1991 [61] as a by-product in the synthesis of fullerenes. However, the formation of filamentous carbon was reported in the early 1970s by Baker et al. [62], [63] and in the mid – 1970s by Oberlin et al. [64]. At the time, the techniques that could characterize the filamentous carbon were poor [65]. From that work by Iijima, it was realized that carbon with sp^2 bonding can exist in different forms shown in Figure 2.4, such as amorphous carbon, carbon nanofibers (CNTs), graphene other than graphite and diamond[66].

After their discovery, CNTs received a great deal of attention from researchers all over the world. This is seen by the vast amount of available literature and publications on this nanomaterial. CNTs possess properties that are unique and interesting such as their extraordinary electrical and thermal

conductivity [67], and high mechanical strength [68] that make them useful in different applications such as hydrogen storage[69], catalysis [70], electronics[69], [71]–[76], biological sensors [77], water purification [78] and polymer science [79] amongst others.

There are mainly two types of CNTs, single-walled CNTs (SWCNTs) and multi-walled CNTs (CNTs). The major and obvious difference between the two types is the number of walls in their structure. SWCNTs contain only a single layer of graphene whereas MWCNTs contain multiple layers of graphene, ranging from 2 – 100 layers rolled to form a tube. Other structures such as few-walled [80] and double-walled CNTs [80]–[82] have been reported.

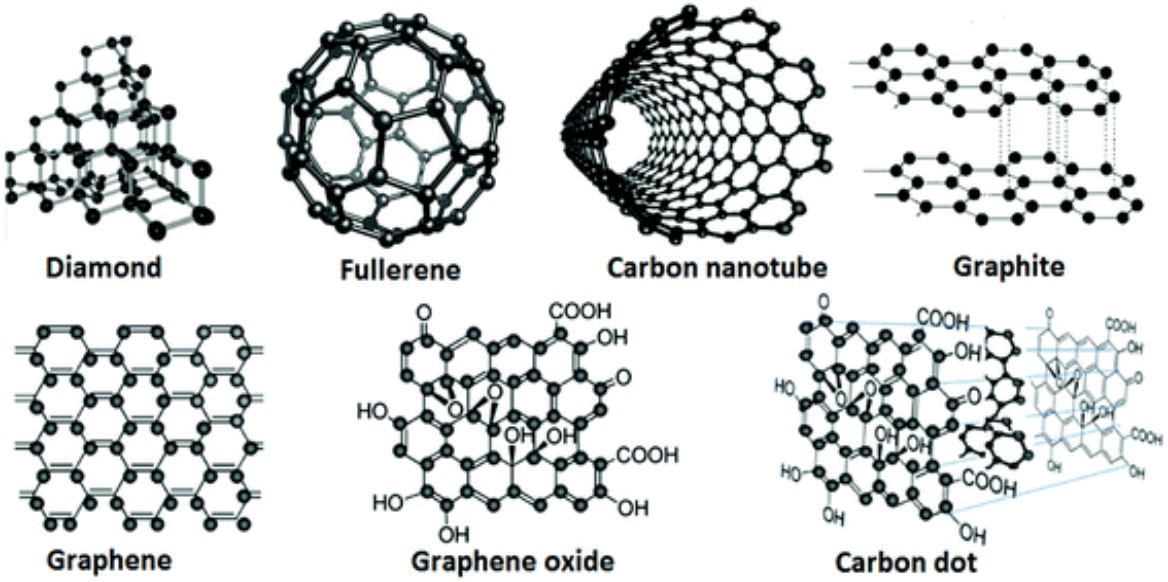


Figure 2.4: Different forms of carbon and carbon nanomaterials [225]

The graphene sheet structure can be rolled up in more than one way to yield different CNT forms Figure 2.5. This orientation in single-walled carbon nanotubes can be specified by a vector called the chiral vector C and can be defined as,

Equation 2.12

$$C = na_1 + ma_2$$

which determines how the graphene sheet is rolled up. The indices (*n, m*) are integers and define the diameter and chiral vector that give rise to different structures, a_1 and a_2 are the unit cell vectors of the two – dimensional lattice formed by sheets of graphene.

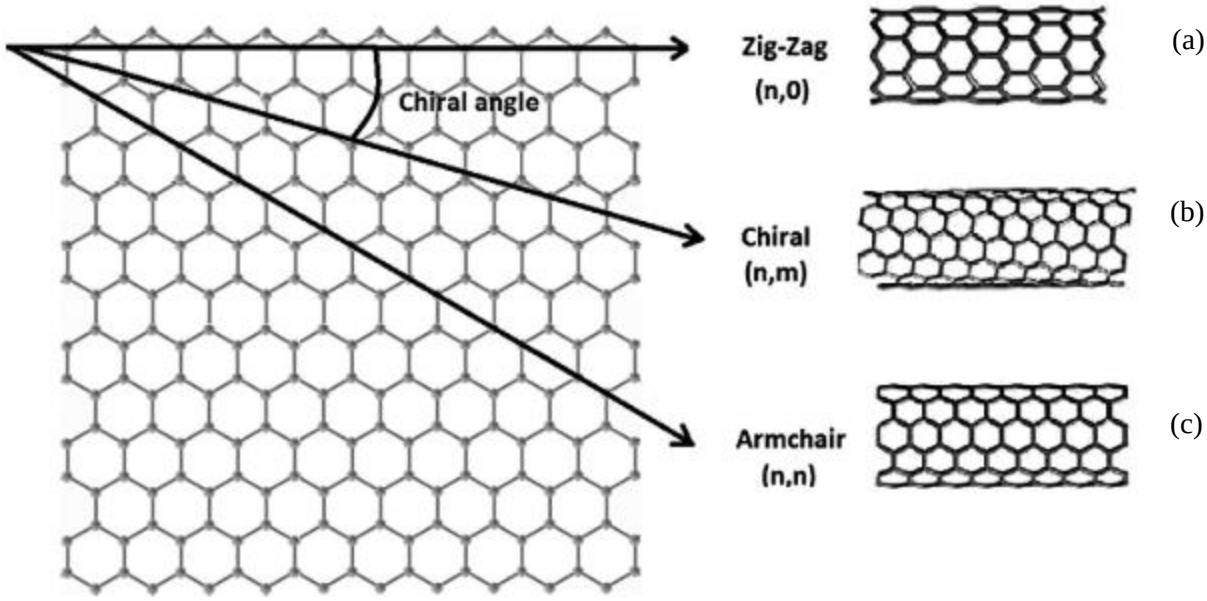


Figure 2.5: Graphene sheet rolled up in various ways to form (a) zigzag, (b) chiral and (c) armchair SWCNTs

The length of the chiral vector C is the circumference of the nanotube and given by the equation:

Equation 2.13

$$c = |C| = a\sqrt{(n^2 + nm + m^2)}$$

Where *a* is the length of the unit cell vector a_1 or a_2. Using the circumference *c*, the diameter of the carbon nanotube can be represented as:

Equation 2.14

$$D = c/\pi$$

The angle between the chiral vector and the zigzag nanotube axis is called the chiral angle θ is given by:

Equation 2.15

$\theta = tan^{-1}\left[\frac{m\sqrt{3}}{m+2n}\right]$

Thus the nanotube can be specified by its *(n,m)* indices or equivalently by θ. When $m = 0\ or\ (\theta = 30°)$ the CNT structure formed is zigzag (Figure 2.5a) while $m = n\ or\ (\theta = 0°)$ gives armchair (Figure 2.5c) and when $m \neq n$ the nanotubes are chiral (Figure 2.5b) CNTs and θ takes a value between *0°* and *30°*. The difference in these structures is noticeable by the open ends. The values of (*n, m*) affect the electronic, mechanical, and optical properties of CNTs [83]. This classification is mostly used to describe single-walled carbon nanotubes (SWCNTs). Multi-walled carbon nanotubes (MWCNTs) can be formed like a scroll, whereby the graphene sheet wraps around itself manifold times or the coaxial cylindrically curved graphene sheets when the carbon nanotube contains another one inside it [84]. Eatemadi et al [83] also described the Russian Doll and Parchment model for MWCNTs.

2.5.1 Synthesis Methods of CNMs (CNTs)

Several techniques have been used in the synthesis of CNTs since their discovery. The most common of these techniques are laser ablation, arc discharge, and chemical vapour deposition (CVD). Each of these techniques has advantages and disadvantages and they have been modified with different recipes to overcoming some of the challenges. This is also done to get CNTs with a specific type of morphology, the number of walls, better quality, and yield for the intended use. The CVD, however, has been the most favoured method among researchers worldwide.

Arc Discharge

The arc discharge method is one of the most common and oldest techniques used to produce carbon nanotubes. It was through this method that Iijima [61] first synthesized CNTs. For CNT synthesis, two graphite electrodes, the anode (positive) and a cathode (negative) are used to produce an arc by digital current (DC). The electrodes are placed ~1 mm apart in an inert gas-filled environment such as helium (He), argon (Ar), or nitrogen (N_2) at pressures of 50-500 torr. The diameter of the cathode is 8-12 mm and the is anode 6-8 mm. The inert gas serves to increase the speed of carbon deposition. A direct current of 50-120 A and a current density of ~150 A/cm^2 are driven by a voltage of ~30 v to generate high-temperature (>4000 ℃) plasma between the two graphite electrodes. The high-temperature plasma region then causes sublimation of carbon on the anode (positive) electrode which in turn deposits on the cathode (negative) electrode resulting in the

formation of CNTs and other carbonaceous material. As the anode is consumed, it is brought closer to the cathode to maintain the stability of the discharge. The reaction time for nanotubes is mostly in shorter periods of 2-20 minutes [84]. Normally, the purity and quality of the CNTs are dependent on the reaction conditions such as flow rate, gas pressure, and metal concentration. The crystallinity of the CNTs produced by this method is very high. However, the number of impurities is also significantly higher compared with the other methods and the yields are relatively low. The quality of CNTs depends on the current, the lower the current the better the quality of the CNTs [84]. CNTs can be produced with or without a catalyst in the arc discharge technique [85]. When a catalyst is used, SWCNTs are usually formed. A schematic representation of the arc discharge method is shown in Figure 2.6.

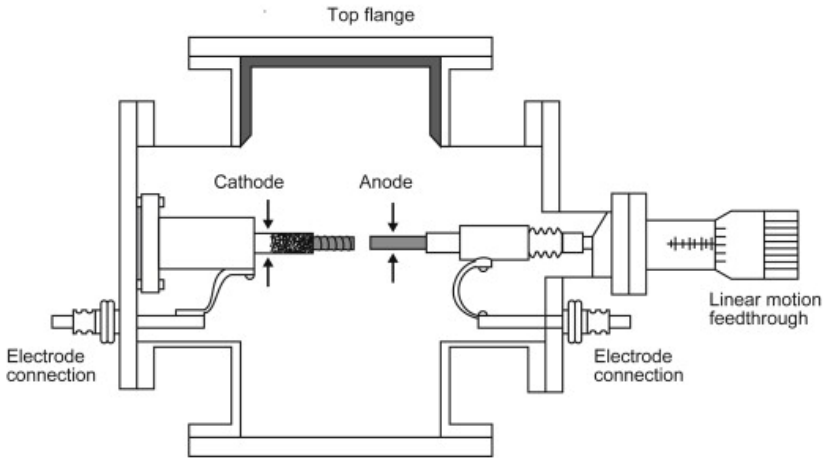


Figure 2.6: A schematic representation of the arc discharge method [84]

The laser ablation method is much like the arc discharge except that a laser beam is used instead of an arc discharge to vaporize the carbon target and deposit it onto the substrate. It is depicted in Figure 2.7. The synthesis of CNTs by this method was developed by Smalley's research group at Rice University [87]. A laser beam source (YAG or CO_2) is used to create a high temperature (>3000 °C) on a carbon target such as graphite under an inert atmosphere of helium (He) or argon (Ar) kept at a constant pressure of 500 torr. As the laser beam vaporizes the carbon target,

condensation rapidly occurs resulting in the formation of CNTs and other carbonaceous by-products.

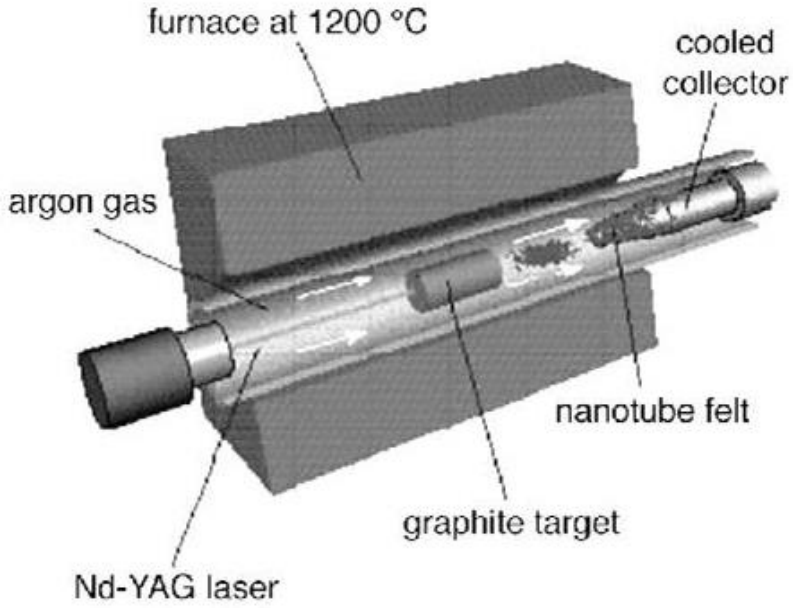


Figure 2.7: A typical laser ablation instrument for CNT synthesis [87]

Doping the carbon target with transition metal catalysts (Fe, Co, and Ni) results in the formation of SWCNTs and due to this, laser ablation has been exclusively used to produce SWCNTs. The purity of the nanotubes formed by this process is very high compared (up to about 90% pure) to the arc discharge and possesses better graphitization [85]. Good quality nanotubes are obtained at 1200 ℃, lower temperatures result in the formation of defects in the structure.

Chemical Vapour Deposition

The chemical vapour deposition technique can be defined as the deposition of a solid that takes place in a vacuum chamber from a chemical reaction in the vapour phase. This technique is simple and economical for the synthesis of carbon nanotubes/fibres. The carbon nanotubes produced by the CVD are purer and it shows great potential for mass production of CNTs compared with the laser vaporisation and arc discharge techniques. It offers more control of the synthesis parameters to allow for the selective production of CNTs with predefined properties. Thus, the CVD technique has become the standard method for CNT synthesis.

To synthesize carbon nanotubes using the CVD method, heat, catalyst, and carbon source/precursor compounds are required for a process that takes place in a tubular furnace [88]. This reactor contains a furnace, a temperature controller to set the temperature, a quartz tube that contains a ceramic boat or crucible to carry the catalyst, an inlet, and a gas outlet. During CNT growth, gas-phase carbon-rich molecules are pyrolyzed in the presence of supported transition metal catalysts at high temperatures (500-1100 ℃). CNTs are subsequently deposited in the form of precipitated solid carbon.

The carbon-containing molecules can be in any form (gas, solid, liquid) but most of the carbon sources used are in the gas phase. With proper conditions, CNTs can be synthesized from a large variety of carbon-containing molecules. This was demonstrated by Vishwanathan et al. in a review paper where several carbon-containing molecules from natural sources were discussed [89]. In another review, Kumar et al. [90] outlined several natural and waste hydrocarbon precursors such as vegetation waste and palm oil for CNT synthesis among others. The most common precursor compounds used are acetylene [91], [92], methane [93], [94], ethylene [95], [96], benzene [97], ethanol [98], [99] and carbon monoxide (CO) [100], [101] to name a few. Hydrocarbons are the most preferred carbon sources due to their low thermodynamic stability. The decomposition of acetylene, ethylene, and benzene is allowed at all temperatures and occurs readily. An exception is methane, which is the most stable hydrocarbon. This information can be extracted from the change in Gibbs free energy of formation ($\Delta_f G$) [102], [103]. The carbon sources also affect the morphology formation of CNTs. Linear hydrocarbons such as acetylene, ethylene, and methane thermally decompose into atomic carbon or linear dimers/trimers of carbon (C_2, C_3), and usually form straight hollow CNTs. Whereas cyclic hydrocarbons such as benzene, xylene, cyclohexane, and fullerenes produce curved CNTs having bridged structures inside the tube walls[104], [105]. This shows that the precursor compounds play a critical role in the CNT synthesis. Proper selection of the carbon precursor can lead to a longer catalyst lifetime, increase the CNT growth rate, quality, and yield. Generally, low-temperature CVD (500-900 ℃) yields MWCNTs, while high-temperature CVD (900-1200 ℃) forms SWCNTs. The SWCNTs have higher energy of formation owing to their small diameters, high curvature bears, and high strain. This could explain why from most hydrocarbons, it is easier to produce MWCNTs than SWCNTs which grow from a selected few carbon sources like methane and CO. They are stable at temperatures between 600-900 ℃ [107]. The carbon precursors that are commonly used for MWCNTs (acetylene, benzene etc.) are

unstable at high temperatures and result in the formation other carbonaceous by products such as amorphous carbon[106], [108].

Under the CVD method, many other methods have been developed. These include fluidized-bed CVD (FBCVD), floating catalyst (FC-CVD) CVD, plasma-enhance CVD (PECVD), microwave-assisted CVD (MWCVD) to name a few [109].

2.5.2 Growth of CNMs from carbon dioxide

The growth of CNMs from CO_2 is reviewed based on several synthesis techniques. These include the chemical reaction of CO_2 with alkali metals as catalysts, the CVD, and electrolysis. The reaction conditions and yields are summarized in (Table 2.1) for the chemical reactions and the CVD method.

Table 2.1: Summary of synthesis parameters and results of CNMs structures obtained by chemical reaction

References	Reductant	Temperature (℃)	Pressure (atm)	Morphology	Yield
Motiei [110]	Mg	1000	9869.23 (10kbar)		10%
Lou [114]	Li	720		Double Helical CNTs	70%
	Li	600			<70%
	Na	720		bamboo CNTs	-
	Na	600		bamboo CNTs	
Zhang [116]		600-1000		Mesoporous graphene, CNTs, hollow carbon boxes	0.3-1g
Lou [117]	$NaBH_4$	700	1000	Y-junction CNTs, CNTs, graphite amorphous carbon	4.20%

By Chemical Reaction

The CNT synthesis from CO_2 was first reported by Motiei et al. [110]. They produced carbon and MgO by reacting supercritical carbon dioxide with Mg at 1000 ℃ and 10 kbar for 3 hours in an autoclave. The total yield of the carbonaceous products relative to the CO_2 starting material was 15.5%. Only 10% of this material was CNTs (Figure 2.8a) and 1-2% were fullerenes from High Resolution (HR)TEM observations. Raman spectrum of the CNTs showed a good crystallinity since the intensity of the D band which is associated with the presence of defects was very low [111]–[113].

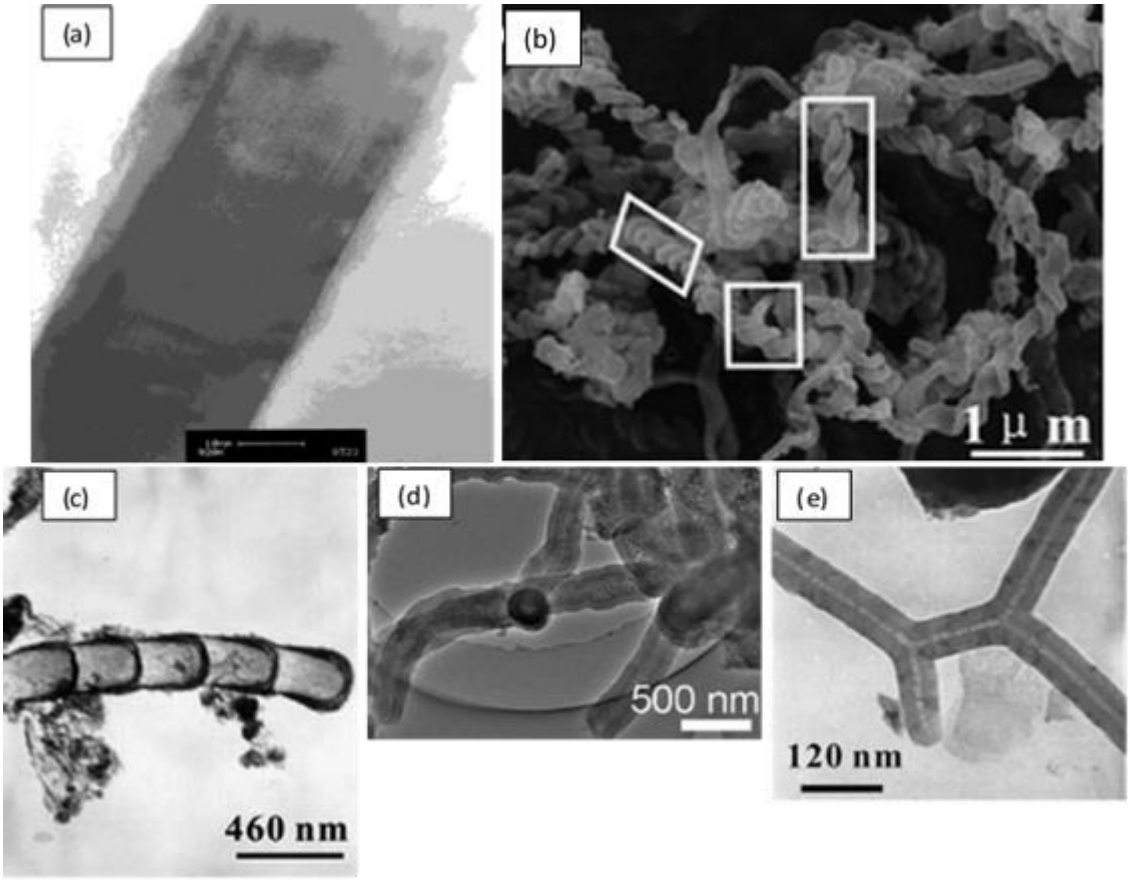


Figure 2.8 : Electron Microscopy CNTs images by (a) Motiei using Mg metal, (b) Lou using Li and (c) Na, (d) Zhang using Mg metal and (e) by Lou using NaBH4 [110], [114], [116], [117]

Lou [114] formed CNTs by following the same procedure as Motiei. However, lithium (Li) and sodium (Na) were used as catalysts instead of Mg and the reaction time was also increased to 10h. The temperature was decreased to between 600-750 ℃ with an autogenic pressure. Under these reaction conditions, CNTs with different morphologies were formed (Figure 2.8b, c). CNTs containing 70% double-helical nanostructures (Figure 2.8b) were synthesized at 720℃ using (Li) as a reductant. When the temperature was decreased to 600 ℃ and the mass of CO_2 increased, they observed a decline in the yield of CNTs. This can be attributed to the retardation of the growth rate of the nanotubes due to the decreased temperature [115]. The yield (70%) and purity of CNTs synthesized under these conditions are still higher than what Motiei et al. (15.5 %) obtained. When sodium was used as a reductant under the same reaction conditions, only bamboo-shaped CNTs

(Figure 2.8c) were formed. EDS analysis showed carbon as being the only product and the yield of the CNTs formed was not reported in this instance. The electron diffraction pattern of the CNTs corresponded with the one of graphite. The work conducted by these two authors demonstrates the importance of choosing a suitable reductant since different morphologies were obtained under different reductants.

Zhang et al. [116] manipulated the temperature to obtain carbon nanomaterials of different morphologies using the same reductant (Mg) as Motiei. The CNMs were synthesized at temperatures ranging from 600-1000 ℃. The carbon nanotubes observed were grown at 800 ℃ with a yield of 0.8 g from 10 g of Mg (Figure 2.8d), and contained significant amounts of amorphous carbon, while mesoporous graphene (MPG) and hollow carbon boxes (HCB) were synthesized at 600 and 1000 ℃, respectively. Raman and XRD spectra showed a shift to lower wavenumbers which is associated with an increase in the amount of graphitized carbon.

Lou et al. [117] used sodium borohydride ($NaBH_4$) as a reductant in the synthesis of Y-junction CNTs at 700 ℃ and 1000 atm for 8 hrs (Figure 2.8 e). The presence of the Y-junction CNTs were confirmed by TEM images and comprised of only 10% of the carbon product. The XRD patterns contained a sharp peak at $2\theta = 26°$ indicating few defects in the structure of the Y-junction CNTs. The Raman spectrum contained a very strong D-band (1349 cm^{-1}) peak which indicates a significant amount of defected, poorly graphitized, amorphous carbon[118], [119]. Lou et al. attribute this to the special nanostructure of the Y – junction CNTs with the bamboo-shaped structure. A High Resolution (HR) TEM showed nearly parallel lines and were said to be graphite atomic phases with a distance of 0.34 nm. The Raman spectrum contained a very strong D band (1349 cm^{-1}) peak which indicates a significant amount of defected carbon [118], [119]. Lou et al. attribute this to the special nanostructure of the Y-junction CNTs with the bamboo-shaped morphology. The growth mechanism of the Y-junction CNTs was investigated by varying parameters in a series of experiments. They found that temperature and the type of reductant played a crucial role which agrees with Lou et al. as mentioned above. At a temperature below 700 ℃, no Y-junction CNT structures were formed, and the result was the same when other alkali metals were used as reductants. This further emphasizes the importance of temperature and the choice of reductant in a supercritical CO_2 system.

In the above reactions, an autoclave was used to synthesize the carbon nanostructures with varying morphologies. Extremely high pressures and enclosed containers that can withstand the pressures are required to ensure a supercritical state when using this technique. From the above, it is observed that significant amounts of impurities such as amorphous carbon are produced by this technique. At lower temperatures only amorphous carbon forms and therefore, high synthesis temperatures are required. Furthermore, different allotropes of carbon are produced in the same synthesis reaction. Some of the shortcomings/weaknesses/disadvantages of this method can be overcome by the chemical vapour deposition technique.

Chemical Vapour Deposition (CVD) method

The CVD method has been the most extensively used method for the growth of nanotubes and nanofibers. Unlike the autoclave method, CNTs can be produced at lower pressures without the need for special equipment using the same carbon source in a gas phase. Although high flow rates favour CNTs growth, structures with good crystallinity, purity, and yield are obtained. Xu and Huang [120] used CO_2 as a carbon source to synthesize CNTs using the CVD technique over a Fe/CaO supported catalyst in a molar ratio of 1:10 (Figure 2.9a). While whereas Allaedini et al. [121] used Ni/MgO as a catalyst and $scCO_2$ as a precursor. The CO_2 flowed at 750 sccm and H_2 was equal to 1500 sccm for the former author, while the latter author used CO_2 at 900 sccm and H_2 at 1500 sccm as shown summarized in Table 2.2. The yield was determined using different methods, thus comparing them would be inaccurate. Allaedini et al. used the percentage of carbon present in the sample from EDS analysis whereas Xu and Huang obtained the yield using the initial weight of the catalyst. The yield obtained by Xu and Huang was more than 50 % at a temperature of 790 ℃ and above 810 ℃ CNTs could not be grown. The synthesized CNTs also showed good crystallinity from Raman spectroscopy. However, Allaedini et al. used a much higher temperature of 1100 ℃ and obtained 27.38 % MWCNTs (Figure 2.9b). At this temperature CO_2 was in its supercritical state. The Raman spectrum showed the same crystallinity as Xu and Huang. The CNT from both studies also had contrasting morphologies and diameters. Xu and Huang further stipulate that CNTs prepared by CO_2 show much higher purity than hydrocarbons. The importance of temperature was demonstrated in Xu and Huang, since an increase in temperature from 790 to 810 ℃ the CNTs morphology changed from straight and crooked to branching. The effect of catalyst

support was also investigated, and it was found that only CaO support could produce CNTs. This could explain why Allaedini obtained a lower yield since they used MgO as support.

Table 2.2: Synthesis conditions of CNTs from CO_2 using the CVD and the optimized parameters

References	Catalyst	Temperature (°C)	Flow rate (sccm)		Pressure (atm)	Carbon source concentration	Time (minutes)	Yield
			Carbon source	Carrier gas				
Xu and Huang [120]	Fe/CaO (1:10)	790-810	CO_2 (750)	H_2 (1500)			45	50%
Allaedini (2015)[121]	Ni/MgO	1100	CO_2 (900)	H_2 (1500)	9869.23 (10kbar)		60	27.38%
Simate et al. [122]	Fe/CaO (10g)	800	CO_2 (400)	H_2		5000 ppm	45	
Li, Wen& Ren[123]	Fe/SiO_2 (100mg)	750	C_2H_2 (20)	NH_3 (80)	0.79 (600torr)		120	600%
Allaedini (2016) [125]	Ge/MgO	1100	CO_2 (963.3)	Ar (900)			60	39.05%
Lee [126]	CoO-MoO/Al_2O_3	762	CH_4	N_2			276	350%
See [127]	Fe/Al_2O_3 (120g)	850& 650	C_2H_4 (98.34& 73.75)	H_2 & N_2		10% and 25%	40	

Both researchers discussed the mechanism and revealed the crucial role played by hydrogen in providing additional carbon atoms for CNTs synthesis. The high flow rates observed in these two studies would defeat the purpose or reducing the production costs of CNTs. Furthermore, the very few to no synthesis parameters were varied to investigate their influence on the properties and structure of CNTs and optimize their production. However, Simate et al. [122] examined the influence of some of the parameters influence the production of CNTs.

Simate et al. [122] utilized a swirled floating catalyst CVD (SFC-CVD) reactor to investigate the effect of temperature, CO_2 flow rate, and concentration of CO_2 on the production rate of CNTs.

The CNTs were grown at temperatures of 750 – 840 ℃ and CO_2 flow rates of 50-400 sccm using Fe/CaO as a catalyst (Figure 2.9c). They found that increasing the reaction temperature to 800℃ increases the rate of production and thereafter it decreases. The decreased production rate at high temperatures was attributed to CO_2 decomposition, Boudouard reaction requirements and kinetics of carbon diffusion. The same trend applies for the concentration and flow rate of CO_2 i.e., the production rate increases as they increase up to a certain level (5000 ppm and 400 sccm). The high carbon concentration led to the rate of formation of adsorbed surface carbon to increase, exceeding the carbon diffusion rate. They also developed a kinetic model equation for the growth of CNTs from CO_2. The Raman spectrum showed that the as-synthesized CNTs have remarkable crystallinity as the temperature increases from 750 – 840 ℃. The purity of the CNTs in this study is higher than Xu and Huang. Li, Wen and Ren [123] also found that at high pressure the concentration of carbon atoms is high, the rate at which the carbon atoms dissolve increases. However, the graphitization was found to be poor at high pressures than at low pressures. Garg et al. [124] found that the CNTs growth rate deteriorated and diameter increased when the methane flow rate was decreased.

Synthesis conditions of CNTs are one of the primary determiners of the yield and quality of CNTs as has been already established. Optimization of these parameters is highly beneficial for finding the optimum conditions that will produce CNTs of the desired quality, yield, and purity at a commercial scale. There are several ways to find the optimum conditions for CNTs growth. Softwares such as Design Expert or Minitab can be used, or it can be conducted manually by varying the synthesis parameters. However, we will only consider studies that employed optimization software. The software has several approaches which include the one factor at a time method, statistical design of experiments (DoE), etc. The DoE can investigate the effect of input factors on the response or desired output [128]. It includes response surface methodology (RSM), completely randomized design (CRD), two-level factorial design (FD) [126], [127], [129], [130].

Allaedini et al. [125] made use of central composite design (CCD), a method of RSM to optimize the synthesis of CNTs from CO_2 and get the best response. The effect of CO_2 flow rate, catalyst

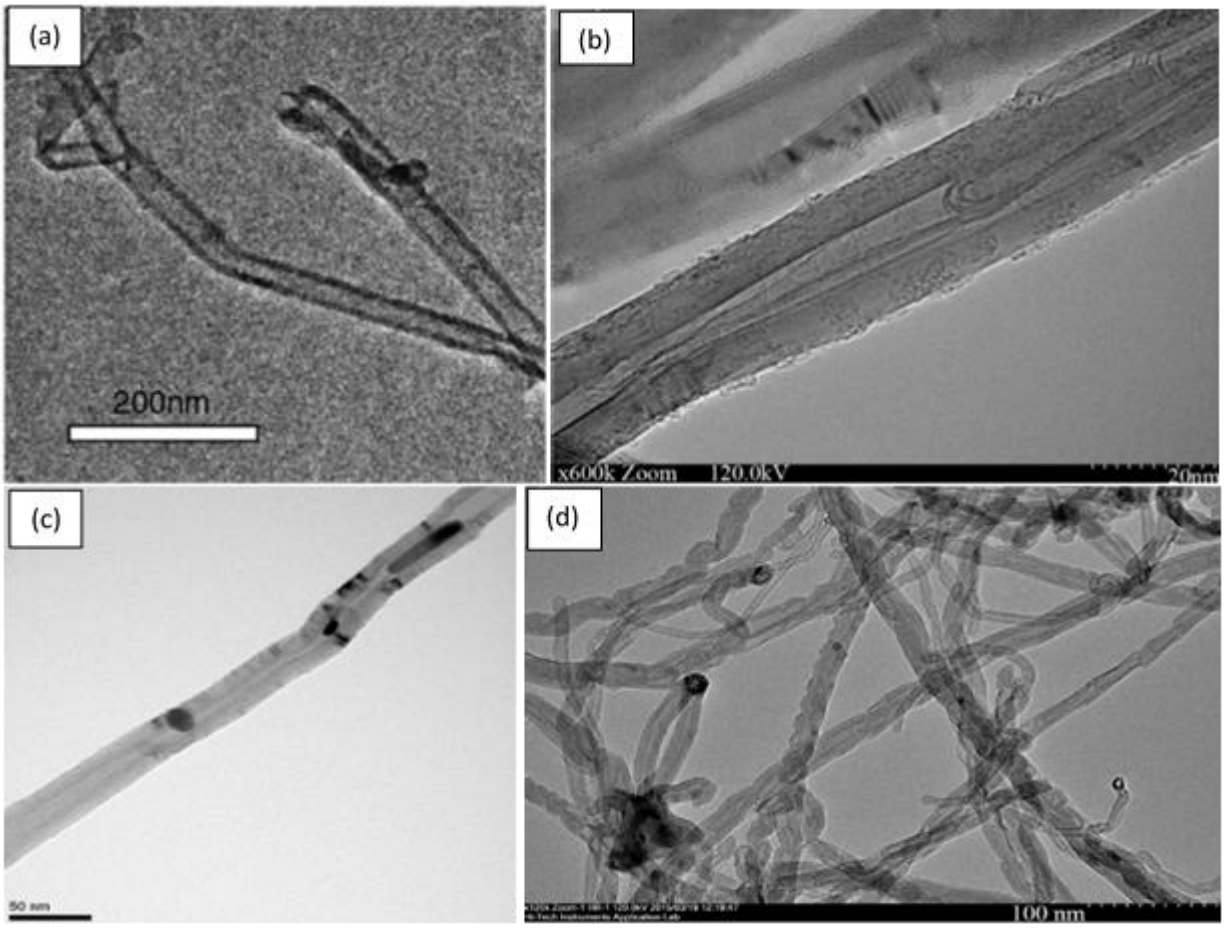


Figure 2.9: TEM micrographs of CNTs obtained from different studies of CO_2 as a precursor (a) Straight CNTs, (b) purified CNTs, (c) CNTs structures synthesized at optimum temperatures of 800℃ and (d) 1100℃ [120], [121], [122], [125]

loading, and temperature on the yield and morphology of CNTs were the responses selected. Ge/MgO was used as a catalyst via the CVD technique at CO_2 flow rates, catalyst loading, and temperature ranging from 600-900 cm^3/min, 8-10 g, and 700-1100 ℃, respectively. From the 20 experiments they conducted, they found temperature to be the most significant factor. The highest yield of CNTs (54.58 g) occurred at a temperature of 1226 ℃, catalyst loading of 10.6 g, and CO_2 flow rate of 963 cm^3/min). At lower temperatures (700& 900 ℃), only blocked-shaped and cubic-shaped carbon were obtained (the boxed shape carbon nanomaterial was also obtained by Zhang as mentioned above). EDS and TGA results showed an increase in the amount of carbon deposited as temperature increased. Carbon nanotubes were only observed at a temperature of 1100 ℃ (Figure 2.9d). Both the Raman spectrum and XRD patterns showed that as the temperature increased, the crystallinity of the CNTs improved. This is currently the only study that optimized CNMs production from CO_2, much more work still needs to be done that will investigate other parameters such as carrier gas flow rate (H_2), synthesis time, catalyst and support ratios and other

transition metals catalysts. Some of these parameters were investigated by other authors using different carbon sources.

Methane is a stable hydrocarbon and decomposes at higher temperatures, Lee et al. [126] used it as a carbon source on an alumina-based catalyst to grow CNTs. Six variables (the amount of catalyst, temperature, time, metal loading, methane, the flow rate of methane, and carrier gas nitrogen), were screened using a fractional factorial series to find the three most influential parameters on the yield and crystallinity (I_D/I_G ratio) of CNTs. These parameters were optimized in RSM and the optimum synthesis conditions were found at a temperature of 762 ℃, time of 2.3 hrs, metal loading of 27 %, and I_D/I_G ratio of 0.595.

See et al. [127] conducted a parametric study to investigate the effects of temperature, feedstock concentration, fluidization ratio, deposition time, and their interactions using a statistical design methodology on CNTs yield and quality. MWCNTs were synthesized from ethylene and Fe-alumina supported catalyst in a fluidized bed reactor. They found that for 10 % ethylene concentration, the optimum yield was obtained at 6 SLPM (Standard Liter Per Minute) and 850 ℃. While at 25 % ethylene, it was obtained at 3 and 4.5 SLPM, 650 ℃. The temperature was found to be more influential on the CNTs production than the flow rate. The yield increased directly with an increase in temperature at flow rates above 3 SLPM. High temperatures and shorter reaction times were required to produce high-quality CNTs. Higher fluidization ratios led to poor conversion rates.

Several research groups have demonstrated that oxygen-containing compounds or oxidants such as water (H_2O), CO_2, and alcohols greatly improve the yield and quality of CNTs. Hata et al. [131] promoted the growth of SWCNTs by the addition of a small and controlled amount of water to ethylene. They produced SWCNTs with high purity and yield. H_2O was said to act as a weak oxidizer that removes amorphous carbon without damaging the CNTs. It does this by promoting and preserving catalytic activity. The effect of CO_2 as a promoter or co-feed has also been investigated.

Magrez et al. [132] reported a mixed equimolar ratio reaction between C_2H_2 and CO_2 to enhance the yield of CNTs. The MWCNTs were produced from $Fe_2Co/CaCO_3$ in 30 minutes at temperatures of 680 ℃. They stipulate that the lifetime of the catalyst is extended as well as the

initial growth rate, this, in turn, increases the yield of the CNTs. They assumed that CO_2 is acting as an etching agent that prevents catalyst poisoning and it also limits acetylene polymerization. Huang et al. [81] used CO_2 to promote the growth of vertically aligned CNT forests on a silicon wafer catalyst. Ethylene (C_2H_4, 100 sccm) was a carbon source with argon (250 sccm) and hydrogen (200 sccm) as carrier gases at a temperature of 750 ℃ and a duration of 60 minutes. It was found that without the addition of CO_2, significant amounts of amorphous carbon were formed. When CO_2 was added, amorphous carbon was present in small quantities. As the concentration of CO_2 was increased from 0 mol% to 36.8 mol%, the intensity ratio (I_G/I_D) of the CNTs also increased indicating good quality. The same trend was observed for the mass when CO_2 concentration was increased. Varying the concentration also changed the morphology of the carbon products from convex-shaped to radial block-shaped at low concentrations and then to bowl-shaped at high concentrations. Without CO_2, nearly 50 % of DWCNTs were formed and SWCNTs were below 20 %. With CO_2, the amounts of SWCNTs increased with an increase in CO_2 concentration.

Wen et al. [133] observed the same results as the above research groups in terms of the effect of CO_2 on the yield and quality of CNTs. The conversion of methane and carbon dioxide to SWCNTs took place at 900 ℃ on a Fe/Mo/MgO supported catalyst for 15 min. The SWCNTs obtained with CO_2 showed much high purity and crystallinity than methane alone. The effect was the same with the yield, an increase from 17.5 % to 28.7 % was observed from TGA when CO_2 was added. CO_2 was also found to be a better catalyst regenerating agent than CO_2 since it yielded higher carbonaceous material.

By electrolysis

Electrolysis is used to drive an oxidation-reduction reaction in a direction it does not spontaneously occur. The reaction is driven by an electric current and can be used by electrolysis to split a compound into its elemental components. Therefore, CO_2 can be directly split into carbon and O_2 by this method.

Jiawen et al. did extensive work on the transformation of carbon dioxide to carbon nanotubes by molten carbonate electrolysis [134]–[138]. They split CO_2 into solid carbon (CNTs) and oxygen, they call this C2CNT methodology. In their work [134] they demonstrated the splitting of CO_2 into

a new type of carbon nanotube, a CNT – wool. The carbon nanotube wools were grown in 50 g lithium carbonate (Li_2CO_3) at 770 °C, using a variety of cathodes. The Monel and copper cathodes produced high yields and good quality CNTs with different morphologies. In another study [137] that was conducted by the same research group, they combined various molten electrolytes to form pure CNTs or CNFs in high yields. The CNTs or CNFs were grown on a steel cathode at a current ranging from 0.8 – 1.00 A and a temperature of 770 ℃ for 1 hr. Boron–doped CNTs at high yields (>90 %) were formed by mixing Lithium metaborate ($LiBO_2$) and $LiCO_3$ electrolytes. They found that at higher levels of $LiBO_2$ doping (>10 wt%), the amount of amorphous material in the CNT product increased. With less than 10 % by mass $LiBO_2$ and 50g Li_2CO3, good quality CNTs were obtained and ~10 % of amorphous carbon was present. The Raman spectroscopy patterns of the CNTs indicated that the number of defects increased with the level of doping.

Douglas et al. [139] used atomic layer deposition, electrode composition, and current density to direct the formation of iron-based catalysts and grow CNTs. They used 40 g Lithium carbonate electrolyte at a temperature of 750 ℃ and a constant current for 1 hour. To access the effect of electrodes on the synthesis of CNTs, 3 different anodes and cathodes were investigated. In the case of the 3 different cathodes investigated, the anode was deactivated to allow the growth of CNTs to be controlled by the composition of the cathode. These electrodes were subjected to low (25 mA/cm^2) and high (100 mA/cm^2) current densities. For the galvanized steel cathode, only 30 % of CNTs were grown at low current densities, however, when the current density was high a 99 % yield was obtained. The increase in yield was attributed to the faster carbon deposition kinetics and greater Fe migration through the ZnO coating, driven by the increased electric field to the electrode surface. In the case of stainless steel, no CNTs were observed at all current densities. The 3rd cathode, 1010 steel did not produce any CNTs or amorphous carbon at low current densities, whereas at high current densities a yield of 90 % was obtained. TEM images showed highly crystalline graphitic walls which are consistent with Raman spectroscopy patterns. For the anodes, untreated Ni wire, thermally oxidized Ni wire and Ni wire coated with ~50nm of alumina. In the case of untreated Ni wire, CNFs were formed with minor CNTs containing large diameters. The thermally oxidized Ni wire formed hollow-centre CNTs with large diameters and lastly, the coated Ni wire produced straight CNTs with dense diameters.

2.5.3 Growth Mechanism

The growth mechanism of CNTs is somewhat unclear despite all the efforts made to define it both experimentally and theoretically. The mechanisms that have been proposed are often contradicting. However, the two most widely accepted mechanisms are the Vapour-Liquid-Solid (VLS) and Vapour-Solid-Solid (VSS) mechanism originally suggested by Wagner and Ellis for silicon whiskers growth [140]. There are three steps in the VLS mechanism. First, the carbon-containing gas adsorbs and dissociates on the surface catalyst nanoparticles to form elementary carbon atoms. Secondly, the carbon atoms dissolve in the bulk of the nanoparticle to form a metastable liquid carbide and diffuse within the particle. Then, carbon solid precipitates at the rear end of the particle to form CNTs. In the VSS mechanism, which is derived from the VLS mechanism, the carbon-containing gas dissociates into carbon atoms and then diffuses on the catalyst nanoparticle.

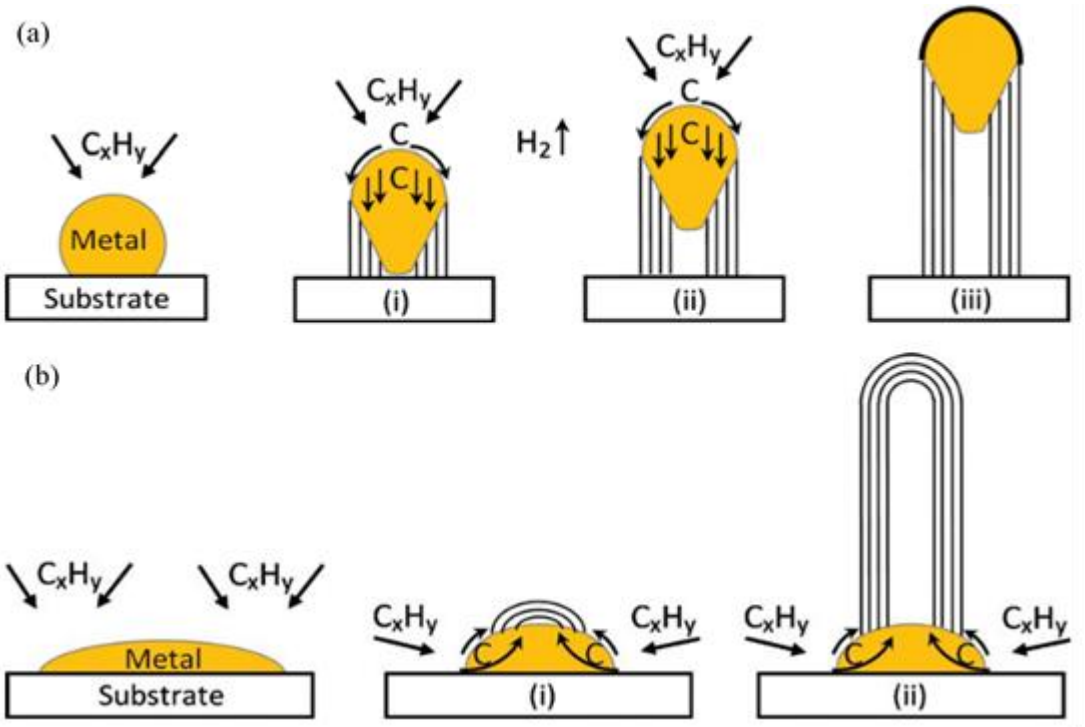


Figure 2.10: CNTs broadly accepted growth mechanism: (a) tip growth and (b) base/root growth mechanism [108]

They precipitate in the form of CNTs. Furthermore, the growth of CNTs on substrates has been divided into two growth models: the root/base and tip growth models (Figure 2.10). In the tip growth model, the catalyst is lifted off from the surface of the catalyst due to weak catalyst-substrate interactions (Figure 2.10a). On the contrary, in the root/base growth model, the catalyst

and substrate remain in contact while the CNT grows due to a strong catalyst substrate (Figure 2.10).

2.5.4 Carbon nanomaterials Synthesis parameters

Carbon nanotubes can be grown under various synthesis conditions and are affected by a significant number of parameters. The synthesis parameters influence their yield, crystallinity, purity, morphology, and structure. Under the correct conditions, CNTs of superior quality can be grown using the CVD technique. The parameters and conditions under which CNTs can be grown have been widely investigated. These include catalyst, substrate, pressure, temperature, carbon precursor and carrier gas flow rates, catalyst preparation method, type of carbon precursor, and catalyst loading. In this subsection, only three of the mentioned parameters will be investigated and they are temperature, flow rate, and mass of catalyst.

Temperature

The reaction temperature is one of the most important and leading parameters that significantly affect carbon nanotube production and its properties. As such, it remains the most investigated parameter in CNT synthesis, and it is also considered an important economic factor. The temperature range for CNTs production varies over a large range and different types of CNTs are observed. A usual trend is that lower temperatures (500-600 ℃) forms CNTs in lower quantities and higher temperatures (700-800 ℃) results in higher yields. Much higher temperatures (>900 ℃) decrease the yield of CNTs with an increase in amorphous carbon. Yang et al. [115] synthesized CNTs on stainless steel microfibrous composites at temperatures from 600-700 ℃. They observed an increase in the length and density of CNTs when the temperature was increased due to an increase in the growth rate of the CNTs. They stipulate that as the reaction continues, the growth rate slowly decreases and terminates abruptly due to the support of morphological evolution. They stipulate those higher temperatures can slow down the process and increase the growth time forming CNTs with higher density and length. Santangelo et al. [141] calibrated reaction parameters to improve thermal stability and crystalline quality of CNTs. They found that the best crystalline quality and highest oxidative resistance were obtained at 700 ℃. A yield of more than 14 g with 94 % purity CNTs per gram of catalyst was obtained while at 600 ℃ a drastic decrease in yield was seen. Maruyama et al. [98] demonstrated the synthesis of high purity

SWCNTs at lower temperatures (700-800 ℃) which generally form at high temperatures (>1200 ℃) by using alcohol as a carbon source.

Flow rate

Carrier gases such as nitrogen (N_2), argon (Ar), Helium (He), and hydrogen (H_2) are used in the CVD synthesis of CNTs to create an inert atmospheric and prevent the CNTs from being oxidized. They also serve to reduce the catalyst to nanoparticles. The flow rate is one of the parameters to be considered and affects the properties and production of CNTs. Khorrami and Lofti [142] investigated the effect of H_2 and N_2 mixture gas flow rates on CNTs growth rate using a copper (Cu) catalyst. CNTs of different morphologies and structures were observed at different flow rates. At 100 and 150 standard cubic centimetres per minute (sccm) large amounts of CNTs were seen while at 200 sccm nearly no CNTs were present. With yield, the formation of CNTs was decreasing with increasing the carrier gas flow rates. At the lower flow rates, the CNTs had a good crystallinity. Tripathi et al. [143] optimized the flow rate and flow duration of the carbon precursor acetylene, to synthesize CNTs. The flow rate was varied from 10-50 sccm. Their results showed that yield, diameter, and length of CNTs increase with the flow rate of acetylene up to 20 sccm. Thereafter, the yield and length started decreasing but incremental increases in diameter occurred.

Catalyst

Catalysts are necessary and play a central role in the formation of carbon nanotubes using the CVD technique. The catalyst properties can influence the yield, quality, morphology, and size of the CNT to be formed. Their function is to decompose the carbon-containing gas at temperatures lower than their spontaneous decomposition temperature and allow the diffusion of carbon intermediates and their chemical interaction. They act as nucleation sites for CNTs growth, Shah and Tali even refer to the catalyst nanoparticle as the father of the resulting carbon nanotube [106]. A great deal of attention has been paid to the catalyst in nanotube formation. The most used catalyst are transition metals (Fe, Ni, and Co) for CNT growth by CVD. Besides Fe, Ni, and Co, late [144], [145] and early transition metals [107], [146], [147], and lanthanides [148] have also been reported to be active for CNT growth.

Several factors affecting the growth of carbon nanotubes growth and their properties can be attributed to the catalyst properties. Several researchers stipulated that the catalyst size determines

the tube diameter of the resulting nanotube. Cheung et al. [149] proved this connection by using iron (Fe) nanoparticles with diameters of 3, 9, 13 nm to grow carbon nanotubes of average diameters of 3, 7, and 12 nm, respectively. It has also been stipulated that catalyst nanoparticles with smaller diameters generally result in SWCNTs and larger diameter catalysts grow MWCNTs[150], [151]. Liao et al. [152] investigated the effect of Co-Mo catalyst composition on CNT growth. They found that a catalyst with low Co content (<15 %) produced long CNTs while a catalyst with high Co content (>80 %) produced onion-like structures. Narkiewicz et al. [153] investigated hydrocarbon decomposition on Fe, Ni, and Co catalysts. They observed that cobalt and iron formed MWCNTs at 700℃ whereas, with nickel, many disordered carbon structures were found. Mhlanga et al. [154] studied several parameters that affect CNTs synthesis including the catalyst preparation. The catalysts were prepared using three different methods i.e., wet impregnation, deposition-precipitation, and reverse micelles. The yield obtained from catalysts prepared by wet impregnation and deposition precipitation was relatively higher than reverse micelles.

Bimetallic catalysts have been shown to exponentially increase the yield CNTs. Kathyayini et al. [155] synthesized MWCNTs on different supports and carbon sources using Fe, Co, and a mixture of iron-cobalt catalysts at 700 ℃. The best carbon deposit yield was obtained when the mixture of iron and cobalt were catalysts, while the yield of iron alone was very poor. Hardeman et al. [156] reported the growth of CNT forest using Fe-Co bimetallic catalysts. They discovered that the height of the forests was much higher compared to pure Fe or Co. On a MgO support, Tsoufis et al. [157] synthesized MWCNTs with a combination of Fe and Ni transition metals in a ratio of 1:1 with varying metal loadings (1-50 wt%). The highest yield was obtained with 15 wt% Fe and 15 wt% Ni at 800 ℃ for 30 minutes. While high-quality CNTs were found at Fe 1 wt% and Ni 1 wt% at 900 ℃ for a reaction time of 30 min. It was realized that to obtain good quality CNTs in high yields, reaction time, temperature and metal loading are critical parameters.

2.6 Coal

Coal remains the most abundantly consumed fossil fuel for electric power generation. It falls into the group of hydrocarbon-rich fossil fuels that are vastly used throughout the world as an energy source. It primarily formed from dead plant matter that accumulated in swamps, decayed into peat, and was converted to coal by being exposed to extreme pressure and temperature conditions. Like

other fossil fuels, its formation took place over millions of years, and for that reason, it is referred to as a non-renewable source of energy.

In South Africa, it is estimated coal reserves are at 50 billion tons. To meet the country's energy demands, more than 200 million tons of coal are produced each year putting it in the 5th place of the largest producers of coal worldwide [158]. According to the South African department of mineral resources and energy [159], 70 % of the coal produced is used to provide the country's energy needs which makes it one of the countries that are highly dependent on coal combustion to produce electricity. Coal is also converted to gas and liquids. In addition to the coal produced and consumed locally, South Africa also exports about 28 % of the coal it produces, making it the 4th largest country in the world exporting coal [160].

2.6.1 Coal Rank/Classification

The rank of coal refers to its degree of metamorphism or maturity [161]. High-ranking coals tend to be more mature and have high carbon content whereas lower-ranking coals correspond to less metamorphism and contain high contents of ash and moisture [162]. There are three different classes or ranks of coal that are being consumed, namely; anthracite, bituminous, and lignite coals [163]. Their classification is based on their heating value and relative carbon content. As seen in Table 2.3, anthracite has a heating value ranging from 13 500 to 15 600 Bt/lb and high carbon content of 92-98 %. Anthracite is breakable and lustrous. It is subdivided into anthracite, semi-anthracite, and meta-anthracite based on carbon content[164]. Bituminous coal has a lower concentration of carbon and heating value than anthracite, ranging from 46-86 % and 8300-15600 Bt/lb, respectively. It is the most abundant type of coal. Bituminous also contains subbituminous coal. After bituminous coal is lignite, the lowest class of coal among the different types. It constitutes the lowest carbon content and heating value at 46-60% and 5500-8600 Bt/lb, respectively [165]. Other classifications or specifications of coal that are used include ash content, proximate and ultimate analyses, volatile matter, total moisture, ash fusion temperature, and forms of sulphur.

Table 2.3: Types of coal based on their heating value and carbon content

	Heating Value (Bt/lb)	Relative carbon content (%)
Anthracite	13500-16500	89-98
Bituminous	8300-15600	46-89
Lignite	5500-8600	46-60

2.6.2 Composition and mineralogy of coal

The composition of coal is strongly influenced by its geochemical history and contains both organic and inorganic matter [166]. Its composition varies widely from one source to another and contains major, minor, and trace elements. The common major elements are carbon (C), nitrogen (N), sulfur(S), silicon (Si), aluminium (Al), oxygen (O), and iron (Fe). Minor elements such as potassium (K), calcium (Ca), sodium (Na), titanium (Ti) and magnesium (Mg) have been detected [161], [167], [168]. The common elements in trace amounts are arsenic (As), cadmium (Cd), chromium (Cr), mercury (Hg), and selenium (Se) [169]. Its composition also affects the composition of fly ash.

Table 2.4: Minerals found in coal

Classification	Mineral Name
Major Minerals	Quartz Kaolinite Illite Montmorillonite Pyrite Calcite
Minor Minerals	Analcime Apatite Barite Chalcopyrite
Trace Minerals	Chromite Gibbsite Gypsum Halite Magnetite

Various minerals have been detected and identified in coal samples. These are dependent on the coal source. The mineral matter found in this fossil fuel is the most significant factor in problems that may arise during its use such as slagging, sintering, pollution, and corrosion [170]. Generally, coal contains major, minor, and trace elements as listed in Table 2.4. These minerals result in ash when combusted.

2.6.3 Coal Consumption

In 2011-2015, coal power generation supplied 29 % of electricity worldwide and despite the use of renewables, the share of coal is expected to increase to 38-46 % by 2030-3035 [171]. Data gathered by International Energy Agency (IEA) [172] revealed that in 2018, coal power generation accounted for 27 % of all energy consumed. China is the leading consumer of coal and accounted for 50.2 % of the world's consumption in 2015. It is followed by the US (11.7 %) and India (8 %) (Figure 2.11). In South Africa, 119.2 million tons (2.4 %) of coal was consumed in the year 2014 and it is in the top ten of world coal consumers [173].

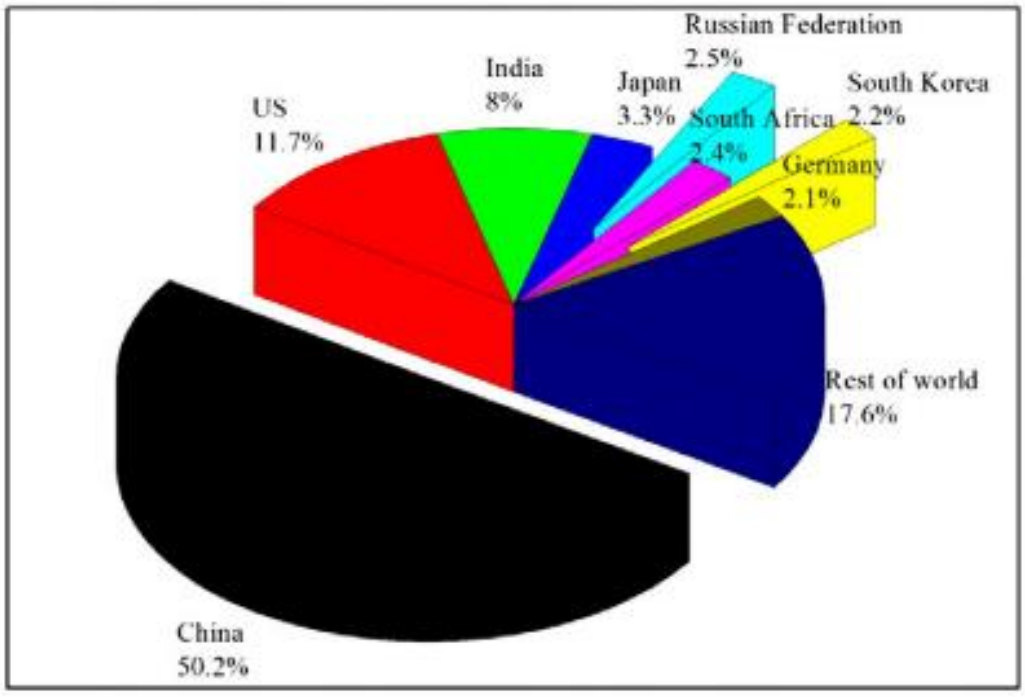


Figure 2.11: Global consumption of coal [173]

2.7 Coal Combustion in South Africa

The combustion of coal for electricity production is one of the leading usages of coal. In South Africa, the major utilities that combust coal are ESKOM and Sasol. The former uses it for electricity production and the latter uses it to produce syngas and generate electricity. Different methods to burn coal can take different routes depending on several factors such as coal usage and harmful gases released [167].

The method used by Eskom and Sasol is known as pulverized fuel combustion (PFC). This method of coal combustion, depicted in Figure 2.12, is standard in many countries around the world [174]. Low rank/low grade (sub)bituminous coal is first pulverized in huge grinding mills into fine powders before it is blown into chambers and combusted at high temperatures. This increases its surface area and enables it to burn more quickly. During this process, the heat generated is used to convert water into steam at high pressures. This steam is used to rotate the blades of giant fans called turbines at high speeds, generating electricity [158].

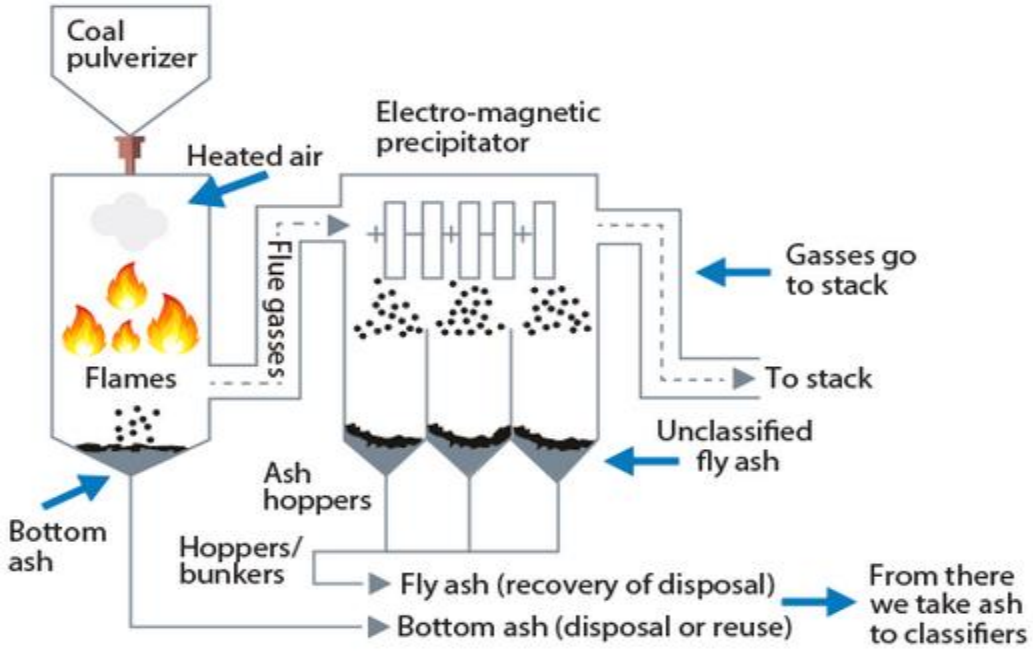


Figure 2.12: A typical pulverized fuel combustion process [161]

Coal ash is formed from the incombustible mineral matter in coal. It contains bottom ash and fly ash. Bottom ash is the larger, heavier, and denser component of coal ash which falls to the bottom

of the boiler during combustion and is collected in the ash hopper of the boiler [175]. While fly ash contains lighter-particulate matter, that is suspended in flue gas and collected by electrostatic precipitators and makes up most of the coal ash (75-85 %). The coal at Sasol is pre-combusted whereas at ESKOM is it post-combusted and the fly ash produced from these methods differ in physical and chemical properties. Some of the boilers at Sasol make use of low NOx burners which is known to increase the amount of unburnt carbon content [176]. Loss on Ignition (LOI) is the amount of unburnt carbon in fly ash.

2.8 Fly ash

Fly ash is the largest industrial waste produced. Currently, it is estimated that the global production of fly ash is 750 million tons (Mt) annually [177]. This can be attributed to the increase in the number of coal-fired power plants and high demands for electricity. The amount of fly ash that is currently being used is at a very low 25 % worldwide [178] which is a very small portion compared with the amount that is formed. South Africa produces 34.4 Mt (28.9 %) of fly ash per annum and only about 7 % of it is used [179]. In 2015, the fly ash utilization rates in China, India and US were 70 %, 62 % and 50 %, respectively [180]. Compared to these countries, South Africa stands at the bottom in utilizing its fly ash. The production and utilization rates of fly ash from different countries are given in Figure 2.13.

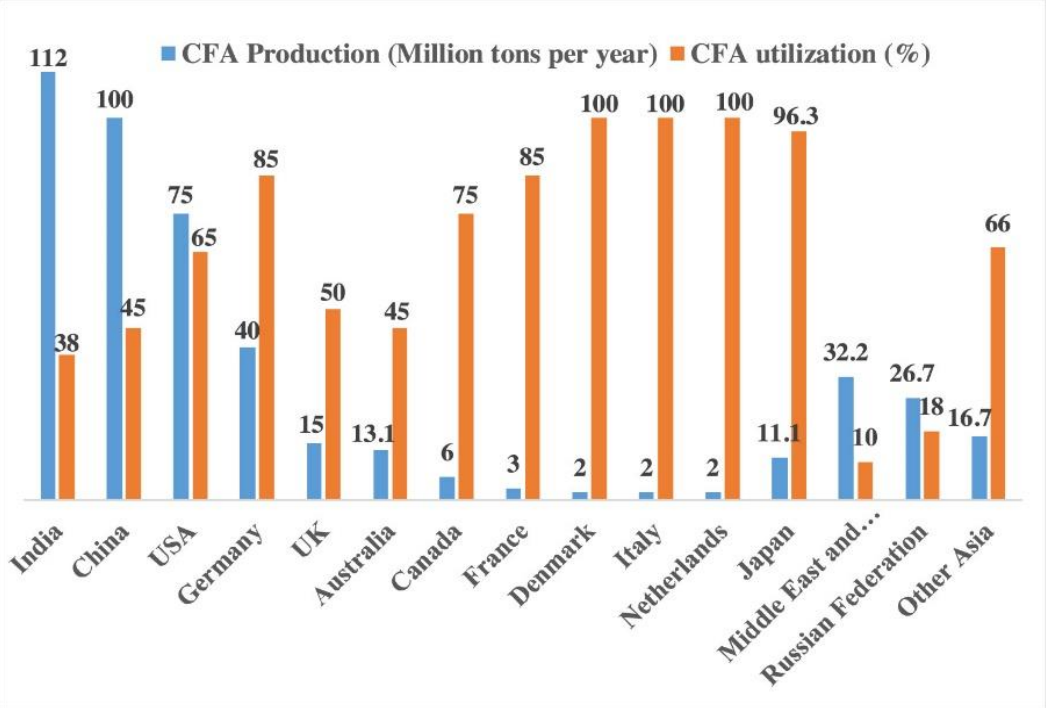


Figure 2.13: Fly ash production and utilization rates from different countries [180]

2.8.1 Fly ash physical properties

Understanding the properties of fly ash is important since they determine how it is used and disposed of [181]. The properties of this coal combustion product are largely dependent on the combustion conditions, source of coal, boiler type, and how it is collected. Depending on the contents of iron and unburnt carbon, fly ash can be white-grey to dark grey or orange to brown [173]. It is light in texture, heterogeneous, and amorphous in nature having spherical glassy particles with diameters that range from 1-100 μm. The spherical particles as shown in Figure 2.14 include cenospheres, plerospheres, irregular-shaped debris, fluidized bed combustion ash (FBC), and unburnt carbon. The fine particles in fly ash have a low to medium-bulk density (0.54-0.86 g/cm^3) and a high surface area (300-500 m^2/kg) [182].

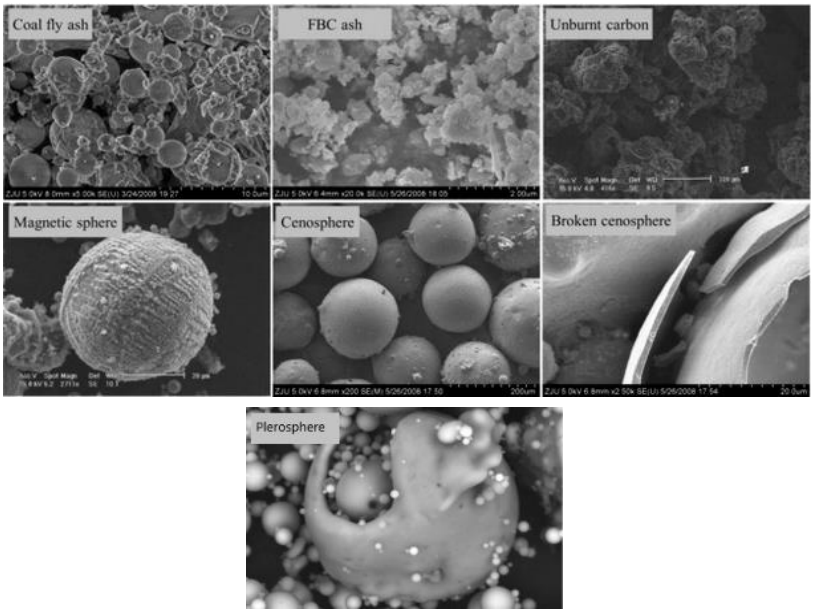


Figure 2.14: Various types of morphologies of fly ash [179] [181][182]

2.8.2 Mineralogy and chemical properties

The chemical composition of fly ash varies considerably and is dependent upon the combustion method and type of coal being burnt. It has been said that over 316 individual minerals and 188 minerals groups have been identified in different coal fly ashes [183].

However, the common components that have been identified from different fly ash samples worldwide in large proportions include silica (SiO_2), alumina (Al_2O_3), calcium oxide (CaO). Other trace elements that are found are titanium (Ti), Magnesium (Mg), Manganese (Mn), phosphorus (P), potassium (K), sodium (Na), chromium (Cr), Sulphur (S), arsenic (As), zinc (Zn), molybdenum (Mo), lead (Pb), cadmium (Cd), cobalt (Co) and copper (Cu)[184]. Its pH value varies from 1.2-7, 8-9, 11-13 and can be classified as acidic ash, mildly alkaline ash, and strongly alkaline ash, respectively [185].

2.9 Fly ash classification

Fly ash classification stems from the American Society for Testing Materials (ASTM C618) based on the industrial application of fly ash [186]. Namely, two common types of fly ash exist, Class F and Class C. They are classified according to the amount of SiO_2, Al_2O_3, and Fe_2O_3 content. The ash containing more than 70 % SiO_2, Al_2O_3, and Fe_2O_3 is defined as Class F whereas Class C fly ash contains a combined content of SiO_2, Al_2O_3, and Fe_2O_3 between 50 % and 70 %. According to ASTM, normally Class C fly ash has a calcium (as CaO) content of more than 15 % while for Class F fly ash, it is lower than 5 %. What is also generally observed is that sub-bituminous and lignite coals produce Class C fly ash when combusted and Class F results from the combustion of anthracite and bituminous coals [187]. The high silica (SiO_2) content in Class F ash makes it to be pozzolanic with no cementitious properties. However, in a finely divided form, it chemically reacts with calcium hydroxide [$Ca(OH)_2$)] at room temperature to produce compounds exhibiting cementitious properties. Class C fly ash on other hand, has self-cementing abilities, meaning in the presence of water it hardens and becomes solid over time [178].

2.10 Applications of fly ash

2.10.1 Agriculture

The use of fly ash in agriculture has several benefits especially in improving the properties of soils that enhance the growth of plants. Fly ash provides some essential micro-nutrients for soil such as K, P, S, Ca, and Mg, and macronutrients such as Fe, B, Zn, Co, Mn, Cu, and Mo that are beneficial for plant growth. It has found several uses as an insecticide, improving soil texture, bulk density, porosity, water holding capacity, hydraulic conductivity, aeration [188]–[191]. The presence of

pozzolanic minerals in fly ash also improves the quality of the soil. These properties of fly ash directly affect plant growth, bulk density, ability to retain water, and porosity.

Sikka& Kansal [192] investigated the effects of fly ash on dry-matter yield, nutrient composition of 60 days old rice and wheat plants. An increase in the N, S, Ca, Na and Fe nutrients was observed while P and Zn decreased. The fly ash used did not influence the dry-matter yield and nutrient composition of wheat. However, the Fe concentration in wheat increased significantly from 139 ppm to 161 ppm at 8 % addition of fly ash. Chang et al [193] performed several experiments with five different soil types mixed with fly ash. Among the five soil types, Reyes silty clay showed an increase in the bulk density from 0.89 g/cc to 1.01 g/cc. Prabakar et al. [194] investigated the load-bearing capacity of soil mixed with fly ash and it was found that increasing the addition of fly ash increases the shear strength non-linearly, and linearly for both shear stress and cohesion.

The water-holding capacity is a very important phenomenon in the growth of crops and plants. In general, the higher the water-holding capacity of soils the less likely the leaching of nutrients losses will occur [195]. Soils with a high water-holding capacity greatly improve the crop's quantity and quality in yield and decrease the adverse effects of droughts and erosion. Fly ash can change the soil texture and increase water-holding capacity permanently when applied at high rates. This was observed by Ghodrati et al. [196] when the water-holding capacity of the soil was raised from 12 % to 25 % with 30 % fly ash. Khan& Khan [197] reported an increase in porosity, water-holding capacity, conductivity, pH, etc. with a gradual increase in fly ash concentrations (0, 10, 20…100 %) in the normal field soil.

The growth of crops is generally optimum at pH between 6.5 and 7. Coal fly ash, which is acidic or basic, can be applied to buffer the pH of soils depending on the coal source and combustion conditions [198]. Introducing fly ash (which is generally alkaline) to acidic soils can raise the pH of the soil and this is explained by the release of Al, Ca, OH, and Na ions [177]. The lime in fly ash reacts with the acidic constituents in soil and releases these ions that benefit crop plants. Class C fly ash has proven to be able to raise the pH of acidic soil more efficiently than Class F fly ash, thus it has been used at excessively high rates. For most of class f ash, its ability to ameliorate the acidity of soils is limited unless it has a higher component of CaO.

The application of fly ash in agriculture can be enhanced by blending it with organic and inorganic materials such as lime, gypsum, farm manure, composts, red mud, and acid-forming organic by-

products like sewage sludge, animal manure and poultry. The co-application of these materials has several advantages which include reducing the bioavailability of toxic metals, increasing the content of soil organic matter, enhancing the availability of nutrients, indirectly stimulating microbial activity, and buffering soil pH [188], [189], [191].

Although fly ash has some benefits in agriculture, it also has some detrimental and undesirable effects on crops, soils, and groundwater due to high concentrations of heavy metals that are potentially toxic, change in soil salinity, and radionuclides. Utilizing un-weathered fly ash could result in the accumulation of elements such as B, Se, Mo, and Fe which are toxic at high concentrations and decrease crop yields [199]. Higher rates of fly ash in soils might lead to the activation of toxic elements which could hinder microbial activity [200].

2.10.2 Environmental protection/adsorbent

The fly ash particles have high porosity, large specific surface area, alkalinity, and a significant amount of unburnt carbon with a negatively charged surface at high pH and many other unique characteristics. These properties of fly ash give the impression that it can be used as an efficient high-capacity adsorbent for treating environmental pollutants. Its direct application as an adsorbent for gaseous and aqueous pollutants has been investigated. By 1984, fly ash had shown great promise as an adsorbent for copper (Cu^{2+}) ions removal from industrial wastewaters [201].

To remove boron from seawater and desalinated seawater, Polat et al. [202] conducted several batch experiments using different types of fly ash and coals as adsorbents. They found that approximately 90 % of boron could be successfully removed from the seawaters due to the interaction of coal and fly ash under the appropriate conditions. Cho et al. [203] investigated the removal of heavy metals (Zn, Pb, Cd, and Cu) from aqueous solutions under varied reaction conditions. They found that the percentage removal of the heavy metals increased as the pH increased. When the pH was 8, 95 % of the metals were removed. Aksu and Yener [204] studied the adsorption of phenol using fly ash as a substitute for activated carbon. Adsorption of 27.9 mg/g for phenol was reported compared to 108 mg/g for activated carbon at 100 mg/l for phenol concentration. Kim et al. [205] demonstrated the fabrication of multipurpose composite polyurethane membrane from TiO_2 and fly ash for the adsorption of heavy metals. The fly ash fibrous membrane had a higher and faster adsorption capacity. Mohan et al.[206] studied the

removal of dyes from wastewaters using fly ash and it was to be comparable to that of other low-cost commercially available adsorbents.

2.10.3 Construction

The use of fly ash in the construction industry has gained tremendous attention and is currently the leader in the applications of fly ash. Concrete in the construction industry is of high importance and this is seen by the amount of concrete used worldwide, Blissett et al. [177] further mention that the humans' species do not use any other material in greater quantities than concrete except for water. It is also the basis of almost all of the construction projects that take place and has been shown to have a significant number of benefits such as high strength, easily moldable, affordable, adaptability, and readily available [181].

Fly ash can be described as either being pozzolanic or cementitious depending on the content of CaO. This property enables it to be used extensively either as a raw material or in cement replacement for ceramics, construction fills, road base, etc. The addition of fly ash in cement enhances the durability and strength of concrete, reduces the heat of hydration, permeability, cost of concrete, and resists sulfate attack [181]. Commonly in a commercial application, the amount of fly ash added ranges from 15-20 wt.%. However, they can get as high as 70 wt.% for concrete in constructions such as pavement, parking lots, and walls. The use of high levels of low-lime fly ash as a constituent of cement in concrete was examined by McCarthy and Dhir [207]. They found that up to 45 wt% levels of fly ash can be combined with Portland cement to form a range of concrete strengths. However, early strength, a critical feature in concrete, can be reduced compared to Portland cement. Felekoglu [208] investigated the potential of three types of Turkish fly ashes from different sources for high-volume fly ash (HVFA) concrete production. The results showed that for structural applications, HVFA can only be produced by using fly ash with appropriate physical and chemical properties within the limits specified.

Fly ash-based geopolymers are promising alternatives to building materials due to their interesting properties like high mechanical strength, good thermal stability, surface hardness amongst others [177],[209]. They rapidly harden at room temperature with mortar containing compressive strengths and concrete strength of 80-120 MPa and 70 MPa, respectively. Nath and Sarker [210] studied fly ash-based geopolymers appropriate for curing conditions. To accelerate the curing of

geopolymer, Portland cement, and low-calcium fly ash were added. Compressive strength of more than 50 MPa was achieved for mortar samples and 40 MPa for concrete samples. Temuujin et al. [211] prepared geopolymer mortars with varying degrees of sand aggregate and examined their physical and mechanical properties. They found that the compressive strength of fly ash-based geopolymer mortar depended on the strength of the geopolymer binder. Joseph and Matthew [212] presented the engineering properties of geopolymer concrete made from alkali-activated fly ash. The geopolymer had a higher value of Poisons ratio and modulus of elasticity than ordinary concrete cement. Ma et al. [213] reviewed the structural performance of geopolymers and their analysis. They found that geopolymers can replace ordinary concrete since they possess better mechanical strength, higher durability, and more desirable structural performances.

The utilization of fly ash in the construction industry is largely affected by seasonal changes in countries like the US and the EU. The high rates of fly ash production are more conducive in winter whereas, in the construction industry, cement is much more required in summer where building projects are at their peak. In the summer months, coal generators tend to be restricted to double shifting which leads to the Loss of Ignition (LOI) of the ash to be increased, resulting in poor quality of fly ash and mixture of aggregation.

2.10.4 Fly ash as a catalyst

The application of fly ash in heterogeneous catalysis has attracted the attention of many researchers around the world. The main characteristics of heterogenous catalysts such as aluminosilicates make them suitable to be used as catalysts, catalyst supports, adsorbents, and sensors to name a few. Their properties include larger surface areas, tunable pore sizes, and large porous structures. In fly ash, the aluminosilicates which have been exposed to higher temperatures enable them to be thermally stable and suitable to be used as catalyst or catalyst supports for various reactions. As catalyst support, fly ash has shown higher catalytic activities for ammonia decomposition, catalytic reduction of NO_x and SO_x, methane oxidation, dye decomposition, and CO_2 reforming of methane [178].

Jain et al. [214] prepared fly ash catalyst supported on CaO for fine chemical production and tested its catalytic activity by Knoevenagel condensation. The results showed a higher conversion of benzaldehyde to the desired product with high purity. Titanium dioxide (TiO_2) is a good semi-

conductor for photocatalytic reactions. Yu [215] coated fly ash with TiO_2 for the removal of NO and found that higher rates of NO removal were more favoured at higher temperatures than at low temperatures. This improvement was a result of the phase transformation of iron oxide, magnetite into hematite (Fe_2O_3). Wang [216] tested fly ash as potential catalyst support for nickel (Ni) in carbon dioxide reforming of methane. It was demonstrated that treating the ash before Ni loading has the potential to improve the catalytic activity and stability of the resultant catalysts.

Fly ash has been used as a catalyst in the synthesis of carbon nanomaterials (CNMs). Compared to the commonly used catalysts for CNM formation, fly ash is cost-effective, recyclable, and readily available at the megaton scale. It can be used without any pre-treatments or be treated with various transition metal catalysts. CNMs have been one of the most researched fields in the past three decades with different recipes and formulations being reported. However, the number of available studies on the production of CNM using fly ash is very limited. The conditions that were used to synthesize CNMs are summarized in Table 2.5.

Table 2.5: Summary of synthesis conditions used in the growth of CNMs from fly ash catalysts

Ref.	Catalyst	Temp (℃)	Carbon source and Carrier gas	Time (minutes)	Yield
Dunens [217]	Fly ash with 5 and 2.5wt% Fe	650	C_2H_4,H_2,N_2 (1:1:2)	120	0.8-25%
Yasui [218]	Raw fly ash	697-797	CH_4,He (1:1) C_2H_5OH,He (3:10)	60	
Nath [42]	25wt% Fly ash and PVA	500	PVA N_2 (5L/min)	10	45.5%
Salah [221]	Carbon-rich fly ash	550-950	C_2H_2 (0-50) Ar (100)	15-60	
Rambau [222]	Raw Fly ash	650	C_2H_4 (250) H_2:Ar (1:5)	60	
Hintsho [39]	Raw Fly ash	400-700	C_2H_2 (100) H_2 (100)	30	

Dunens et al. [217] synthesized Multiwall carbon nanotubes (MWCNTs) on Australian fly ash catalysts by fluidized bed chemical vapour deposition (FBCVD). In this study, fly ash was impregnated with different metal loadings of iron nitrate and calcinated in the air at 650 ℃ for 2 hrs. The CNTs were produced at 800 ℃ for 12 hrs under a 1:1 ratio of H_2:N_2 carrier gases with

ethylene as a carbon source. The TGA results showed that fly ash impregnated with 5 wt% Fe had the highest catalyst activity for CNMs (Figure 2.15a) whereas the raw fly ash did not produce any CNT under the selected conditions. They explained that the increased Fe content in fly ash increased the hydrocarbon decomposition rate and provided more reactive sites for CNT growth. While the catalytic inactivity of the as-received fly ash was attributed to the inherent heterogeneity of the iron location and composition of the untreated fly ash.

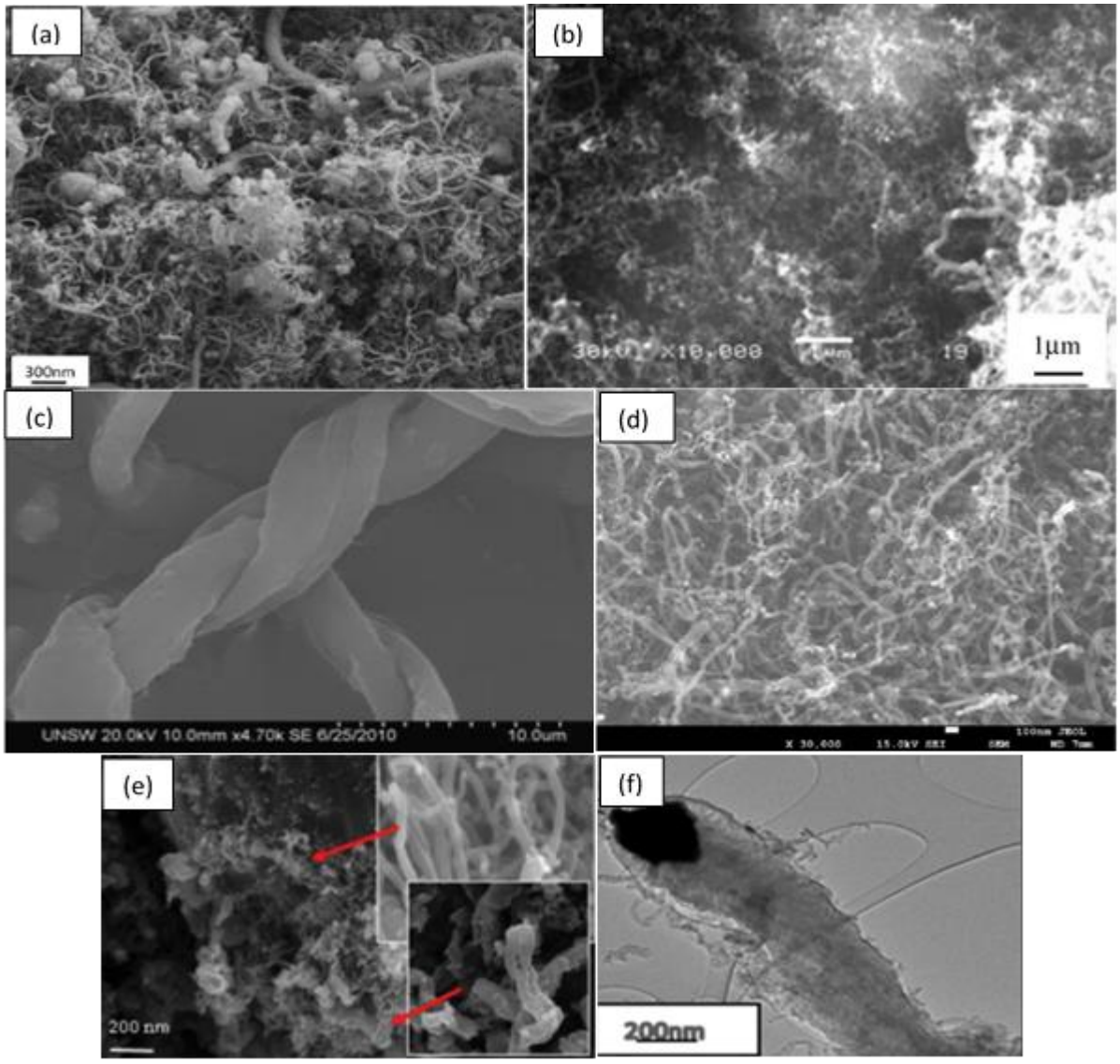


Figure 2.15: Electron microscopy images of (a) CNFs entwined with MWCNTs from 5 wt% Fe and fly ash, (b) CNTs from ethanol and carrier gas (3:10) and fly ash, (c) CNT ribbons from PVA and 25 wt% fly ash, (d) CNTs obtained at the optimum conditions of 650 ℃, 300 torr [217]–[219], [221], [222].

Yasui et al. [218] reported on the fabrication of CNTs from Japanese fly ash in a thermal CVD (TCVD). They stipulated that this process could result in simple, cost-effective, and large amounts of CNTs. The synthesized CNTs using fly ash was intended to be applied in electronic material such as electromagnetic and optical absorber. Furthermore, the principal oxides in fly ash, alumina, and silica, are low dielectric constant materials that are used in electronic devices and high-frequency materials. Methane and ethanol were used as carbon precursors with He and N_2 as carrier gases at different temperatures. On using methane as a carbon source and He as carrier gas at 897 ℃, very few CNTs were observed. However, the yield was increased when ethanol was used as a carbon source and CNT growth could occur at a temperature of 697 ℃. A further increase in the yield was reported when the temperature and ethanol were raised to 797 ℃ and 3:10, respectively (Figure 2.15b) They established that the carrier gases had no effect on the results obtained. From the Raman spectrum, the D-band (degree of disorder) at 1390 cm^{-1} had a broader peak than the G-band (degree graphitized carbon) resulting in defects, poor graphitization of the CNTs, and high yields of amorphous carbon.

Nath and Sahajwalla [219] produced CNTs from a different technique than the other authors. The CNTs were synthesized from fly ash catalyzed pyrolysis of a composite film of polyvinyl alcohol (PVA). The fly ash in this study was used as received. The synthesis was carried out in a horizontal tube furnace at 500 ℃ under N_2 as a carrier gas for 10 minutes. The pyrolysis was between mixtures of PVA and fly ash, powder PVA, PVA, and composite films. Only the pyrolysis of PVA with 25 wt% fly ash formed CNTs with a yield of 45.5 % (Figure 2.15c). From this, CNT ribbons and fibers with different morphological geometries were produced CNT ribbons with a range of diameters and lengths. The self-assembled CNT ribbons exhibited high flexibility and permanently twisted structures. The intensity of the D-band was lower than the G-band, indicating well graphitized CNT ribbons. They stipulated that the ribbons have the potential to be used in fabricating high-strength composite materials with polymer and metals.

Fly ash is also a by-product of heavy oil or crude oil from water desalination plants. The major component in this fly ash is unburnt carbon, which exceeds 80 % and sometimes can reach up to 90 %. Salah [220] ultrasonically treated a solution of carbon-rich fly ash in water and grew CNTs in a low-pressure CVD (LPCVD). This carbon-rich fly ash from Saudi Arabia served as both a catalyst and co-precursor along with acetylene and N_2 as a carrier gas. The reaction took place at

a temperature of 700 ℃ and pressure of 15 Torr, while acetylene and nitrogen were flowing at 50 and 200 sccm, respectively, for 20 minutes. CNTs were formed in high yields and had a high degree of wall graphitization as evidenced in the Raman spectrum. In this work, he stipulates that this method converts carbon-rich fly ash completely to CNTs and is suitable for large-scale production at a low cost.

In an attempt to find the optimum reaction conditions for the growth of CNTs from this carbon-rich fly ash using LPCVD, Salah et al.[221] in another work, investigated the parameters affecting their growth using the same method as above [220]. These parameters are temperature, time, gas pressure, and flow rate. The optimum synthesis conditions were temperature of 650 ℃, the gas pressure of 300 torr, growth time of 60 min, C_2H_2: Ar ratios of 30:100, and resulted in full conversion of fly ash to CNTs with a range of diameters and lengths (Figure 2.15d). At higher temperatures, a mixture of thick CNTs and unreacted fly ash was observed whereas lower temperatures had poor growth. The CNTs obtained from higher pressures showed better results than the ones at lower pressures, which had a mixture of fly ash nanotubes. The length and diameters of the CNTs were found to increase with the growth time, increasing acetylene flowrate resulted in an increase in amorphous carbon. In this study, the mechanism of CNT formation from fly ash was also discussed and that this fly ash contains a significant number of hydrocarbons. They predict that this fly ash can be applied as composites for polymers and rubbers.

Rambau et al.[222] reported on the different combinations of fly ash, extracted iron oxide from fly ash, and ethylene and waste tyres pyrolysis oil to produce CNMs. The magnetic iron oxide in fly ash was extracted via acid digestion and used as catalyst and support along with the as-received fly ash. Ethylene and pyrolysis oil vapour were used as precursor compounds. The CNTs were grown in a CVD furnace at 650 ℃ under argon and hydrogen gases for 60 minutes. The SEM images of CNMs from fly ash and ethylene showed CNMs with a wide variety of diameters and lengths (Figure 2.15e). Pyrolysis oil vapour precursor and fly ash catalyst produced CNMs that were anchored on the surface of cenospheres. The morphology of CNMs from ethylene and extracted magnetic Fe portrayed clustered cylindrical structures whereas, with pyrolysis oil vapour the CNM observed had thin tubular structures at low quantity. The Raman spectra showed CNMs with good graphitization and minor defects.

Using South African fly ash, Hintsho et al. [223] synthesized thick CNFs (Figure 2.15f). from acetylene under different temperature conditions (400-700 ℃). The ash was fly ash was used as received in a tubular furnace with both acetylene and H_2 flowing at 100 ml/min for 30 min. At a high temperature (700 ℃), the degree of graphitization was found to be high for the CNMs from Raman Spectroscopy. Thermal analysis (TGA) results were coherent with the Raman spectroscopy, they showed that the nanomaterials had an oxidation temperature that was greater than 550 ℃ and the CNMs synthesized at 700 ℃ had the highest oxidation temperature. This indicates a material with good graphitization. In this study, the formation of CNFs from fly ash was attributed to the presence of iron in the form of iron carbide. This was done by XRD, EDS, and Mössbauer spectroscopy.

2.11 Carbon Dioxide as a carbon source and fly ash as a catalyst for CNMs production

The studies on the combination of CO_2 and fly ash as a carbon source and catalyst are very limited. Hintsho et al. [223] demonstrated the use of the two waste products to produce CNMs. The fly ash was untreated while CO_2 was used in three different ways: as a sole carbon source, as an additive to acetylene, and in advance to reaction with acetylene. The CNMs were grown at temperatures between 500 and 1000 ℃ using the CVD furnace with H_2 as carrier gas. Then it was flushed with H_2 for 15 min followed by acetylene into the furnace for 30 min. CO_2 as a sole precursor formed CNMs only at 900 ℃. The CNMs were produced in low yields and were confirmed by Raman spectroscopy which portrayed a high D-peak of disordered carbon and a low G-peak of graphitic carbon. A three-fold increase in the yield was obtained from 500-700 ℃ when CO_2 was added to acetylene. The high intensity of the G-band and low intensity of the D-band from the Raman spectroscopy showed an improvement in the crystallinity of CNMs. In the third case, CO_2 was used as a carbon source before acetylene to avoid dangerous chemicals from occurring. It was introduced into the furnace at a set flow rate and allowed to react with fly ash at a set temperature for 30 min. Regularly and irregularly shaped nanofibers were formed along with small amounts of CNTs. An increase in yield was observed at 500-600 ℃ and decreased at 700 ℃. The same trend was observed for crystallinity. Since low yields and poor quality of the carbonaceous products were obtained, the carbon-rich fly ash was used by Salah et al. [220].

2.12 Fly ash disposal

The disposal of wastes from different processes has always been a problem for industry and fly ash is not any different. Its management and disposal are a major problem to thermal power plants generators require a vast amount of land. Fly ash should be disposed of in a manner that is safe in all aspects and will not have short- or long-term detrimental effects on human health, vegetation, economy, aquatic life, and animals. This heterogeneous inorganic material constitutes some toxic metals such as lead (Pb) and chromium (Cr), which can be a consequence of some serious health concerns and are harmful to the environment[224]–[227].

In Tennessee (US), a fly ash pond containing 3.8 billion Litres of water and 4.1 million tons of fly ash collapsed and infiltrated several residential areas, contaminating the Emory River. This event took place in the December of 2008. However, the clean-up was only concluded in 2015 and cost a total of $1.1 billion [228]. Kumar et al. [229] analysed the leaching behaviour of 17 combinations of columns with fly ash and three soil types and found higher concentrations of metals than the drinking water quality guidelines for the column filled with fly ash only. In another study, Singh et al. [230] attempted to assess groundwater contamination due to fly ash disposal in ash by simulating the dumpsite conditions using batch leaching tests. Only a few elements were selected for the leachate test and the average concentration of these elements in groundwater was found to be higher than the prescribed concentrations in drinking water.

In the past, fly ash was disposed into the atmosphere. This created environmental and health concerns which prompted the development of other methods. There are mainly two methods of disposing of fly ash, dry disposal, and wet disposal. In the dry disposal method, fly ash captured and collected from electrostatic precipitators (ESP) is transported by trucks and conveyors to landfills and dumpsites. In wet disposal, fly ash is mixed with water and transported as slurry from the thermal power plants to ash ponds near the plant [224]. Wet disposal is the most popular and widely used method of fly ash disposal since it is cost-effective. Despite being cheaper, wet disposal does not protect the environment from the leaching of heavy metals into the soil and groundwater contamination [231].

2.13 Conclusion and Summary of CNMs production from fly ash and CO_2

Remarkable achievements have been in the synthesis of CNMs in the last 30 years. Significant progress has been made in the synthesis techniques which brought about the realization of industrial production of CNMs and their application in commercial products. While some applications of carbon dioxide and fly ash have been realized and reached maturity, the use of fly ash and carbon dioxide in the production of carbon nanomaterials is still limited on a lab scale. One of the major challenges of CO_2 is its stability that requires extreme synthesis conditions for growing CNTs in good yield and quality. Suitable catalysts and modified CVD reactors to suit CO_2 might crack the secrets its holds in producing these materials. The morphology of the nanostructures obtained from the reduction of CO_2 is greatly influenced by temperature and the type of reductant used. The mechanism by which CNMs grow by this method has not been fully explored. The parameters for its use as a carbon source have been optimized for CNTs production on the CVD. However, high temperatures were shown to be more favourable. The use of CO_2 as a co-feed has shown tremendous success and potential to produce pure SWCNTs in high yields. This is the most successful method in this review that used CO_2 SWCNTs production in the CVD, the next step in this method would be to produce SWCNTs on an industrial scale. Electrolysis is also one promising technique since it is more affordable than CVD.

The quality of the CNMs produced from fly ash is generally low, depending on the type of fly ash used and contains unreacted fly ash particles. As we have demonstrated, in some instances a mixture of CNFs and CNTs was formed from fly ash instead of a single product. Controlling the formation of the desired material becomes paramount and this also relates to the growth mechanism experienced by fly ash for CNMs which needs to be explored further. Besides fly ash, the general growth mechanism of CNMs is still not clear. No studies have been conducted to achieve high yield and good quality products through optimizing the synthesis conditions in fly ash. The presence of iron in fly ash plays an important role as observed in some of the studies, its higher content results in good yields. The temperature was shown to be the most important and influential parameter on the CNMs synthesis. The availability of studies where they are both used collectively is very limited. Research efforts should focus more on the use of fly ash and CO_2 as raw materials without any pre-treatments or mixing them with other compounds to have a significant contribution in their mitigation.

2.14 References

[1] "CO_2 Carbon Dioxide Properties, Uses, Applications - Recovery from Industrial Sources - Concentration in Air," *Universal Industrial Gases, Inc*. [Online]. Available: http://www.uigi.com/carbondioxide.html. [Accessed: 16-Aug-2020].

[2] *Gaseous Carbon Waste Streams Utilization: Status and Research Needs*. Washington, DC: NATIONAL ACADEMIES Press, 2019.

[3] D. Y. C. Leung, G. Caramanna, and M. M. Maroto-Valer, "An overview of current status of carbon dioxide capture and storage technologies," *Renew. Sustain. Energy Rev.*, vol. 39, pp. 426–443, 2014.

[4] E. T. Kho, T. H. Tan, E. Lovell, R. J. Wong, J. Scott, and R. Amal, "A review on photo-thermal catalytic conversion of carbon dioxide," *Green Energy Environ.*, vol. 2, no. 3, pp. 204–217, 2017.

[5] C. Song, "CO2 Conversion and Utilization: An Overview," *ACS Symp. Ser.*, vol. 809, pp. 1–30, 2002.

[6] H. Vidas, B. Hugman, A. Chikkatur, and B. Venkatesh, "Analysis of the costs and benefits of CO2 sequestration on the US outer continental shelf," 2012.

[7] K. Z. House, C. F. Harvey, M. J. Aziz, and D. P. Schrag, "The energy penalty of post-combustion CO2 capture & storage and its implications for retrofitting the U.S. installed base," *Energy Environ. Sci.*, vol. 2, no. 2, pp. 193–205, 2009.

[8] S. D. Kenarsari *et al.*, "Review of recent advances in carbon dioxide separation and capture," *RSC Adv.*, vol. 3, no. 45, pp. 22739–22773, 2013.

[9] W. L. Theo, J. S. Lim, H. Hashim, A. A. Mustaffa, and W. S. Ho, "Review of pre-combustion capture and ionic liquid in carbon capture and storage," *Applied Energy*, vol. 183. Elsevier Ltd, pp. 1633–1663, 2016.

[10] B. Erlach, M. Schmidt, and G. Tsatsaronis, "Comparison of carbon capture IGCC with pre-combustion decarbonisation and with chemical-looping combustion," *Energy*, vol. 36,

no. 6, pp. 3804–3815, 2011.

[11] A. Padurean, C. C. Cormos, and P. S. Agachi, “Pre-combustion carbon dioxide capture by gas-liquid absorption for Integrated Gasification Combined Cycle power plants,” *Int. J. Greenh. Gas Control*, vol. 7, pp. 1–11, 2012.

[12] A. Samanta, A. Zhao, G. K. H. Shimizu, P. Sarkar, and R. Gupta, “Post-combustion CO2 capture using solid sorbents: A review,” *Industrial and Engineering Chemistry Research*, vol. 51, no. 4. pp. 1438–1463, 2012.

[13] T. C. Drage *et al.*, “Materials challenges for the development of solid sorbents for post-combustion carbon capture,” *J. Mater. Chem.*, vol. 22, no. 7, pp. 2815–2823, Feb. 2012.

[14] J. C. Abanades, G. Grasa, M. Alonso, N. Rodriguez, E. J. Anthony, and L. M. Romeo, “Cost structure of a postcombustion CO2 capture system using CaO,” *Environ. Sci. Technol.*, vol. 41, no. 15, pp. 5523–5527, 2007.

[15] R. M. Davidson and IEA Coal Research. Clean Coal Centre., *Post-combustion carbon capture from coal fired plants : solvent scrubbing*. IEA Clean Coal Centre, 2007.

[16] L. Raynal, P. A. Bouillon, A. Gomez, and P. Broutin, “From MEA to demixing solvents and future steps, a roadmap for lowering the cost of post-combustion carbon capture,” *Chem. Eng. J.*, vol. 171, no. 3, pp. 742–752, 2011.

[17] R. Stanger *et al.*, “Oxyfuel combustion for CO2 capture in power plants,” *Int. J. Greenh. Gas Control*, vol. 40, pp. 55–125, 2015.

[18] M. A. Habib *et al.*, “A review of recent developments in carbon capture utilizing oxy-fuel combustion in conventional and ion transport membrane systems,” *International Journal of Energy Research*, vol. 35, no. 9. pp. 741–764, 2011.

[19] S. Solomon, M. Carpenter, and T. A. Flach, “Intermediate storage of carbon dioxide in geological formations: A technical perspective,” *Int. J. Greenh. Gas Control*, vol. 2, no. 4, pp. 502–510, Oct. 2008.

[20] M. A. Celia and J. M. Nordbotten, “Practical modeling approaches for geological storage of carbon dioxide,” *Ground Water*, vol. 47, no. 5, pp. 627–638, Sep. 2009.

[21] Join The Underground, “The Global Status of CCS: 2017,” 2017.

[22] H. Kolbe, “Ueber Synthese der Salicylsäure,” *Ann. der Chemie und Pharm.*, vol. 113, no. 1, pp. 125–127, 1860.

[23] P. B. Joshi, “Carbon dioxide utilization: A comprehensive review,” *Int. J. Chem. Sci.*, vol. 12, no. 4, pp. 1208–1220, 2014.

[24] M. Aresta, A. Dibenedetto, and A. Angelini, “The changing paradigm in CO2 utilization,” *J. CO2 Util.*, vol. 3–4, pp. 65–73, 2013.

[25] M. Shigeru, S. Makoto, K. Isamu, S. Akira, and M. Masayuki, “Synthesis of N,N’-Dimethylurea from Monomethylamine and Carbon Dioxide MORINO,” *Bull. Fac. Fish. Hokkaido, Univ.*, vol. 29, no. 1, pp. 75–88, 1978.

[26] C.-H. Huang and C.-S. Tan, “A Review : CO2 Utilization,” *Aerosol Air Qual. Res.*, vol. 14, pp. 480–499, 2014.

[27] K. Loria, “Safe Carbonated Drinks: Cheers to Improved Quality, Production of CO2,” *Wiley Subscription Services*, 2018. [Online]. Available: https://www.foodqualityandsafety.com/article/carbonated-drinks-safety-quality-production-co2/. [Accessed: 08-Jan-2020].

[28] N. Bryk, “Dry Ice| How products are made,” *Encyclopedia*, 2019. [Online]. Available: https://www.encyclopedia.com/science-and-technology/chemistry/compounds-and-elements/dry-ice. [Accessed: 23-Dec-2019].

[29] U.S. Environmental Protection Agency, “Carbon Dioxide as a Fire Suppressant Examining the Risks,” *Environ. Prot.*, 2000.

[30] R. Bhadra, P. Biswas, and M. Ravi Sankar, “A Literature Review on CO2 Laser Welding,” in *Lasers Based Manufacturing. Topics in Mining, Metallurgy and Materials Engineering. Springer, New Delhi*, 2015, pp. 381–398.

[31] L. Shanping, F. Hidetoshi, and N. Kiyoshi, “Effects of CO2 shielding gas additions and welding speed on GTA weld shape,” *J. Mater. Sci.*, vol. 40, pp. 2481–2485, 2005.

[32] D. Lozowski, “Supercritical CO2 A Green Solvent - Chemical Engineering,” *Chemical*

Engineering, 2010. [Online]. Available: https://www.chemengonline.com/supercritical-co2-a-green-solvent/?printmode=1#disqus_thread. [Accessed: 23-Dec-2019].

[33] T. Wu and B. Han, "Supercritical Carbon Dioxide (CO2) as Green Solvent," in *Innovations in Green Chemistry and Green Engineering: Selected Entries from the Encyclopedia of Sustainability Science and Technology*, P. T. Anastas and J. B. Zimmerman, Eds. New York, NY: Springer New York, 2013, pp. 297–326.

[34] N. W. Krase and V. L. Gaddy, "Synthesis of Urea from Ammonia and Carbon Dioxide," *Ind. Eng. Chem.*, vol. 14, no. 7, pp. 611–615, 1922.

[35] H. Kolbe, "Ueber Synthese der Salicylsäure," *Ann. der Chemie und Pharm.*, vol. 113, no. 1, pp. 125–127, 1860.

[36] T. Iijima and T. Yamaguchi, "Efficient regioselective carboxylation of phenol to salicylic acid with supercritical CO2 in the presence of aluminium bromide," *J. Mol. Catal. A Chem.*, vol. 295, no. 1–2, pp. 52–56, 2008.

[37] D. C. Webster, "Cyclic carbonate functional polymers and their applications," *Prog. Org. Coatings*, vol. 47, no. 1, pp. 77–86, 2003.

[38] S. Fukuoka *et al.*, "A novel non-phosgene polycarbonate production process using by-product CO2 as starting material," in *Green Chemistry*, 2003, vol. 5, no. 5, pp. 497–507.

[39] H. Arakawa *et al.*, "Catalysis research of relevance to carbon management: Progress, challenges, and opportunities," *Chem. Rev.*, vol. 101, no. 4, pp. 953–996, 2001.

[40] M. North, R. Pasquale, and C. Young, "Synthesis of cyclic carbonates from epoxides and CO2," *Green Chem.*, vol. 12, no. 9, pp. 1514–1539, 2010.

[41] S. S. Yu, X. H. Liu, J. G. Ma, Z. Niu, and P. Cheng, "A new catalyst for the solvent-free conversion of CO2 and epoxides into cyclic carbonate under mild conditions," *J. CO2 Util.*, vol. 14, pp. 122–125, 2016.

[42] A. J. Scott and A. Penlidis, "Copolymerization," in *Reference Module in Chemistry, Molecular Sciences and Chemical Engineering*, Elsevier, 2017.

[43] W. H. Brown, "Formic acid," *Encyclopædia Britannica, inc.* 19-Mar-2019.

[44] S. Sankaranarayanan and K. Srinivasan, “Carbon dioxide - A potential raw material for the production of fuel, fuel additives and bio-derived chemicals,” *Indian J. Chem.*, vol. 51, no. 9–10, pp. 1252–1262, 2012.

[45] J. Artz *et al.*, “Sustainable Conversion of Carbon Dioxide: An Integrated Review of Catalysis and Life Cycle Assessment,” *Chem. Rev.*, vol. 118, no. 2, pp. 434–504, 2018.

[46] Z. Zhang *et al.*, “Hydrogenation of carbon dioxide is promoted by a task-specific ionic liquid,” *Angew. Chemie - Int. Ed.*, vol. 47, no. 6, pp. 1127–1129, 2008.

[47] M. Gabrovska, R. Edreva-Kardjieva, D. Crişan, P. Tzvetkov, M. Shopska, and I. Shtereva, “Ni-Al layered double hydroxides as catalyst precursors for CO 2 removal by methanation,” *React. Kinet. Mech. Catal.*, vol. 105, no. 1, pp. 79–99, 2012.

[48] S. Wang, G. Q. Lu, and G. J. Millar, “Carbon dioxide reforming of methane to produce synthesis gas over metal-supported catalysts: State of the art,” *Energy and Fuels*, vol. 10, no. 4, pp. 896–904, 1996.

[49] S. A. Al-Saydeh and S. J. Zaidi, “Carbon Dioxide Conversion to Methanol: Opportunities and Fundamental Challenges Chapter,” *Intech*, p. 13, 2016.

[50] M. Peters, B. Köhler, W. Kuckshinrichs, W. Leitner, P. Markewitz, and T. E. Müller, “Chemical technologies for exploiting and recycling carbon dioxide into the value chain,” *ChemSusChem*, vol. 4, no. 9. Wiley-VCH Verlag, pp. 1216–1240, 2011.

[51] D. Kubarek, “Carbon dioxide-to-methanol process improved by catalyst,” *Penn State News*, 2018.

[52] X. Nie *et al.*, “Mechanistic Understanding of Alloy Effect and Water Promotion for Pd-Cu Bimetallic Catalysts in CO2 Hydrogenation to Methanol,” *ACS Catal.*, vol. 8, no. 6, pp. 4873–4892, 2018.

[53] K. M. K. Yu, I. Curcic, J. Gabriel, and S. C. E. Tsang, “Recent advances in CO2 capture and utilization.,” *ChemSusChem*, vol. 1, no. 11, pp. 893–899, 2008.

[54] A. Coker, “Dimethyl Carbonate,” 2012.

[55] A. Rafiee, K. Rajab Khalilpour, D. Milani, and M. Panahi, “Trends in CO2 conversion

and utilization: A review from process systems perspective," *J. Environ. Chem. Eng.*, vol. 6, no. 5, pp. 5771–5794, 2018.

[56] P. Tundo and M. Selva, "The chemistry of dimethyl carbonate," *Acc. Chem. Res.*, vol. 35, no. 9, pp. 706–716, 2002.

[57] F. F. T. De Groot *et al.*, "The industrial production of dimethyl carbonate from methanol and carbon dioxide," *Chem. Eng. Trans.*, vol. 39, no. Special Issue, pp. 1561–1566, 2014.

[58] C. Arcoumanis, C. Bae, R. Crookes, and E. Kinoshita, "The potential of di-methyl ether (DME) as an alternative fuel for compression-ignition engines: A review," *Fuel*, vol. 87, no. 7. Elsevier, pp. 1014–1030, 2008.

[59] E. Alper and O. Yuksel Orhan, "CO2 utilization: Developments in conversion processes," *Petroleum*, vol. 3, no. 1, pp. 109–126, 2016.

[60] S. Iijima, "Helical microtubules of graphitic carbon," *Nature*, vol. 354, no. 6348, pp. 56–58, Nov. 1991.

[61] R. T. K. Baker, P. S. Harris, R. B. Thomas, and R. J. Waite, "Formation of filamentous carbon from iron, cobalt and chromium catalyzed decomposition of acetylene," *J. Catal.*, vol. 30, no. 1, pp. 86–95, 1973.

[62] R. T. K. Baker, J. J. Chludzinski, N. S. Dudash, and A. J. Simoens, "The formation of filamentous carbon from decomposition of acetylene over vanadium and molybdenum," *Carbon N. Y.*, vol. 21, no. 5, pp. 463–468, 1983.

[63] A. Oberlin, M. Endo, and T. Koyama, "Filamentous growth of carbon through benzene decomposition," *J. Cryst. Growth*, vol. 32, no. 3, pp. 335–349, 1976.

[64] P. Harris, "Transmission Electron Microscopy of Carbon: A Brief History," *C*, vol. 4, no. 1, p. 4, 2018.

[65] Y. M. Manawi, Ihsanullah, A. Samara, T. Al-Ansari, and M. A. Atieh, "A review of carbon nanomaterials' synthesis via the chemical vapor deposition (CVD) method," *Materials (Basel).*, vol. 11, no. 5, 2018.

[66] M. S. D. Ado Jorio, Gene Dresselhaus, *Carbon Nanotubes Advanced Topics in the*

Synthesis, Structure, Properties and Applications, vol. 111. 2007.

[67] R. S. at al. Ruoff and D. C. Lorents, "Mechanical and thermal properties of carbon nanotubes," *Carbon N. Y.*, vol. 33, no. 7, pp. 925–930, 1995.

[68] A. C. Grimsdale, J. Wu, and K. Müllen, "New carbon-rich materials for electronics, lithium battery, and hydrogen storage applications," *Chem. Commun.*, no. 17, pp. 2197–2204, 2005.

[69] P. Serp, M. Corrias, and P. Kalck, "Carbon nanotubes and nanofibers in catalysis," *Appl. Catal. A Gen.*, vol. 253, no. 2, pp. 337–358, 2003.

[70] S. Frank, P. Poncharal, Z. L. Wang, and W. A. de Heer, "Carbon nanotube quantum resistors," *Sci. (Washington, D. C.)*, vol. 280, no. 5370, pp. 1744–1746, 1998.

[71] F. Cheng, Z. Tao, J. Liang, and J. Chen, "Template-Directed Materials for Rechargeable Lithium-Ion Batteries," *Chem. Mater.*, vol. 20, no. 3, pp. 667–681, 2008.

[72] P. Simon and Y. Gogotsi, "Materials for electrochemical capacitors," *Nat. Mater.*, vol. 7, no. 11, pp. 845–854, 2008.

[73] S. Uemura *et al.*, "CARBON NANOTUBE EMITTERS FOR FIELD EMISSION DISPLAYS," in *IEEE/CPMT/SEMI. 28th International Electronics Manufacturing Technology Symposium (Cat. No.03CH37479)*, 2003.

[74] H. Nishijima *et al.*, "Carbon-nanotube tips for scanning probe microscopy: Preparation by a controlled process and observation of deoxyribonucleic acid," *Appl. Phys. Lett.*, vol. 74, no. 26, pp. 4061–4063, 1999.

[75] K. S. Karimov, F. A. Khalid, and M. T. S. Chani, "Carbon nanotubes based strain sensors," *Meas. J. Int. Meas. Confed.*, vol. 45, no. 5, pp. 918–921, 2012.

[76] K. Balasubramanian and M. Burghard, "Biosensors based on carbon nanotubes," *Anal. Bioanal. Chem.*, vol. 385, no. 3, pp. 452–468, 2006.

[77] X. Qu, P. J. J. Alvarez, and Q. Li, "Applications of nanotechnology in water and wastewater treatment," *Water Res.*, vol. 47, pp. 3931–3946, 013.

[78] G. Mittal, V. Dhand, K. Y. Rhee, S. J. Park, and W. R. Lee, "A review on carbon

nanotubes and graphene as fillers in reinforced polymer nanocomposites," *J. Ind. Eng. Chem.*, vol. 21, pp. 11–25, 2015.

[79] S. Inoue, S. Lojindarat, T. Kawamoto, Y. Matsumura, and T. Charinpanitkul, "Spontaneous and controlled-diameter synthesis of single-walled and few-walled carbon nanotubes," *Chem. Phys. Lett.*, vol. 699, pp. 88–92, 2018.

[80] J. Doh and J. Lee, "Prediction of the mechanical behavior of double walled-CNTs using a molecular mechanics-based finite element method: Effects of chirality," *Comput. Struct.*, vol. 169, pp. 91–100, 2016.

[81] J. Huang, Q. Zhang, M. Zhao, and F. Wei, "Process intensification by CO2 for high quality carbon nanotube forest growth: Double-walled carbon nanotube convexity or single-walled carbon nanotube bowls?," *Nano Res.*, vol. 2, no. 11, pp. 872–881, 2009.

[82] A. Eatemadi *et al.*, "Carbon nanotubes: Properties, synthesis, purification, and medical applications," *Nanoscale Res. Lett.*, vol. 9, pp. 1–13, 2014.

[83] A. Aqel, K. M. M. A. El-Nour, R. A. A. Ammar, and A. Al-Warthan, "Carbon nanotubes, science and technology part (I) structure, synthesis and characterisation," *Arab. J. Chem.*, vol. 5, no. 1, pp. 1–23, 2012.

[84] N. Arora and N. N. Sharma, "Arc discharge synthesis of carbon nanotubes: Comprehensive review," *Diamond and Related Materials*, vol. 50. Elsevier B.V., pp. 135–150, 2014.

[85] C. T. Kingston and B. Simard, "Fabrication of Carbon Nanotubes," *Anal. Lett.*, vol. 36, no. 15, pp. 3119–3145, 2003.

[86] M. Loos, "Production of CNTs and Risks to Health," in *Carbon Nanotube Reinforced Composites*, Elsevier, 2015, pp. 103–123.

[87] T. Guo, P. Nikolaev, A. Thess, D. T. Colbert, and R. E. Smalley, "Catalytic growth of single-walled manotubes by laser vaporization," *Chem. Phys. Lett.*, vol. 243, no. 1–2, pp. 49–54, Sep. 1995.

[88] S. D. Mhlanga, K. C. Mondal, N. Naidoo, N. Kunjuzwa, M. J. Witcomb, and N. J. Coville,

"Synthesis and study of carbon microspheres for use as catalyst support for cobalt," *S. Afr. J. Sci.*, vol. 105, no. 7–8, pp. 304–308, 2009.

[89] L. G. Vishwanathan, S. Bhowmik, and M. Sharon, "Natural Precursors for Synthesis of Carbon Nano Materials by Chemical Vapor Deposition Process: A Review," *Int. J. Sci. Res.*, vol. 7, no. 2, pp. 1475–1485, 2018.

[90] R. Kumar, R. K. Singh, and D. P. Singh, "Natural and waste hydrocarbon precursors for the synthesis of carbon based nanomaterials: Graphene and CNTs," *Renew. Sustain. Energy Rev.*, vol. 58, pp. 976–1006, 2016.

[91] W. Z. Li *et al.*, "Large-scale synthesis of aligned carbon nanotubes," *Science (80-.).*, vol. 274, no. 5293, pp. 1701–1703, 1996.

[92] K. Hernadi, A. Fonseca, J. B. Nagy, D. Bernaerts, and A. A. Lucas, "Fe-catalyzed carbon nanotube formation," *Carbon N. Y.*, vol. 34, no. 10, pp. 1249–1257, 1996.

[93] I. Abdullahi, N. Sakulchaicharoen, and J. E. Herrera, "A mechanistic study on the growth of multi-walled carbon nanotubes by methane decomposition over nickel-alumina catalyst," *Diam. Relat. Mater.*, vol. 23, pp. 76–82, M2012.

[94] W. Yang, Y. Feng, and W. Chu, "Catalytic chemical vapor deposition of methane to carbon nanotubes: Copper promoted effect of Ni/MgO catalysts," *J. Nanotechnol.*, vol. 2014, 2014.

[95] A. Hussain *et al.*, "Floating catalyst CVD synthesis of single walled carbon nanotubes from ethylene for high performance transparent electrodes," *Nanoscale*, vol. 10, no. 20, pp. 9752–9759, 2018.

[96] S. C. Lyu *et al.*, "Large-scale synthesis of high-quality double-walled carbon nanotubes by catalytic decomposition of n-hexane," *J. Phys. Chem. B*, vol. 108, no. 5, pp. 1613–1616, 2004.

[97] R. Sen, A. Govindaraj, and C. N. R. Rao, "Carbon nanotubes by the metallocene route," *Chem. Phys. Lett.*, vol. 267, no. 3–4, pp. 276–280, 1997.

[98] S. Maruyama, R. Kojima, Y. Miyauchi, S. Chiashi, and M. Kohno, "Low-temperature

synthesis of high-purity single-walled carbon nanotubes from alcohol," *Chem. Phys. Lett.*, vol. 360, no. 3–4, pp. 229–234, 2002.

[99] Y. L. Li, L. H. Zhang, X. H. Zhong, and A. H. Windle, "Synthesis of high purity single-walled carbon nanotubes from ethanol by catalytic gas flow CVD reactions," *Nanotechnology*, vol. 18, no. 22, 2007.

[100] Y. AN, X. YUAN, S. CHENG, and X. GEN, "Carbon nanotube prepared from carbon monoxide by CVD method and its application as electrode materials," *Rare Met.*, vol. 25, no. 6 SUPPL. 2, pp. 73–76, 2006.

[101] E. V. Shlyakhova, N. F. Yudanov, A. V. Okotrub, Y. V. Shubin, L. I. Yudanova, and L. G. Bulusheva, "Growth of carbon nanotubes via chemical vapor deposition on Co catalyst nanoparticles dispersed in CaO," *Inorg. Mater.*, vol. 44, no. 3, pp. 213–218, 2008.

[102] V. Jourdain and C. Bichara, "Current understanding of the growth of carbon nanotubes in catalytic chemical vapour deposition," *Carbon*, vol. 58. Elsevier Ltd, pp. 2–39, 2013.

[103] J. P. Tessonnier and D. S. Su, "Recent progress on the growth mechanism of carbon nanotubes: A review," *ChemSusChem*, vol. 4, no. 7, pp. 824–847, 2011.

[104] R. E. Morjan, O. A. Nerushev, M. Sveningson, F. Rohmund, L. K. L. Falk, and E. E. B. Campbell, "Growth of carbon nanotubes from C60," *Appl. Phys. A Mater. Sci. Process.*, vol. 78, no. 3, pp. 253–261, 2004.

[105] O. A. Nerushev, S. Dittmar, R. E. Morjan, F. Rohmund, and E. E. B. Campbell, "Particle size dependence and model for iron-catalyzed growth of carbon nanotubes by thermal chemical vapor deposition," *J. Appl. Phys.*, vol. 93, no. 7, pp. 4185–4190, 2003.

[106] K. A. Shah and B. A. Tali, "Synthesis of carbon nanotubes by catalytic chemical vapour deposition: A review on carbon sources, catalysts and substrates," *Materials Science in Semiconductor Processing*, vol. 41. Elsevier, pp. 67–82, 2016.

[107] D. Yuan, L. Ding, H. Chu, Y. Feng, T. P. McNicholas, and J. Liu, "Horizontally aligned single-walled carbon nanotube on quartz from a large variety of metal catalysts," *Nano Lett.*, vol. 8, no. 8, pp. 2576–2579, 2008.

[108] M. Kumar and Y. Ando, “Chemical Vapor Deposition of Carbon Nanotubes: A Review on Growth Mechanism and Mass Production,” *J. Nanosci. Nanotechnol.*, vol. 10, no. 6, pp. 3739–3758, 2010.

[109] X.-D. Wang, K. Vinodgopal, and G.-P. Dai, “Synthesis of Carbon Nanotubes by Catalytic Chemical Vapor Deposition,” *Intech*. 2019.

[110] M. Motiei, Y. R. Hacohen, J. Calderon-Moreno, and A. Gedanken, “Preparing carbon nanotubes and nested fullerenes from supercritical CO2by a chemical reaction [16],” *Journal of the American Chemical Society*, vol. 123, no. 35. pp. 8624–8625, 2001.

[111] T. Belin and F. Epron, “Characterization methods of carbon nanotubes: A review,” *Materials Science and Engineering B: Solid-State Materials for Advanced Technology*, vol. 119, no. 2. pp. 105–118, 2005.

[112] M. S. Dresselhaus, G. Dresselhaus, R. Saito, and A. Jorio, “Raman spectroscopy of carbon nanotubes,” *Physics Reports*, vol. 409. p. 47, 2005.

[113] C. Herrero-Latorre, J. Álvarez-Méndez, J. Barciela-García, S. García-Martín, and R. M. Peña-Crecente, “Characterization of carbon nanotubes and analytical methods for their determination in environmental and biological samples: A review,” *Analytica Chimica Acta*, vol. 853, no. 1. pp. 77–94, 2015.

[114] Z. Lou, C. Chen, Q. Chen, and J. Gao, “Formation of variously shaped carbon nanotubes in carbon dioxide-alkali metal (Li, Na) system,” *Carbon N. Y.*, vol. 43, no. 5, pp. 1104–1108, 2005.

[115] Y. Yang, H. Zhang, and Y. Yan, “Synthesis of CNTs on stainless steel microfibrous composite by CVD: Effect of synthesis condition on carbon nanotube growth and structure,” *Compos. Part B Eng.*, vol. 160, pp. 369–383, 2019.

[116] H. Zhang, X. Zhang, X. Sun, and Y. Ma, “Shape-controlled synthesis of nanocarbons through direct conversion of carbon dioxide,” *Sci. Rep.*, vol. 3, pp. 1–8, 2013.

[117] Z. Lou, C. Chen, H. Huang, and D. Zhao, “Fabrication of Y-junction carbon nanotubes by reduction of carbon dioxide with sodium borohydride,” *Diam. Relat. Mater.*, vol. 15, no. 10, pp. 1540–1543, 2006.

[118] W. M. Silva *et al.*, "Surface properties of oxidized and aminated multi-walled carbon nanotubes," *J. Braz. Chem. Soc.*, vol. 23, no. 6, pp. 1078–1086, 2012.

[119] A. C. Ferrari and J. Robertson, "Interpretation of Raman spectra of disordered and amorphous carbon A.," *Phys. Rev. B*, vol. 61, no. 20, pp. 14095–14106, 2000.

[120] X. j. Xu and S. ming Huang, "Carbon dioxide as a carbon source for synthesis of carbon nanotubes by chemical vapor deposition," *Mater. Lett.*, vol. 61, no. 21, pp. 4235–4237, 2007.

[121] G. Allaedini, S. M. Tasirin, and P. Aminayi, "Synthesis of CNTs via chemical vapor deposition of carbon dioxide as a carbon source in the presence of NiMgO," *J. Alloys Compd.*, vol. 647, pp. 809–814, 2015.

[122] G. S. Simate *et al.*, "Kinetic model of carbon nanotube production from carbon dioxide in a floating catalytic chemical vapour deposition reactor," *RSC Adv.*, vol. 4, no. 19, pp. 9564–9572, 2014.

[123] W. Z. Li, J. G. Wen, Y. Tu, and Z. F. Ren, "Effect of gas pressure on the growth and structure of carbon nanotubes by chemical vapor deposition," *Appl. Phys. A Mater. Sci. Process.*, vol. 73, no. 2, pp. 259–264, 2001.

[124] R. K. Garg, S. S. Kim, D. B. Hash, J. P. Gore, and T. S. Fisher, "Effects of Feed Gas Composition and Catalyst Thickness on Carbon Nanotube and Nanofiber Synthesis by Plasma Enhanced Chemical Vapor Deposition," *J. Nanosci. Nanotechnol.*, vol. 8, no. 6, pp. 3068–3076, 2008.

[125] G. Allaedini, S. M. Tasirin, and P. Aminayi, "Yield optimization of nanocarbons prepared via chemical vapor decomposition of carbon dioxide using response surface methodology," *Diam. Relat. Mater.*, vol. 66, pp. 196–205, 2016.

[126] K. Y. Lee, W. M. Yeoh, S. P. Chai, S. Ichikawa, and A. R. Mohamed, "Optimization of carbon nanotubes synthesis via methane decomposition over alumina-based catalyst," *Fullerenes Nanotub. Carbon Nanostructures*, vol. 18, no. 3, pp. 273–284, 2010.

[127] C. H. See, K. J. MacKenzie, O. M. Dunens, and A. T. Harris, "Multi-parameter optimisation of carbon nanotube synthesis in fluidised-beds," *Chem. Eng. Sci.*, vol. 64, no.

16, pp. 3614–3621, 2009.

[128] K. M. Bower, “What Is Design of Experiments (DOE)? | ASQ,” *ASQ*. [Online]. Available: https://asq.org/quality-resources/design-of-experiments. [Accessed: 22-Mar-2021].

[129] Á. Kukovecz, D. Méhn, E. Nemes-Nagy, R. Szabó, and I. Kiricsi, “Optimization of CCVD synthesis conditions for single-wall carbon nanotubes by statistical design of experiments (DoE),” *Carbon N. Y.*, vol. 43, no. 14, pp. 2842–2849, 2005.

[130] C. Yuangyai and H. B. Nembhard, “Design of experiments: A key to innovation in nanotechnology,” in *Emerging Nanotechnologies for Manufacturing*, Second., Elsevier Science, 2014, pp. 230–254.

[131] K. Hata, D. N. Futaba, K. Mizuno, T. Namai, M. Yumura, and S. Iijima, “Water-assisted highly efficient synthesis of impurity-free single-walled carbon nanotubes,” *Science (80-.).*, vol. 306, no. 5700, pp. 1362–1364, 2004.

[132] A. Magrez, J. W. Seo, V. L. Kuznetsov, and L. Forró, “Evidence of an equimolar C2H2-CO2 reaction in the synthesis of carbon nanotubes,” *Angew. Chemie - Int. Ed.*, vol. 46, no. 3, pp. 441–444, 2007.

[133] Q. Wen, W. Qian, F. Wei, Y. Liu, G. Ning, and Q. Zhang, “CO2-assisted SWNT growth on porous catalysts,” *Chem. Mater.*, vol. 19, no. 6, pp. 1226–1230, 2007.

[134] M. Johnson *et al.*, “Carbon nanotube wools made directly from CO2 by molten electrolysis: Value driven pathways to carbon dioxide greenhouse gas mitigation,” *Mater. Today Energy*, vol. 5, pp. 230–236, 2017.

[135] J. Ren, J. Lau, M. Lefler, and S. Licht, “The Minimum Electrolytic Energy Needed to Convert Carbon Dioxide to Carbon by Electrolysis in Carbonate Melts,” *J. Phys. Chem. C*, vol. 119, no. 41, pp. 23342–23349, 2015.

[136] J. Ren, F. F. Li, J. Lau, L. González-Urbina, and S. Licht, “One-Pot Synthesis of Carbon Nanofibers from CO2,” *Nano Lett.*, vol. 15, no. 9, pp. 6142–6148, 2015.

[137] J. Ren, M. Johnson, R. Singhal, and J. Licht, “Transformation of the greenhouse gas CO2 by molten electrolysis into a wide controlled selection of carbon nanotubes,” *J. CO2 Util.*,

vol. 18, pp. 335–344, 2017.

[138] M. Johnson, J. Ren, M. Lefler, G. Licht, J. Vicini, and S. Licht, “Data on SEM, TEM and Raman Spectra of doped, and wool carbon nanotubes made directly from CO2 by molten electrolysis,” *Data Br.*, vol. 14, pp. 592–606, 2017.

[139] A. Douglas, R. Carter, N. Muralidharan, L. Oakes, and C. L. Pint, “Iron catalyzed growth of crystalline multi-walled carbon nanotubes from ambient carbon dioxide mediated by molten carbonates,” *Carbon N. Y.*, vol. 116, pp. 572–578, 2017.

[140] R. S. Wagner and W. C. Ellis, “Vapor-liquid-solid mechanism of single crystal growth,” *Appl. Phys. Lett.*, vol. 4, no. 5, pp. 89–90, 1964.

[141] S. Santangelo, G. Messina, G. Faggio, M. Lanza, A. Pistone, and C. Milone, “Calibration of reaction parameters for the improvement of thermal stability and crystalline quality of multi-walled carbon nanotubes,” *J. Mater. Sci.*, vol. 45, no. 3, pp. 783–792, 2010.

[142] S. A. Khorrami and R. Lotfi, “Influence of carrier gas flow rate on carbon nanotubes growth by TCVD with Cu catalyst,” *J. Saudi Chem. Soc.*, vol. 20, no. 4, pp. 432–436, 2016.

[143] N. Tripathi, P. Mishra, H. Harsh, and S. S. Islam, “Fine-tuning control on CNT diameter distribution, length and density using thermal CVD growth at atmospheric pressure: an in-depth analysis on the role of flow rate and flow duration of acetylene (C2H2) gas,” *Appl. Nanosci.*, vol. 5, no. 1, pp. 19–28, 2015.

[144] D. Takagi, Y. Homma, H. Hibino, S. Suzuki, and Y. Kobayashi, “Single-walled carbon nanotube growth from highly activated metal nanoparticles,” *Nano Lett.*, vol. 6, no. 12, pp. 2642–2645, 2006.

[145] Y. Qian, C. Wang, G. Ren, and B. Huang, “Surface growth of single-walled carbon nanotubes from ruthenium nanoparticles,” *Appl. Surf. Sci.*, vol. 256, no. 12, pp. 4038–4041, 2010.

[146] Y. Li *et al.*, “How catalysts affect the growth of single-walled carbon nanotubes on substrates,” *Adv. Mater.*, vol. 22, no. 13, pp. 1508–1515, 2010.

[147] L. Bilu *et al.*, “Manganese-catalyzed surface growth of single-walled carbon nanotubes with high efficiency,” *J. Phys. Chem. C*, vol. 112, no. 49, pp. 19231–19235, 2008.

[148] P. K. Avti, Y. Talukdar, M. V. Sirotkin, K. R. Shroyer, and B. Sitharaman, “Toward single-walled carbon nanotube-gadolinium complex as advanced MRI contrast agents: Pharmacodynamics and global genomic response in small animals,” *J. Biomed. Mater. Res. - Part B Appl. Biomater.*, vol. 101 B, no. 6, pp. 1039–1049, Aug. 2013.

[149] C. L. Cheung, A. Kurtz, H. Park, and C. M. Lieber, “Diameter-controlled synthesis of carbon nanotubes,” *J. Phys. Chem. B*, vol. 106, no. 10, pp. 2429–2433, 2002.

[150] E. F. Kukovitsky, S. G. L’vov, N. A. Sainov, V. A. Shustov, and L. A. Chernozatonskii, “Correlation between metal catalyst particle size and carbon nanotube growth,” *Chem. Phys. Lett.*, vol. 355, no. 5–6, pp. 497–503, 2002.

[151] V. I. Merkulov, D. H. Lowndes, Y. Y. Wei, G. Eres, and E. Voelkl, “Patterned growth of individual and multiple vertically aligned carbon nanofibers,” *Appl. Phys. Lett.*, vol. 76, no. 24, pp. 3555–3557, 2000.

[152] X. Z. Liao, A. Serquis, Q. X. Jia, D. E. Peterson, Y. T. Zhu, and H. F. Xu, “Effect of catalyst composition on carbon nanotube growth,” *Appl. Phys. Lett.*, vol. 82, no. 16, pp. 2694–2696, 2003.

[153] U. Narkiewicz, M. Podsiadły, R. Jędrzejewski, and I. Pełech, “Catalytic decomposition of hydrocarbons on cobalt, nickel and iron catalysts to obtain carbon nanomaterials,” *Appl. Catal. A Gen.*, vol. 384, no. 1–2, pp. 27–35, 2010.

[154] S. D. Mhlanga, . M. K. C., M. J. Carter R., Witcomb, and N. J. Coville, “The effect of synthesis parameters on the catalytic synthesis of multiwalled carbon nanotubes using Fe-Co/CaCO3 catalysts,” *S. Afr. J. Chem.*, vol. 62, pp. 67–76, 2009.

[155] H. Kathyayini, N. Nagaraju, A. Fonseca, and J. B. Nagy, “Catalytic activity of Fe, Co and Fe/Co supported on Ca and Mg oxides, hydroxides and carbonates in the synthesis of carbon nanotubes,” *J. Mol. Catal. A Chem.*, vol. 223, no. 1–2, pp. 129–136, 2004.

[156] D. Hardeman *et al.*, “The synergistic effect in the Fe-Co bimetallic catalyst system for the growth of carbon nanotube forests,” *J. Appl. Phys.*, vol. 117, no. 4, p. 044308, 2015.

[157] T. Tsoufis *et al.*, "Catalytic production of carbon nanotubes over Fe-Ni bimetallic catalysts supported on MgO," *Diamond and Related Materials*, vol. 16. pp. 155–160, 2007.

[158] Eskom, "Coal Power." [Online]. Available: https://www.eskom.co.za/AboutElectricity/ElectricityTechnologies/Pages/Coal_Power.aspx. [Accessed: 19-Oct-2020].

[159] "South Africa Coal Reserves and Consumption Statistics - Worldometer." [Online]. Available: https://www.worldometers.info/coal/south-africa-coal/. [Accessed: 20-Oct-2020].

[160] M. Steyn and R. C. A. Minnitt, "Thermal coal products in South Africa," *J. South. African Inst. Min. Metall.*, vol. 110, no. 10, pp. 593–599, 2010.

[161] R. Falcon and A. J. Ham, "Characteristics of Southern African Coals.," *J. South African Inst. Min. Metall.*, vol. 88, no. 5, pp. 145–161, 1988.

[162] S. V. Vassilev, K. Kitano, and C. G. Vassileva, "Some relationships between coal rank and chemical and mineral composition," *Fuel*, vol. 75, no. 13, pp. 1537–1542, 1996.

[163] I. Suárez-Ruiz and J. Crelling, *Applied coal petrology*. Elsevier Ltd, 2008.

[164] H. M. King, "Coal: Anthracite, Bituminous, Coke, Pictures, Formation, Uses." [Online]. Available: https://geology.com/rocks/coal.shtml. [Accessed: 06-Feb-2020].

[165] J. C. Crelling, "Coal Carbonization," in *Applied Coal Petrology*, I. Suárez-Ruiz and J. C. Crelling, Eds. Burlington: Elsevier, 2008, pp. 173–192.

[166] S. V Vassilev and C. G. Vassileva, "A new approach for the combined chemical and mineral classification of the inorganic matter in coal. 1. Chemical and mineral classification systems," *Fuel*, vol. 88, no. 2, pp. 235–245, 2009.

[167] S. Bilgen, "The environmental effects of coal-related activities," *Energy Sources, Part A Recover. Util. Environ. Eff.*, vol. 38, no. 22, pp. 3283–3289, 2016.

[168] S. V. Vassilev, K. Kitano, S. Takeda, and T. Tsurue, "Influence of mineral and chemical composition of coal ashes on their fusibility," *Fuel Process. Technol.*, vol. 45, no. 1, pp.

27–51, 1995.

[169] M. Sager, “Environmental aspects of trace elements in coal combustion,” *Toxicol. Environ. Chem.*, vol. 71, no. 1–2, pp. 159–183, 1999.

[170] R. H. Matjie, Z. Li, C. R. Ward, J. R. Bunt, and C. A. Strydom, “Determination of mineral matter and elemental composition of individual macerals in coals from Highveld mines,” *J. South. African Inst. Min. Metall.*, vol. 116, no. 2, pp. 169–180, 2016.

[171] N. Lior, “Sustainable energy development: The present (2009) situation and possible paths to the future,” *Energy*, vol. 35, no. 10, pp. 3976–3994, 2010.

[172] IEA, “Coal – World Energy Outlook 2019,” Paris, 2019.

[173] Z. T. Yao *et al.*, “A comprehensive review on the applications of coal fly ash,” *Earth-Science Rev.*, vol. 141, pp. 105–121, 2015.

[174] D. Coil, E. Mckittrick, and B. Hig, “Coal Combustion Methods.” pp. 1–2, 2014.

[175] B. K. Saikia, B. Mahanta, U. N. Gupta, O. P. Sahu, P. Saikia, and B. P. Baruah, “Mineralogical composition and ash geochemistry of raw and beneficiated high sulfur coals,” *J. Geol. Soc. India*, vol. 88, no. 3, pp. 339–349, 2016.

[176] L. Bartoňová, “Unburned carbon from coal combustion ash: An overview,” *Fuel Process. Technol.*, vol. 134, pp. 136–158, 2015.

[177] R. S. Blissett and N. A. Rowson, “A review of the multi-component utilisation of coal fly ash,” *Fuel*, vol. 97, pp. 1–23, 2012.

[178] S. Wang, “Application of solid ash based catalysts in heterogeneous catalysis,” *Environ. Sci. Technol.*, vol. 42, no. 19, pp. 7055–7063, 2008.

[179] M. Rycroft, “Exploring the many uses of fly ash,” *Energize*, vol. November 2. pp. 1–6, 2017.

[180] J. Alegbe, O. S. Ayanda, P. Ndungu, N. Alexander, O. O. Fatoba, and L. F. Petrik, “Chemical, Mineralogical and Morphological Investigation of Coal Fly Ash Obtained from Mpumalanga Province, South Africa,” *Res. J. Environ. Sci.*, vol. 12, no. 3, pp. 98–105, 2018.

[181] N. Ghazali, K. Muthusamy, and S. Wan Ahmad, “Utilization of Fly Ash in Construction,” *IOP Conf. Ser. Mater. Sci. Eng.*, vol. 601, no. 1, 2019.

[182] H. J. H. Brouwers and R. J. Van Eijk, “Fly ash reactivity: Extension and application of a shrinking core model and thermodynamic approach,” *J. Mater. Sci.*, vol. 37, no. 10, pp. 2129–2141, 2002.

[183] S. V. Vassilev and C. G. Vassileva, “Methods for characterization of composition of fly ashes from coal-fired power stations: A critical overview,” *Energy and Fuels*, vol. 19, no. 3. pp. 1084–1098, 2005.

[184] G. Xu and X. Shi, “Characteristics and applications of fly ash as a sustainable construction material: A state-of-the-art review,” *Resour. Conserv. Recycl.*, vol. 136, pp. 95–109, 2018.

[185] A. Binal, “The Effects of High Alkaline Fly Ash on Strength Behaviour of a Cohesive Soil,” *Adv. Mater. Sci. Eng.*, vol. 2016, p. 11, 2016.

[186] ASTM 618, *Standard Specification for Coal Fly Ash and Raw or Calcined Natural Pozzolan for Use in Concrete*. ASTM International, 2005.

[187] B. Ramme and M. Tharaniyil, *Coal combustion products utilisation handbook*, Third. WE Energies, 2013.

[188] V. C. Pandey and N. Singh, “Impact of fly ash incorporation in soil systems,” *Agriculture, Ecosystems and Environment*, vol. 136, no. 1–2. Elsevier, pp. 16–27, 2010.

[189] M. Basu, M. Pande, P. B. S. Bhadoria, and S. C. Mahapatra, “Potential fly-ash utilization in agriculture: A global review,” *Progress in Natural Science*, vol. 19, no. 10. Science Press, pp. 1173–1186, 2009.

[190] L. C. Ram *et al.*, “Leaching behavior of lignite fly ash with shake and column tests,” *Environ. Geol.*, vol. 51, no. 7, pp. 1119–1132, 2007.

[191] L. C. Ram *et al.*, “Management of mine spoil for crop productivity with lignite fly ash and biological amendments,” *J. Environ. Manage.*, vol. 79, no. 2, pp. 173–187, 2006.

[192] R. Sikka and B. D. Kansal, “Effect of fly-ash application on yield and nutrient composition of rice, wheat and on pH and available nutrient status of soils,” *Bioresour.*

Technol., vol. 51, no. 2–3, pp. 199–203, 1995.

[193] A. C. Chang, L. J. Lund, A. L. Page, and J. E. Warneke, "Physical properties of fly ash amended soils," *J. Environ. Qual.*, vol. 6, no. 3, pp. 267–270, 1977.

[194] J. Prabakar, N. Dendorkar, and R. K. Morchhale, "Influence of fly ash on strength behavior of typical soils," *Constr. Build. Mater.*, vol. 18, no. 4, pp. 263–267, 2004.

[195] J. Lehmann and G. Schroth, "Chapter 7 Nutrient Leaching," in *Trees, Crops and Soil Fertility*, 2003.

[196] M. Ghodrati, J. T. Sims, and B. L. Vasilas, "Evaluation of fly ash as a soil amendment for the Atlantic Coastal Plain: I. Soil hydraulic properties and elemental leaching," *Water, Air, Soil Pollut.*, vol. 81, no. 3–4, pp. 349–361, 1995.

[197] M. R. Khan and M. W. Khan, "The effect of fly ash on plant growth and yield of tomato," *Environ. Pollut.*, vol. 92, no. 2, pp. 105–111, 1996.

[198] A. A. Elseewi, F. T. Bingham, and A. L. Page, "Availability of sulfur in fly ash to plants," *J. Environ. Qual.*, vol. 7, no. 1, pp. 69–73, 1978.

[199] S. K. Sharma and N. Kalra, "Effect of flyash incorporation on soil properties and productivity of crops: A review," *Journal of Scientific and Industrial Research*, vol. 65, no. 5. pp. 383–390, 2006.

[200] D. C. Adriano, T. A. Woodford, and T. G. Ciravolo, "Growth and Elemental Composition of Corn and Bean Seedlings as Influenced by Soil Application of Coal Ash," *J. Environ. Qual.*, vol. 7, no. 3, pp. 416–421, 1978.

[201] K. K. Panday, G. Prasad, and V. N. Singh, "Mixed adsorbents for Cu(II) removal from aqueous solutions," *Environ. Technol. Lett.*, vol. 7, no. 1–12, pp. 547–554, 1986.

[202] H. Polat, A. Vengosh, I. Pankratov, and M. Polat, "A new methodology for removal of boron from water by coal and fly ash," *Desalination*, vol. 164, no. 2, pp. 173–188, 2004.

[203] H. Cho, D. Oh, and K. Kim, "A study on removal characteristics of heavy metals from aqueous solution by fly ash," *J. Hazard. Mater.*, vol. 127, no. 1–3, pp. 187–195, 2005.

[204] Z. Aksu and J. Yener, "The usage of dried activated sludge and fly ash wastes in phenol

biosorption/adsorption: Comparison with granular activated carbon," *J. Environ. Sci. Heal. - Part A Toxic/Hazardous Subst. Environ. Eng.*, vol. 34, no. 9, pp. 1777–1796, 1999.

[205] H. Joo Kim, H. Raj Pant, J. Hee Kim, N. Jung Choi, and C. Sang Kim, "Fabrication of multifunctional TiO2-fly ash/polyurethane nanocomposite membrane via electrospinning," *Ceram. Int.*, vol. 40, no. 2, pp. 3023–3029, 2014.

[206] D. Mohan, K. P. Singh, G. Singh, and K. Kumar, "Removal of Dyes from Wastewater Using Flyash, a Low-Cost.pdf," *Ind. Eng. Chem. Res.*, vol. 41, no. 15, pp. 3688–3695, 2002.

[207] M. J. McCarthy and R. K. Dhir, "Development of high volume fly ash cements for use in concrete construction," in *Fuel*, vol. 84, no. 11, pp. 1423–1432, 2005.

[208] B. Felekoglu, "Utilisation of Turkish fly ashes in cost effective HVFA concrete production," *Fuel*, vol. 85, no. 12–13, pp. 1944–1949, 2006.

[209] J. C. Swanepoel and C. A. Strydom, "Utilisation of fly ash in a geopolymeric material," in *Applied Geochemistry*, 2002, vol. 17, no. 8, pp. 1143–1148.

[210] P. Nath and P. K. Sarker, "Use of OPC to improve setting and early strength properties of low calcium fly ash geopolymer concrete cured at room temperature," *Cem. Concr. Compos.*, vol. 55, pp. 205–214, 2015.

[211] J. Temuujin, A. Van Riessen, and K. J. D. MacKenzie, "Preparation and characterisation of fly ash based geopolymer mortars," *Constr. Build. Mater.*, vol. 24, no. 10, pp. 1906–1910, 2010.

[212] B. Joseph and G. Mathew, "Influence of aggregate content on the behavior of fly ash based geopolymer concrete," *Sci. Iran.*, vol. 19, no. 5, pp. 1188–1194, 2012.

[213] C. K. Ma, A. Z. Awang, and W. Omar, "Structural and material performance of geopolymer concrete: A review," *Construction and Building Materials*, vol. 186. Elsevier Ltd, pp. 90–102, 20-Oct-2018.

[214] D. Jain, C. Khatri, and A. Rani, "Fly ash supported calcium oxide as recyclable solid base catalyst for Knoevenagel condensation reaction," *Fuel Process. Technol.*, vol. 91, no. 9,

pp. 1015–1021, 2010.

[215] S. Mostafa, H. Asl, A. Ghadi, M. Sharifzadeh, and H. Javadian, “Porous catalysts fabricated from coal fly ash as cost-e ffective alternatives for industrial applications : A review,” *Fuel*, vol. 217. Elsevier, pp. 320–342, 2018.

[216] S. Wang and G. Q. Lu, “Effect of chemical treatment on ni/fly-ash catalysts in methane reforming with carbon dioxide,” *Studies in Surface Science and Catalysis*, vol. 167. pp. 275–280, 2007.

[217] O. M. Dunens, K. J. Mackenzie, and A. T. Harris, “Synthesis of Multiwalled Carbon Nanotubes on Fly Ash Derived Catalysts,” *Environ. Sci. Technol*, vol. 43, pp. 7889–7894, 2009.

[218] A. Yasui, Y. Kamiya, S. Sugiyama, S. Ono, H. Noda, and Y. Ichikawa, “Synthesis of carbon nanotubes on fly ashes by chemical vapor deposition processing,” *IEEJ Trans. Electr. Electron. Eng.*, vol. 4, no. 6, pp. 787–789, 2009.

[219] D. C. D. Nath and V. Sahajwalla, “Application of fly ash as a catalyst for synthesis of carbon nanotube ribbons,” *J. Hazard. Mater.*, vol. 192, pp. 691–697, 2011.

[220] N. A. Salah, “Method of forming carbon nanotubes from carbon-rich fly ash,” US 8,609,189 B2, 2013.

[221] N. Salah, A. A. Al-Ghamdi, A. Memic, S. S. Habib, and Z. H. Khan, “Formation of Carbon Nanotubes from Carbon-Rich Fly Ash: Growth Parameters and Mechanism,” *Mater. Manuf. Process.*, vol. 31, no. 2, pp. 146–156, 2016.

[222] K. M. Rambau, N. M. Musyoka, N. Manyala, J. Ren, H. W. Langmi, and M. K. Mathe, “Preparation of carbon nanofibers/tubes using waste tyres pyrolysis oil and coal fly ash derived catalyst,” *J. Environ. Sci. Heal. - Part A Toxic/Hazardous Subst. Environ. Eng.*, vol. 53, no. 12, pp. 1115–1122, 2018.

[223] N. Hintsho, A. Shaikjee, P. K. Tripathi, P. Franklyn, and S. Durbach, “The effect of CO2 on the CVD synthesis of carbon nanomaterials using fly ash as a catalyst,” *RSC Adv.*, vol. 5, no. 66, pp. 53776–53781, 2015.

[224] A. Dwivedi and M. K. Jain, “Fly ash – waste management and overview : A Review Fly ash – waste management and overview : A Review,” *Recent Res. Sci. Technol. 2014*, vol. 6, no. 1, pp. 30–35, 2014.

[225] D. Paswan, S. M. A, M. Shaikh, A. Nadar, and S. D. Maniyar, “Heavy Metals in Fly Ash ; Its Impact on Human Health and Environment,” in *NICMAR 2nd International Conference On Construction, Real Estate, Infrastructure and Project (CRIP) Managemen*, 2017.

[226] B. Lokeshappa, “Disposal and Management of Flyash,” *2011 Int. Conf. Life Sci. Technol.*, vol. 3, no. 2011, pp. 11–14, 2012.

[227] I. Strapáč, Z. Bedlovičová, and M. Baranová, “Edible Spruce (Morchella esculenta), Accumulator of Toxic Elements in the Environment,” *Folia Vet.*, vol. 63, no. 2, pp. 55–59, 2019.

[228] S. K. Ritter, “A New Life For Coal Ash| Chemical & Engineering News,” *American Chemical Society*, vol. 94, no. 7, pp. 10–14, 2016.

[229] A. Kumar, S. R. Samadder, and V. Kumar, “Assessment of groundwater contamination risk due to fly ash leaching using column study,” *Environ. Earth Sci.*, vol. 78, no. 1, pp. 1–12, 2019.

[230] R. K. Singh, N. C. Gupta, and B. K. Guha, “Fly Ash Disposal in Ash Ponds: A Threat to Ground Water Contamination,” *J. Inst. Eng. Ser. A*, vol. 97, no. 3, pp. 255–260, 2016.

[231] I. Nawaz, “Disposal and Utilization of Fly Ash to Protect the Environment,” *Int. J. Innov. Res. Sci. Eng. Technol.*, vol. 2, no. 10, pp. 5259–5266, 2013.

[232] “12.4: Phase Diagrams - Chemistry LibreTexts.” [Online]. Available: https://chem.libretexts.org/Bookshelves/General_Chemistry/Map%3A_General_Chemistry_(Petrucci_et_al.)/12%3A_Intermolecular_Forces%3A_Liquids_And_Solids/12.4%3A_Phase_Diagrams. [Accessed: 16-Aug-2020].

[233] Center for Climate and Energy Solutions, “Global Emissions: Center for climate and energy solutions,” 2016. [Online]. Available: https://www.c2es.org/content/international-emissions/. [Accessed: 22-Dec-2019].

[234] Q. L. Yan, M. Gozin, F. Q. Zhao, A. Cohen, and S. P. Pang, “Highly energetic compositions based on functionalized carbon nanomaterials,” *Nanoscale*, vol. 8, no. 9. Royal Society of Chemistry, pp. 4799–4851, 2016.

[235] F. Goodarzi and H. Sanei, “Plerosphere and its role in reduction of emitted fine fly ash particles from pulverized coal-fired power plants,” *Fuel*, vol. 88, no. 2, pp. 382–386, 2009.

Chapter 3: Methodology

3.1 Introduction

This chapter outlines and describes the materials used and methods followed in this research study, the equipment and chemicals used are given and listed. The characterization techniques for the fly ash carbon nanomaterials are also explained and listed.

3.2 Materials

The gases used for CNT synthesis were argon (Ar) as a carrier gas and carbon dioxide (CO_2) and acetylene (C_2H_2) as precursor gases. These gases were obtained from AFROX (African Oxygen Limited) and they came with a certificate of analysis indicating the purity of 99.99 %. Post-combustion fly ash was obtained from Electricity Supply Commission (ESKOM) through Lafarge. Pre- combustion fly was sourced from Sasol in Secunda. The catalysts were used as received.

3.3 Synthesis of CNMs

Figure 3.1 depicts the CVD setup used to synthesize CNMs. Varying amounts of raw samples of fly ash were weighed and uniformly spread on a catalyst boat and placed inside the middle of the stainless-steel tube reactor in the CVD. The CVD furnace was set at different temperatures between 750-950 ℃. Argon gas was opened and flowed at 150 sccm. This was done to purge the furnace of any contaminants and detect any leakages from the gases to the reactor. Once the desired temperature was reached, the pressure of argon was increased to the desired value and CO_2 or acetylene was introduced into the CVD system as a carbon source. It flowed for a period of 60 minutes at a specified flow rate. Thereafter, the flow of CO_2 or acetylene was cut off and the furnace was allowed to cool down under the argon atmosphere for an hour, and then it was terminated. The furnace was further allowed to cool overnight to room temperature. The product was collected from the tubular furnace.

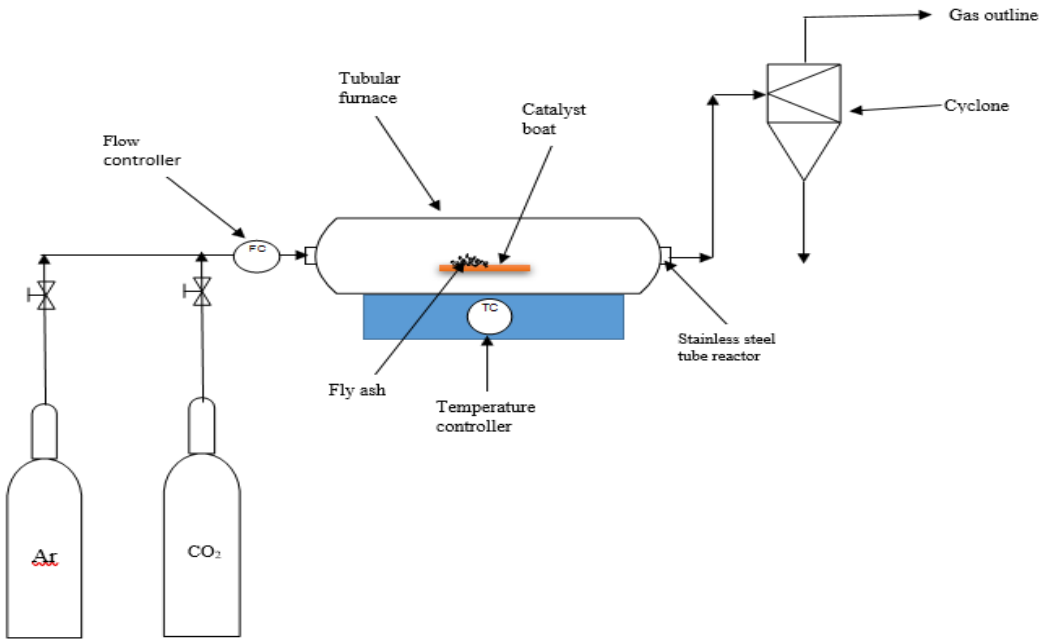


Figure 3.1: Chemical vapour deposition setup used in this study

3.4 Characterization Methods for fly ash and CNMs

A thorough description of the characterization methods used to analyse the two fly ash catalysts and CNMs in this study is given:

SEM, EDS, TGA, TEM, Raman Spectroscopy, XRD, XRF, and a particle size analyser.

3.4.1 Scanning Electron Microscopy (SEM)

The SEM technique is one of the most used characterization methods across many disciplines. In this study, it was used to visualize and examine the surface morphology, diameter, and length of nanomaterials with a very high resolution and a greater depth of field. The SEM micrographs were obtained using a ZEISS Sigma 300VP Field Emission Scanning Electron Microscopy (FESEM) and the images were obtained using ZEISS Smart SEM. It was operating at voltages of 8, 10, 15, and 20 kV. A small amount of the sample was placed on a carbon tape which was placed on a stub and coated twice with Gold and Palladium (Au/Pd). This was then introduced into the SEM.

3.4.2 Energy Dispersive Spectroscopy (EDS)

EDS is a chemical analysis technique in conjunction with SEM analysis. The information obtained from EDS can be used to quantitatively determine the elements present in a sample. One of the main advantages of EDS along with SEM and TEM is sample preparation. It is very minimal and they are not destructive techniques. In this study, a visible area of the fly ash sample was selected and analyzed, and subsequently, individual spheres and non-spherical fragments were also selected. This was done to compare the content of iron between the spherical and irregular particles. An Oxford instruments x-act PentaFET precision detector was used.

3.4.3 Thermogravimetric Analysis (TGA)

Generally, by-products like amorphous carbon are formed during the production of carbon nanomaterials, and impurities such as unreacted metal catalysts are present. Thus, investigating the quality and purity of CNMs is a crucial task for their applications. Thermal gravimetric analysis (TGA) is a destructive technique that is used to investigate the purity and yield of CNMs based on the decomposition temperature of the CNMs. This technique gives a curve of weight loss (%) vs. temperature (℃) and its derivative. From this curve, the quality and level of impurities are determined. The derivative thermogravimetry (DTG) was used to determine the distribution of particles and the quality of the CNMs. Thermal analysis of the CNMs was done using an SDT Q600 thermogravimetric analysis (TGA). This was conducted by using 10 mg of the catalyst, placed in an alumina crucible, and placed inside the TGA furnace. The decomposition took place in air and nitrogen flowing at 50 ml/cm^3 with the temperature increasing at a rate of 30 ℃/min until it reached 800 ℃.

3.4.4 Transmission Electron Microscopy (TEM)

The TEM technique gives information about the internal structure of the specimen. The number of walls, as well as the morphology and diameter of CNT, are obtained from the TEM. The CNMs were visualized on an FEI Tecnai T12 Transmission Electron Microscopy (TEM). To prepare the sample for analysis, the product was dissolved in 10 ml ethanol. It was subsequently sonicated for 10 minutes and a drop of the solution was subsequently deposited on a copper grip and placed on a lacy carbon film.

3.4.5 Raman Spectroscopy

Raman spectroscopy is a powerful tool that is useful to determine the crystallinity of the CNMs. Generally, the peaks in Raman exhibit two bands, namely the D (defective) and G (graphitic) band occurring at 1350 cm^{-1} and 1580 cm^{-1}, respectively. These occur namely for carbon nanofibers (CNFs) and multi-walled carbon nanotubes (MWCNTs). The D band is associated with the presence of defects (disordered carbon) in CNMs' wall structures. While the G band correlates with an E_{2g} mode of graphite and is related to the vibrations of sp^2 carbon-bonded atoms in a two-dimensional hexagonal lattice, such as in a graphitic layer. The relative intensity ratio (I_D/I_G) of these two peaks is used to determine the degree of graphitization of the CNMs. Raman spectra were acquired using the 514.5 nm line of a Lexel Model 95 SHG argon-ion laser as an excitation source and a Horiba LabRAM HR Raman spectrometer equipped with an Olympus BX41 microscope attachment. The incident beam was focused onto the sample using a 100x objective (N.A.=0.90) and the backscattered light was dispersed via a 600 lines/mm grating onto liquid nitrogen cooled CCD detector. The data was acquired using LabSpec v5 software. The laser power at the sample was approximately 0.4 mW to minimize localised heating effects.

3.4.6 X-ray fluorescence (XRF)

XRF analysis was used to determine the chemical composition of fly ash. About 2.5 g of the fly ash was placed in a crucible and heated in a furnace at 1050℃ for a period of 35 min and then it was left to cool in the air to room temperature. This was pulverized using a pestle and mortar, followed by mixing 1 g of fly ash with 5 g of flux, then heated in a modutemp at 1000 ℃ and a fused bead was formed and used for analysis.

3.4.7 X-ray diffraction (XRD)

XRD was used to identify the mineral phases present in the fly ash particles and the carbonaceous products when acetylene was the carbon source. The analysis was conducted using a Bruker D2 phaser Benchtop X-ray diffraction (XRD) equipped with Cu Kα radiation [λ = 1.54184 Å] in the 2-theta range of 5 to 90°, at 0.02° with a counting time of 31.4s per step.

3.4.8 Particle Size Analyser

The particle size distribution (PSD) was determined using a Nanotrac Wave, Particle size, and Zeta Potential Analyzer. The catalyst was dissolved in water, then collected using a dropper, and was added dropwise to the particle size analyser. The data was acquired with Microtrac FLEX 10.6.1 software.

Chapter 4: Fly Ash Characterization

4.1 Introduction

Fly ash is an inorganic fine material that is formed from the combustion of coal during power generation. It is composed of a variety of chemical compounds. The major ones exist as oxides including silica (SiO_2), alumina (Al_2O_3), calcium oxide (CaO), iron oxide (FeO), magnesium oxide (MgO), potassium oxide (K_2O), and titanium oxide (TiO_2) [1]–[3]. Fly ash composition varies by a large margin and it's mostly dependent on the coal source, capturing, and combustion technology. It can be white-grey to dark grey or orange to brown in colour, depending on the chemical composition [3]. Most countries are largely reliant on coal combustion for industrialization and the improvement of life. This leads to massive quantities of this material being produced [4]. These large quantities of fly ash are either disposed of in lagoons or dams and ash dumpsites [5]. There are costs such as transportation and maintenance of disposal sites associated with the act of discarding fly ash [6]. Furthermore, the disposal methods have caught the attention of environmentalists. It has been reported that the toxic metals found in fly ash could result in pollution and leaching to underground water [7]. A cost-effective and safe disposal method of fly ash is utilizing this inorganic material and converting it to useful products. It has been widely applied in the construction industry and agriculture, as an adsorbent and catalyst, and polymer composites [5]–[7]. Despite the research conducted on the potential applications of fly ash, substantial quantities of this inorganic material are still disposed and remain unused. The current global figure of fly ash utilization is approximately 25 %. In the US, China and India only 65 %, 45 %, and 38 % of fly ash are respectively utilized [11]. In developing countries like South Africa, only 10 % is used. These figures are extremely low compared to the amount of fly ash produced and this calls for further research into finding or improving its beneficiation.

South Africa is the leading producer of electricity from coal in Africa [12]. Thus, fly ash is being produced on the megaton scale. Currently, two major utilities i.e., Sasol and Eskom produce fly ash in large quantities. Differences exist in both materials in terms of their physical and chemical properties. Sasol fly ash (S-FA) is produced from pre-combustion, while Eskom fly ash is from post-combustion. In pre-combustion, the coal is partially combusted and therefore contains some unburnt carbon. While post-combustion at Eskom, the coal is completely combusted. In this

chapter, we seek to compare and characterize these two heterogeneous materials and determine which one would be a catalyst best suitable for CNMs' production from CO_2.

4.2 Results and Discussion

The SEM images of Eskom (post-combustion) and Sasol (pre-combustion) fly ashes are depicted in Figure 4.1. They reveal that both of these coal combustion products are comprised of spherical particles of varying sizes mixed with irregularly shaped fragments. Smaller spheres and irregular fragments are attached and resting on the surface of bigger spheres, Figure 4.1a& b. Most of the surfaces on Eskom fly ash (E-FA) appear finer and well-rounded with some pores (Figure 4.1c). While some spheres from Sasol fly ash (S-FA) appear to have coarser, chipped, and uneven surfaces that are poorly rounded (Figure 4.1d). The chipped surfaces of the spheres seen in both materials reveal that they are filled inside which indicates the presence of plerospheres [13]. Cenospheres are also present. A physical inspection of the fly ashes revealed that the colour is

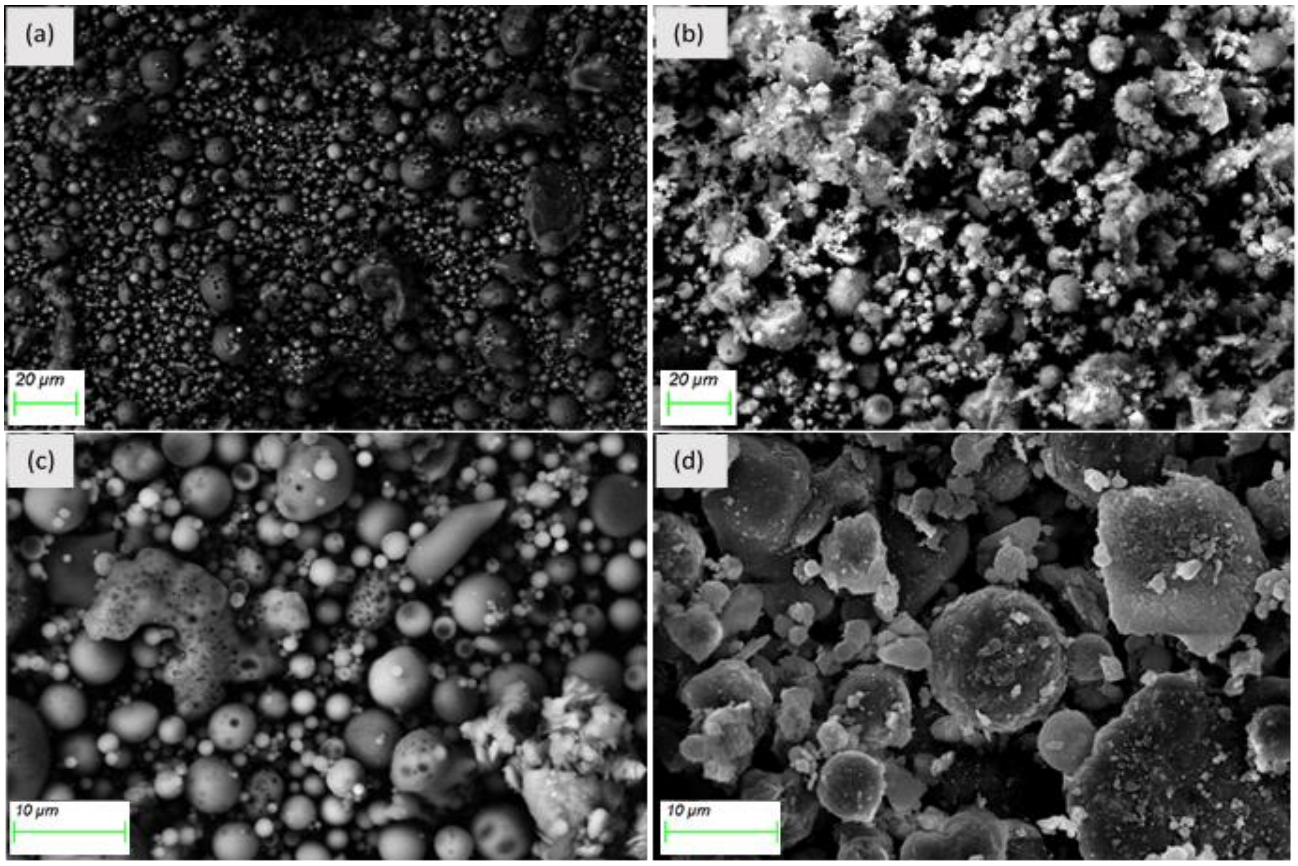


Figure 4.1: SEM micrographs of (a) Eskom and (b) Sasol fly ashes. A closer inspection of the fly ash particles showing (c) smaller spheres, broken granular fragments in E-FA and (d) course surface of S-FA spheres mixed with higher fraction of irregular

darker in Sasol than in Eskom's fly ash due to the different combustion conditions of the coal [4]. The particle size of the catalyst is also an important measure in carbon nanotube/fibre synthesis.

The particle size distribution (PSD) of both fly ashes obtained using a Zeta Potential Analyzer is depicted in Figure 4.2. The variation of the sizes of both ashes appears to be closely similar (2.8-88 μm). However, S-FA is observed to contain the highest number of smaller and larger particles than E-FA. Lastly, S-FA has significant amounts of non-spherical material compared to E-FA as observed in the SEM micrographs above. The composition of the samples was determined using EDS (Energy-dispersive X-ray Spectroscopy) and XRF (X-ray Fluorescence) techniques.

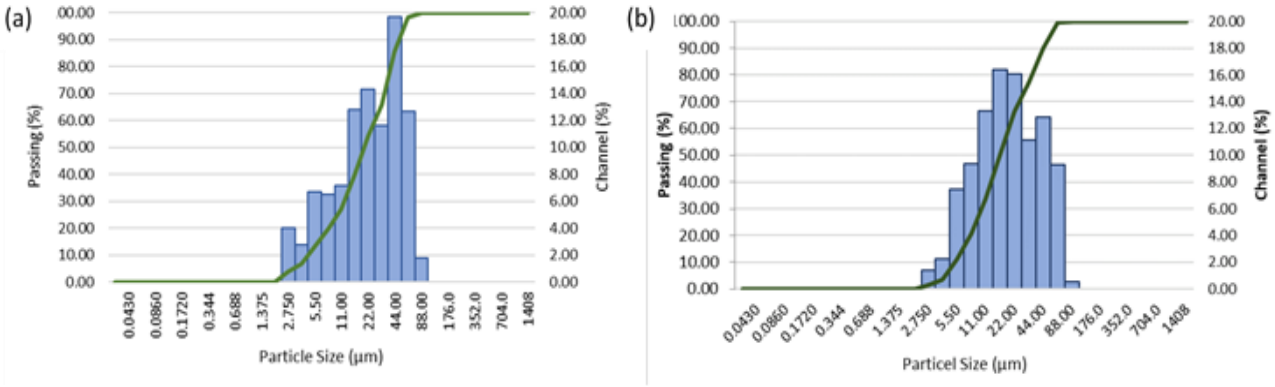


Figure 4.2: Comparison of the particle size distributions of raw (a) Sasol and (b) Eskom fly ash

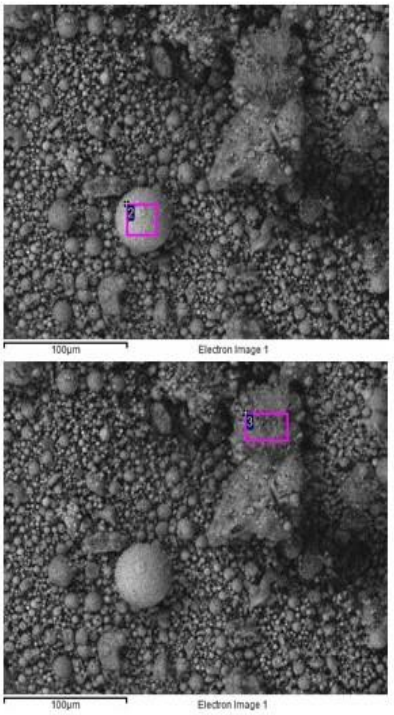
Table 4.1 depicts the overall chemical composition as oxides of both fly ash samples. SiO_2 and Al_2O_3 are the principal components in both catalysts as expected. However, their amounts are higher in E-FA compared to S-FA. Iron (Fe) is also one of the components abundant in S-FA than E-FA. It is one of the commonly used catalysts for CNMs growth. Thus, a higher yield of CNMs would be expected from S-FA. Furthermore, a significant difference in the LOI (Loss on Ignition) is observed. It is a measure of the unburnt carbon content in fly ash and it is used in the construction industry to determine the suitability of fly ash to be used as a replacement for Portland cement [9], [11], [14]. Sasol's coal combustion product has a higher LOI (8.5 wt%) than Eskom, which is extremely low (0.9 wt%). Sasol uses the pre-combustion method which is not total combustion

because there is a large amount of CO in the flue gases [15], [16]. This justifies the large amount of LOI in S-FA compared to E-FA which uses the post-combustion method.

Table 4.1: Chemical composition of Sasol and Eskom fly ash obtained from XRF

Component	Sasol (wt%)	Eskom (wt%)
SiO_2	46.4	53.88
Al_2O_3	25.25	33.12
CaO	7.73	4.00
Fe_2O_3	4.51	3.33
MgO	2.5	1.17
TiO_2	1.39	1.65
K_2O	0.81	0.71
Na_2O	0.78	0.28
P_2O_5	0.71	0.40
MnO	0.06	0.04
Cr_2O_3	0.03	0.05
NiO	0.01	0.01
LOI	8.5	0.90

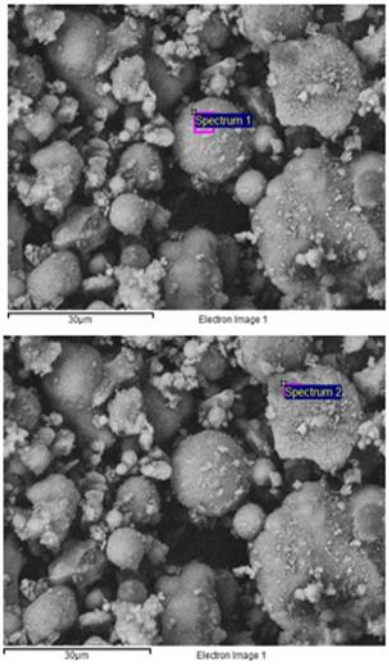
In the EDS technique, a visible area of the fly ash sample was selected and analysed. Subsequently, individual spheres and non-spherical fragments were also selected for elemental quantitative analysis. Depicted in Figure 4.4 are the selected spherical and irregular particles from Eskom fly ash. Fe was found to be less abundant on the irregular fragments than spherical particles. This observation was consistent when the analysis was conducted on different areas in the fly ash. However, Sasol fly ash (Figure 4.3) showed the opposite result in terms of the abundance of iron. It was found to be more abundant in the irregular fragments. The results obtained when a whole area was selected samples are consistent with the XRF analysis in both fly ashes as shown in Table 4.2



Element	Weight%
O K	44.9
Mg K	0.73
Al K	2.5
Si K	17.48
Ca K	1.72
Fe K	32.67

Element	Weight%
O K	52.15
Na K	0.37
Mg K	0.38
Al K	17.76
Si K	18.85
K K	0.95
Ca K	3.54
Ti K	4.31
Fe K	1.69

Figure 4.4: EDS analysis of raw Eskom fly ash of selected individual particles (spherical and irregular fragment)



Element	Weight (wt%)
O	46.75
Na	0.86
Mg	0.96
Al	18.25
Si	25.92
Ca	7.57
Ti	1.42

Element	Weight (wt%)
O	46.53
Na	0.22
Mg	13.92
Al	9.99
Si	9.32
Cl	1.95
Ca	11.76
Ti	0.77
Fe	5.54

Figure 4.3: EDS analysis of raw Sasol fly ash showing elemental composition of a spherical particle (spectrum 1) and an irregularly fragment (spectrum 2)

Table 4.2: Quantitative elemental analysis of Eskom and Sasol fly ash from EDS

Elements	**O**	**Si**	**Al**	**Ca**	**Fe**	**Ti**	**K**	**Mg**	**Na**	**P**	**S**
Eskom (wt%)	47.9	22.4	20.5	3.0	2.80	1.1	0.6	0.9	0.4	0.2	0.2
Sasol (wt%)	62.9	16.51	9.94	5.79	2.89	1.99	0.99	0.59			

Carbon was not included in Table 4.2 since the samples were placed on carbon tape for the analysis and it would be detected during analysis and give inaccurate results. The chemical composition was found to be consistent with other fly ash studies [17]–[20].

XRD was used to determine the phases formed from the coal combustion processes. The XRD spectra in Figure 4.5 revealed that mullite ($3Al_2O_3 \cdot 2SiO_2$) and quartz (SiO_2) are the major phases followed by calcite ($CaCO_3$) and magnetite (Fe_2O_4) as the minor phases in both materials. In the spectrum of Eskom fly ash, calcite was not detected whereas it was found in Sasol fly ash. This is coherent with the XRF results obtained in Table 4.1, where CaO contents were higher in S-FA than in E-FA. Hintsho et al. [21] confirmed iron as the main catalyst producing CNFs from results obtained in XRD and BET analyses.

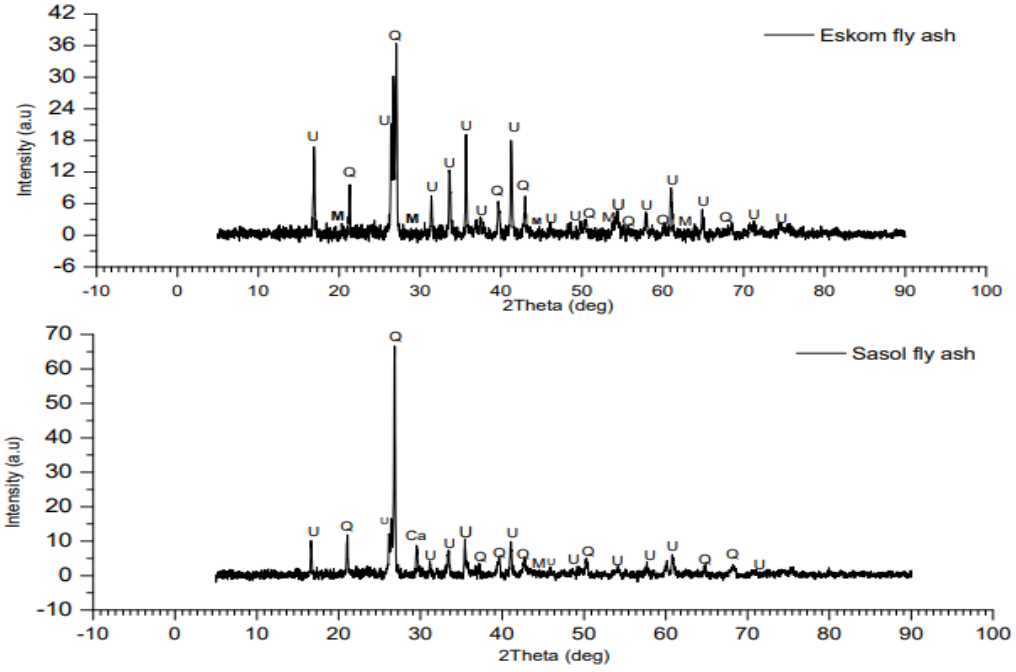


Figure 4.5: XRD patterns of Eskom and Sasol fly ashes showing phases that are present. U-Mullite, Q-quartz, Ca-calcite, M-magnetite

4.3 Conclusion

Fly ash from Eskom (post-combustion) and Sasol (pre-combustion) in South African was characterized. This was done to compare them as catalysts for carbon nanomaterial synthesis using the chemical vapour deposition (CVD) technique. SEM images showed the presence of spheres containing cenospheres and plerospheres. The particle size distribution of the materials was the same. However, Sasol fly ash contained a higher concentration of large particle sizes. Their chemical, elemental, and phase compositions were determined by XRF, EDS, and XRD analysis, respectively. XRF analysis showed Eskom fly ash had significantly low contents of unburnt carbon whereas Sasol fly ash contained higher composition of unburnt carbon and iron. XRD showed sharp peaks of aluminosilicate phases, small calcite, and hematite phases which corresponded with the XRF and EDS results. From these results, it can be predicted that Sasol fly ash (pre-combustion) will yield CNMs in high quantities than Eskom fly ash (post-combustion).

4.4 References

[1] S. Wang, "Application of solid ash based catalysts in heterogeneous catalysis," *Environ. Sci. Technol.*, vol. 42, no. 19, pp. 7055–7063, 2008.

[2] R. Sett, "Flyash: Characteristics, Problems and Possible Utilization," *Adv. Appl. Sci. Res.*, vol. 8, no. 3, pp. 32–50, 2017.

[3] Z. T. Yao *et al.*, "A comprehensive review on the applications of coal fly ash," *Earth-Science Rev.*, vol. 141, pp. 105–121, 2015.

[4] R. S. Blissett and N. A. Rowson, "A review of the multi-component utilisation of coal fly ash," *Fuel*, vol. 97, pp. 1–23, 2012.

[5] I. Nawaz, "Disposal and Utilization of Fly Ash to Protect the Environment," *Int. J. Innov. Res. Sci. Eng. Technol.*, vol. 2, no. 10, pp. 5259–5266, 2013.

[6] R. A. Kruger, "Introduction to the utilization of coal combustion products," in *Coal Combustion Products (CCPs): Characteristics, Utilization and Beneficiation*, Elsevier, 2017, pp. 99–119.

[7] A. Kumar, S. R. Samadder, and V. Kumar, "Assessment of groundwater contamination risk due to fly ash leaching using column study," *Environ. Earth Sci.*, vol. 78, no. 1, pp. 1–12, 2019.

[8] J. C. Swanepoel and C. A. Strydom, "Utilisation of fly ash in a geopolymeric material," in *Applied Geochemistry*, 2002, vol. 17, no. 8, pp. 1143–1148.

[9] N. Ghazali, K. Muthusamy, and S. Wan Ahmad, "Utilization of Fly Ash in Construction," *IOP Conf. Ser. Mater. Sci. Eng.*, vol. 601, no. 1, 2019.

[10] M. J. McCarthy and R. K. Dhir, "Development of high volume fly ash cements for use in concrete construction," in *Fuel*, 2005, vol. 84, no. 11, pp. 1423–1432.

[11] B. Ramme and M. Tharaniyil, *Coal combustion products utilisation handbook*, Third. WE Energies, 2013.

[12] K. Reynolds-Clausen and N. Singh, "South Africa's power producer's revised Coal Ash Strategy and Implementation Progress," in *2017 World of Coal Ash Conference*, 2017, pp.

1–10.

[13] F. Goodarzi and H. Sanei, “Plerosphere and its role in reduction of emitted fine fly ash particles from pulverized coal-fired power plants,” *Fuel*, vol. 88, no. 2, pp. 382–386, Feb. 2009.

[14] A. Bhatt, S. Priyadarshini, A. Acharath Mohanakrishnan, A. Abri, M. Sattler, and S. Techapaphawit, “Physical, chemical, and geotechnical properties of coal fly ash: A global review,” *Case Stud. Constr. Mater.*, vol. 11, Dec. 2019.

[15] M. Steyn and R. C. A. Minnitt, “Thermal coal products in South Africa,” *J. South. African Inst. Min. Metall.*, vol. 110, no. 10, pp. 593–599, 2010.

[16] L. Bartoňová, “Unburned carbon from coal combustion ash: An overview,” *Fuel Process. Technol.*, vol. 134, pp. 136–158, Jun. 2015.

[17] J. Alegbe, O. S. Ayanda, P. Ndungu, N. Alexander, O. O. Fatoba, and L. F. Petrik, “Chemical, Mineralogical and Morphological Investigation of Coal Fly Ash Obtained from Mpumalanga Province, South Africa,” *Res. J. Environ. Sci.*, vol. 12, no. 3, pp. 98–105, 2018.

[18] N. Hintsho, A. Shaikjee, P. K. Tripathi, P. Franklyn, and S. Durbach, “The effect of CO2 on the CVD synthesis of carbon nanomaterials using fly ash as a catalyst,” *RSC Adv.*, vol. 5, no. 66, pp. 53776–53781, 2015.

[19] R. H. Matjie, M. Ginster, C. Van Alphen, and A. Sobiecki, “Detailed Characterisation of Sasol Ashes,” *World Coal Ash*, 2005.

[20] J. S. Mahlaba, E. P. Kearsley, and R. A. Kruger, “Physical, chemical and mineralogical characterisation of hydraulically disposed fine coal ash from SASOL Synfuels,” *Fuel*, vol. 90, no. 7, pp. 2491–2500, 2011.

[21] N. Hintsho *et al.*, “Direct synthesis of carbon nanofibers from South African coal fly ash,” *Nanoscale Res. Lett.*, vol. 9, no. 387, 2014.

Chapter 5: Synthesis of CNMs from CO_2 using Sasol and Eskom Fly ash as catalyst

5.1 Introduction

Carbon nanomaterials such as carbon nanotubes (CNTs) and carbon nanofibers (CNFs) have gained the attention and interest of researchers all over the world. This huge interest in them emanates from their unique properties such as good mechanical strength, high electrical and thermal conductivity [1]–[8]. Their properties and characteristics are significantly influenced by synthesis parameters such as temperature, catalyst thickness and reaction time, etc [9]–[11]. Gaining precise control of these parameters is key to ensuring CNMs with desired properties are synthesized. It is particularly because of this ability to control parameters with ease that chemical vapour deposition (CVD) is the most widely used technique for CNMs synthesis [12]. Other methods such as laser ablation and arc discharge are also used [13], [14]. However, they require extremely high temperatures, and the control of parameters is limited. The CVD allows for several compounds to be used as sources of carbon and different catalysts for growing CNMs at moderate temperatures. Most of the carbon-containing compounds can be used as CNMs precursors. However, the most common sources of carbon are hydrocarbons and carbon monoxide (CO) [15]. While transition metals such as Fe, Ni, Co, and their alloys are commonly used on supports [16]–[19]. Most of these carbon sources and catalysts are expensive and toxic. The catalyst also requires pre-treatment and preparation.

Carbon dioxide (CO_2) and fly ash are harmful industrial waste products that are known to be produced in large quantities. Fly ash is a fine powder that is formed from the combustion of coal during power generation. CO_2 exists naturally in the atmosphere and is needed by plants for survival. However, anthropogenic CO_2 sources such as the use of burning fossil fuels and cement production contribute significantly to global warming and its effects are well documented [20]–[22]. Studies using CO_2 as a carbon source for CNMs production have been reported [23]–[25]. Its use as a carbon source stems from its affordability, abundance, and non-toxicity. CNTs were also reported in good yields in some of these studies. Fly ash has also been reported as a catalyst in the formation of CNMs [26]–[31]. It is affordable and available in large amounts. Although its applications exist, they are limited and require further research to explore some of its potential applications. Fly ash is generally kept in landfills or lagoons. However, instead of storing it, it can

be used to make useful products such as CNMs and contribute towards mitigating its effect on the environment. In South Africa, two major utilities produce fly ash in large quantities; Sasol, and Eskom. Their catalytic ability to produce CNMs is compared. In this chapter, temperature, flow rate, and mass are the parameters varied to investigate the optimum conditions that give good crystalline materials in high yields. This chapter is structured as follows; Section 5.2 outlines the experimental methods. Section 5.3 discusses the effects of the synthesis parameters on the yield, purity, and crystallinity of CNMs using Sasol fly ash (subsection 5.3.1) and Eskom fly ash (subsection 5.3.2). Section 5.4 concludes the chapter.

5.2 Experimental and Characterization Methods

Raw Sasol and Eskom fly ash were used as catalysts for CNMs production. Sasol Fly ash (S-FA) was obtained from Secunda and the Eskom fly ash (E-FA) was obtained at Lethabo power station through Lafarge. The CNMs synthesis took place in a tubular chemical vapour deposition (CVD) furnace containing a stainless-steel tube reactor. Measured amounts of the catalyst were placed at the centre of the reactor in the CVD furnace. Argon (Ar) gas was allowed to flow at 150 sccm until the desired synthesis temperature was reached. Subsequently, the Ar gas flow was increased, and carbon dioxide (CO_2) gas was opened for 60 minutes. The furnace was turned off and allowed to cool down under Ar gas for 60 minutes and then it cooled down overnight without the inert gas. The influence of the studied synthesis parameters are summarized in Table 5.1 for both catalysts. The yield and purity of the synthesized carbon nanomaterials were determined using an SDT Q600 thermogravimetric analysis (TGA) and derivative thermogravimetry (DTG). Field Emission Scanning Electron Microscopy (FESEM) was used to visualize and identify the carbonaceous products as well as their morphology. Raman spectra were acquired to determine the crystallinity of the CNMs. Generally, the peaks in Raman exhibit two bands, namely the D (defective) and G (graphitic) band occurring at 1350 cm^{-1} and 1580 cm^{-1}, respectively [32]–[34]. The relative intensity ratio (I_D/I_G) of these two peaks is used to determine the degree of graphitization of the CNMs. A low I_D/I_G ratio indicates a low level of defects, which implies the material has a good crystallinity [23].

Table 5.1: Reaction parameters varied for the synthesis of CNMs from Sasol and Eskom fly ash

Run	Temperature (°C)	CO_2 (sccm)	Argon (sccm)	Catalyst Mass (mg)
1	950	962	1202	600
2	950	601	1202	600
3	850	601	1202	600
4	750	601	1202	600
5	850	300.1	901.5	600
6	950	300.1	901.5	600
7	750	300.1	901.5	600
8	850	962	1202	600
9	750	962	1202	600
10	750	300.1	480.7	600
11	850	300.1	480.7	600
12	950	1202	1202	600
13	750	962	1202	800
14	750	962	1202	1000
15	850	300.1	901.5	1200

5.3 Results and Discussion

The growth rate of CNMs is influenced by several factors which affect the quantity and quality of nanomaterials. There is still some controversy surrounding the growth mechanism of CNMs. However, the current growth model that is widely accepted can give compelling explanations about the influence certain parameters have on the yield and crystallinity of CNMs. The mechanism of CNMs growth can be summarized in three stages: (i) adsorption and dissociation of carbon atoms on the catalyst surface, (ii) diffusion of carbon atoms through the catalyst, and (iii) precipitation of solid carbon as CNMs (CNTs/CNFs) [9]–[12]. All these stages are affected by the temperature, type of catalyst, flow rates of the carrier gas, and carbon source gas.

5.3.1 CNMs synthesis from Sasol Fly Ash

The effect of temperature, flow rate, and catalyst amount was investigated to determine the conditions to synthesize CNMs from Sasol fly ash. The best results obtained from these investigated parameters are summarized in Table 5.2 below.

Table 5.2: Summary of the best synthesis conditions obtained from each of the parameters investigated in Sasol fly ash

Temperature (℃)	Flow rate (sccm)		Mass (mg)	Yield (wt%)	I_D/I_G
	CO_2	Ar			
750	300.1	901.5	600	4	0.8
750	962	1202	600	4.6	0.84
750	962	1202	1000	4.1	0.96

Effect of Temperature

The temperature was varied from 750 ℃ (run 7) through 850 ℃ (run 5) to 950 ℃ (run 6), while the flow rate of CO_2/Ar was maintained at 300.1/901.5 sccm and catalyst mass was 600 mg. The collected product from the furnace showed some changes in terms of their texture and colour. They appeared slightly darker and harder than before. For all the temperatures, yields <95% were obtained.

The TGA and DTG curves for different synthesis temperatures are depicted in Figure 5.1a and Figure 5.1b, respectively. The decomposition temperatures of amorphous carbon and CNTs or CNFs are found at 200-400 ℃ and 450-650 ℃ regions, respectively, in the TGA [35]. At synthesis temperatures of 750 ℃ (run 7) in Figure 5.1a, it can be seen that amorphous carbon is present. In its region, there is a rapid decrease in the mass loss of the product. The decomposition of CNTs and CNFs occurred between the 400-700 ℃ region with a mass loss of 4 %. Residual fly ash particles remain as impurities at temperatures >700 ℃. The DTG curve is used to determine the distribution of products and oxidation temperatures of the materials. The DTG thermograms in Figure 5.1b, show multiple peaks in the 620-680 ℃ region, indicating the formation of more than one carbonaceous material. They are probably CNTs and CNFs containing various diameters. The formation of more than one product occurred because of the heterogeneous nature of the fly ash

catalyst and its non-uniform particle size. The oxidation temperature, which is the temperature at which mass loss is at a maximum in the DTG was found at 680 °C. This implies that CNMs with good crystallinity were obtained.

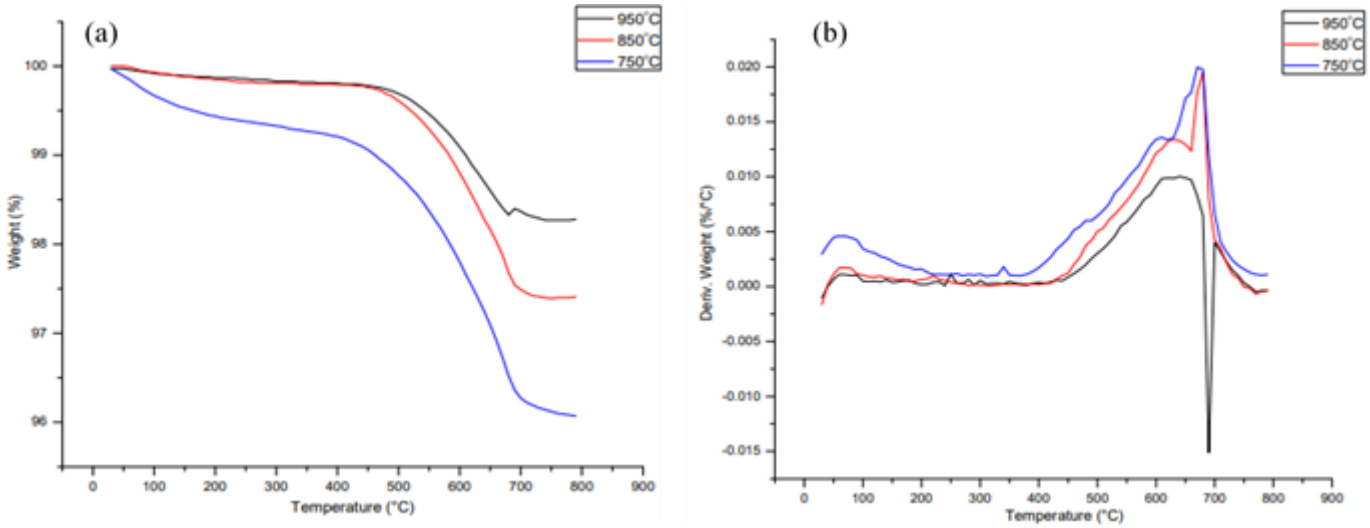


Figure 5.1: Thermal analysis of the as-synthesized CNMs at various temperatures (a) TGA curve showing decomposition temperatures and (b) derivative thermogravimetric curve showing oxidation temperature

The SEM images of CNMs produced at a temperature of 750°C (run 7) are shown in Figure 5.2. Net and carpet-like CNT/CNFs of various lengths and diameters were formed on top of the fly ash sphere are shown (Figure *5.2*a), with some branching. These structures seem to be beginning the

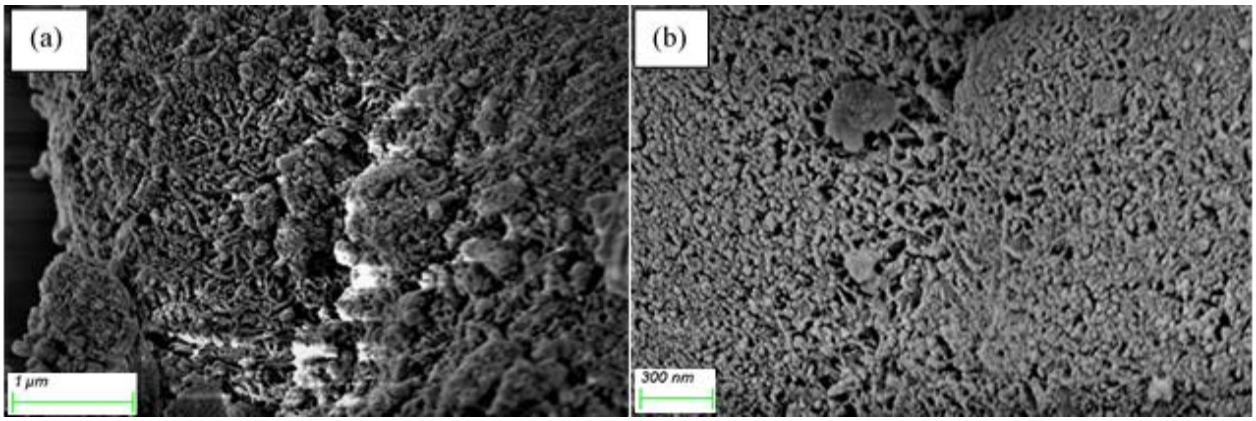


Figure 5.2: SEM images of CNMs grown at 750°C showing (a) mixture of CNMs with fly ash and (b) net-like CNMs

formation of CNMs and getting attached to the spheres. This happens while the fly ash particles deform (becoming hollow on their surface).

Although catalyst supports were not used in this study, this could suggest that the CNMs were formed via the root-growth mechanism. Some unreacted fly ash fragments are also observed (Figure 5.2b). The Raman spectroscopy obtained at this temperature is shown in Figure 5.3. Strong D and G peaks were obtained at 1369cm^{-1} and 1608cm^{-1}, respectively. However, the G band has a stronger intensity than the D band. This indicates that a material with high graphitic content than defects was formed. The I_D/I_G ratio was 0.8, showing that the CNMs have a good crystalline structure as seen in the DTG analysis at this temperature (750℃).

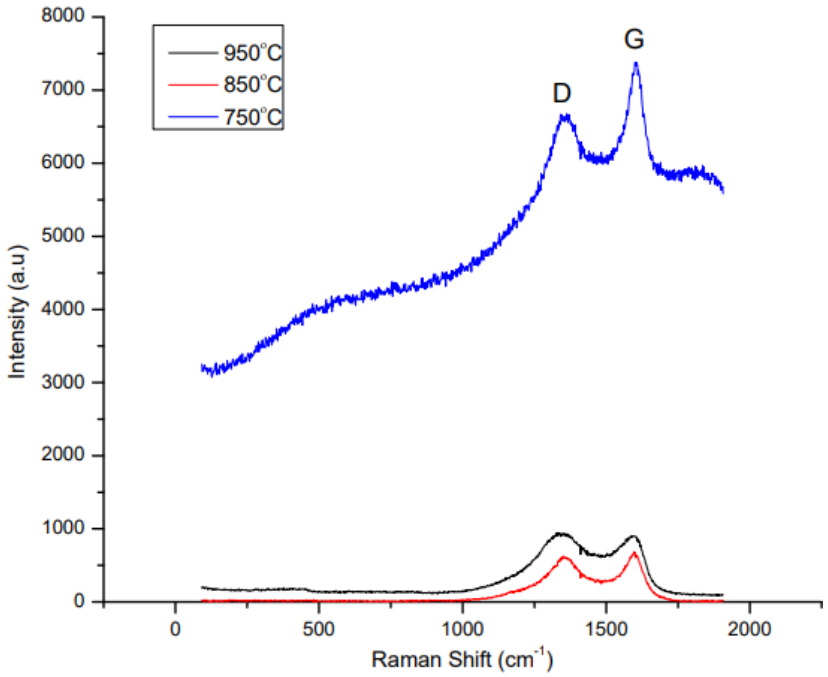


Figure 5.3: Raman Spectra obtained from CNMs synthesized using Sasol fly ash at different temperatures

When the temperature was increased (850-950℃), a decrease in the yield of CNMs was observed (Figure 5.1a). Generally, an increase in temperature is known to increase the yield of CNMs [36], [37]. However, at 950℃ (run 6) the highest decrease was observed. The decrease in the yield is because CO_2 is more chemically stable at high temperatures. Thus, activating it in the reaction is difficult [23]. This affects stages (i)& (ii) in the growth mechanism since insufficient carbon atoms

are being decomposed and diffused through the catalyst. A decrease in the production of CNTs was also observed by Simate et al. [25] at temperatures greater than 840 ℃ when CO_2 was used as a carbon source. They attributed this observation to the Bourdouard reaction requirements and the decomposition of CO_2. They explained that during the decomposition of CO_2, CO is released. The disproportionation reaction of CO is restricted kinetically at low temperatures and it is restricted thermodynamically at high temperatures. Subsequently, the production rate of CNMs decreases. The initial decomposition temperature of the nanomaterials in the TGA is relatively similar (480-500 ℃), which means they possess relatively the same thermal stabilities. The DTG curve, Figure 5.1b, shows that the oxidation temperatures of the nanomaterials are close. This indicates that the crystallinity is also the same. The products synthesized at 950 ℃ showed a small mass gain between the 700 and 750 ℃ region in the TGA curve due to oxidation reactions.

The SEM images of the nanomaterial obtained at 850 ℃ (run 5) are depicted in Figure 5.4. A splashed liquid-like substance on the surface of the sphere is seen, Figure 5.4a. This is CO_2 decomposed on the surface of the spheres forming CNMs. In Figure 5.4a, a different structure is obtained than in Figure 5.4b at the same temperature. This was seen throughout all the investigated parameters. This can be rationalized by the influence of the catalyst shape on the structure of CNMs. As seen in the images, the structures are grown on different surfaces i.e., a sphere in Figure 5.4a and an irregular fragment in Figure 5.4b. This has also been seen by other researchers where the shape of the catalyst influenced the structure of the CNM [36], [37]–[39]. The D and G bands were obtained at 1354.3 and 1598.7 cm^{-1}, respectively for 850 ℃. Their I_D/I_G is 0.91 which is higher than the intensity ratio obtained at 750℃, implying that CNMs with lower crystallinity were grown.

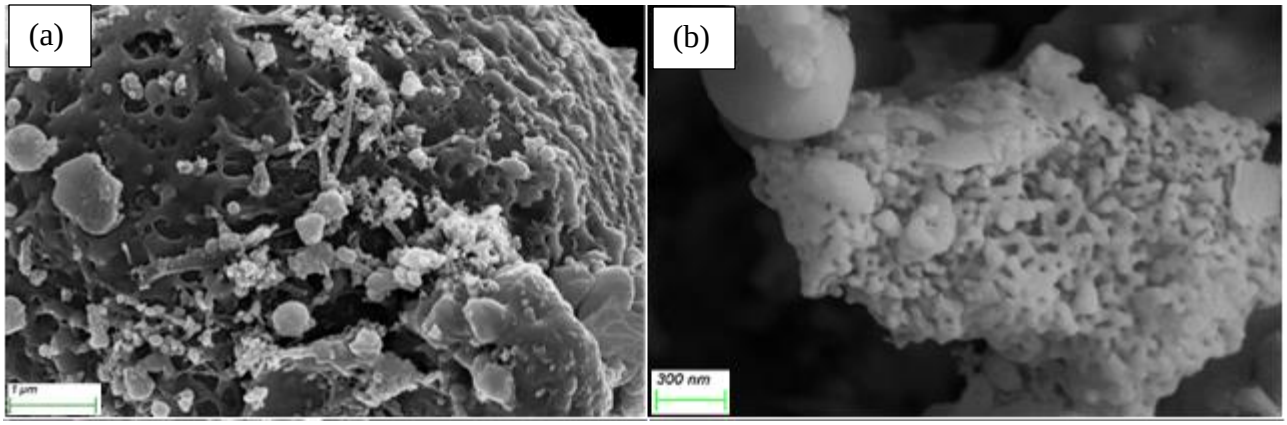


Figure 5.4: CNMs synthesized from Sasol fly ash at 850℃ showing (a) a splashed like liquid-substance on the surface of fly ash resembling CNMs and (b) an irregular and deformed fly ash

The SEM micrographs of the products grown at 950 ℃ are depicted in Figure 5.5 a& b. In Figure 5.5a, a deformed and conglomerate structure is observed showing the poor growth of CNMs which is consistent with the TGA results. This is also observed in Figure 5.5b, where strands of short lengths are grown on an irregular fly ash fragment. The D band had a Raman shift of 1339 cm^{-1} and the G band was 1600 cm^{-1} (Figure 5.3) with an I_D/I_G ratio of 1.05. This shows that higher temperatures form structures with defects or poor crystallinity. From these findings, it is seen that a temperature of 750 ℃ forms CNMs in better quantities and quality than higher temperatures.

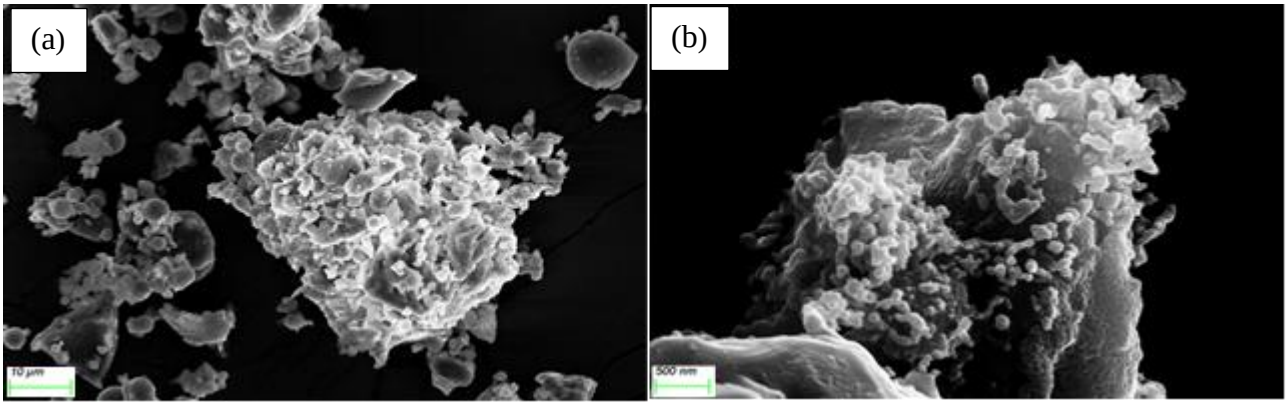


Figure 5.5: CNMs from Sasol fly ash obtained at a temperature of 950℃ showing (a) deformed fly ash particle and (b) short-length rod-like structures

Effect of flow rate

The flow rate in the CVD synthesis of CNMs is one of the key parameters to achieve high yields and remarkable crystallinity. It affects stages (i)& (ii) in the growth mechanism. To observe the effects of CO_2/Ar (carbon dioxide and argon) flow rates, the temperature, catalyst mass, and time were held constant at 750 ℃, 600 mg, and 60 minutes, respectively. In run 3 (Table 5.1) the inlet pressure was also investigated.

The TGA thermograms shown in Figure 5.6a reveal that in all the flow rates investigated, extremely low yields were obtained, as seen with the temperature. The yield, purity, and crystallinity of the products obtained at CO_2/Ar flow rates of 300.1 sccm/ 901.5 sccm are the same

as the temperature at 750 ℃ (run 5) in Figure 5.4. Thus, they are not discussed further. A CO_2/Ar flow increase to 601/1202 sccm (run 3) resulted in a decrease in the yield which happened because of a decrease in pressure as seen in Figure 5.6. This reverts to the growth mechanism in stages (i)& (ii). At low pressure, the concentration of adsorbed carbon species is low, the amount of carbon atoms dissolving and diffusing into the catalyst is limited. The CNMs' growth becomes suppressed, resulting in low yields. Li et al. [40] investigated the effect of gas pressure on the growth and structure of CNTs and they observed the same effect. The effect the decrease in pressure had on the crystallinity is observed in the DTG curve, Figure 5.6b. A broad peak at an oxidation temperature of ~600 ℃ is found, indicating a non-uniform nanomaterial.

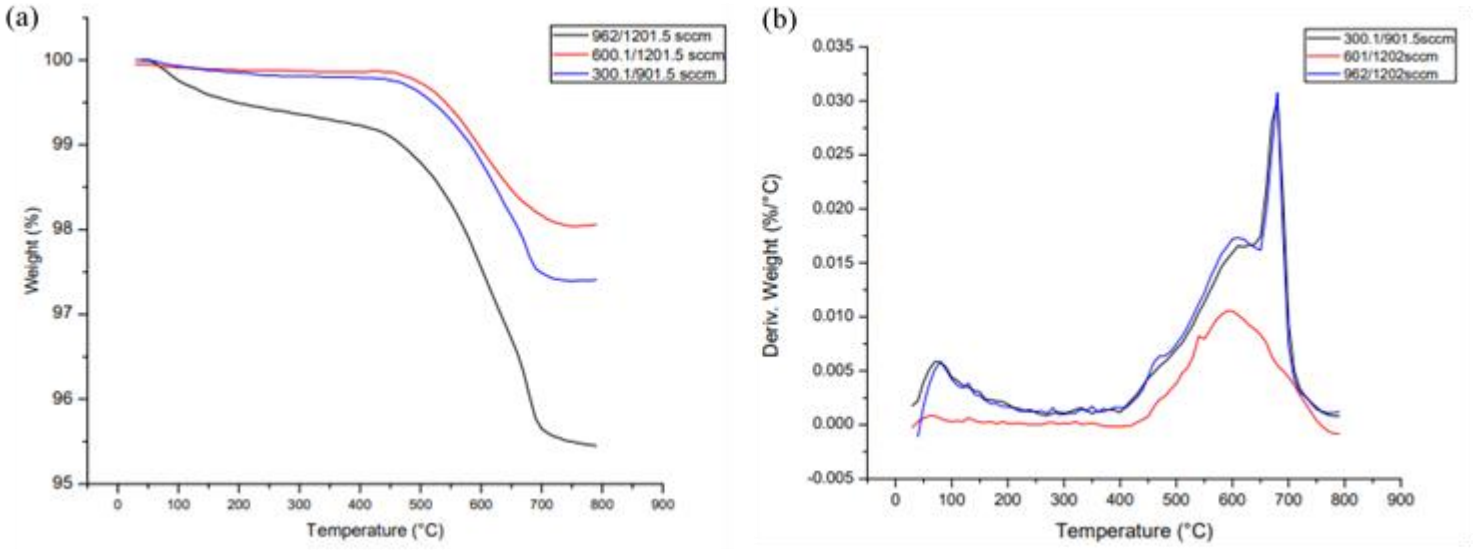


Figure 5.6: Thermograms of Sasol CNMs at various flow rates of CO_2/Ar, (a) TGA and (b) DTG

The SEM visuals of the carbonaceous products synthesized at CO_2/Ar flow rates of 601/1202 sccm are shown in Figure 5.7. Poor growth of the nanomaterials is observed. In Figure 5.7a, the formed products show a dried chunk of fly ash material with some thick structures. While in Figure 5.7b flat-like structure is grown. This observation is due to the decreased pressure and the lack of adsorbed carbon atoms. The effect of the decreased pressure and increased flow rate is also observed in the Raman spectroscopy, Figure 5.8. The D band at 1354.3 cm^{-1} is higher than the G band at 1605.3 cm^{-1} indicating the presence of nanocarbons with significant amounts of disordered

carbon in the product. This is also corroborated by the high I_D/I_G ratio, which is 1.17, implying a low degree of graphitization and a high level of defects.

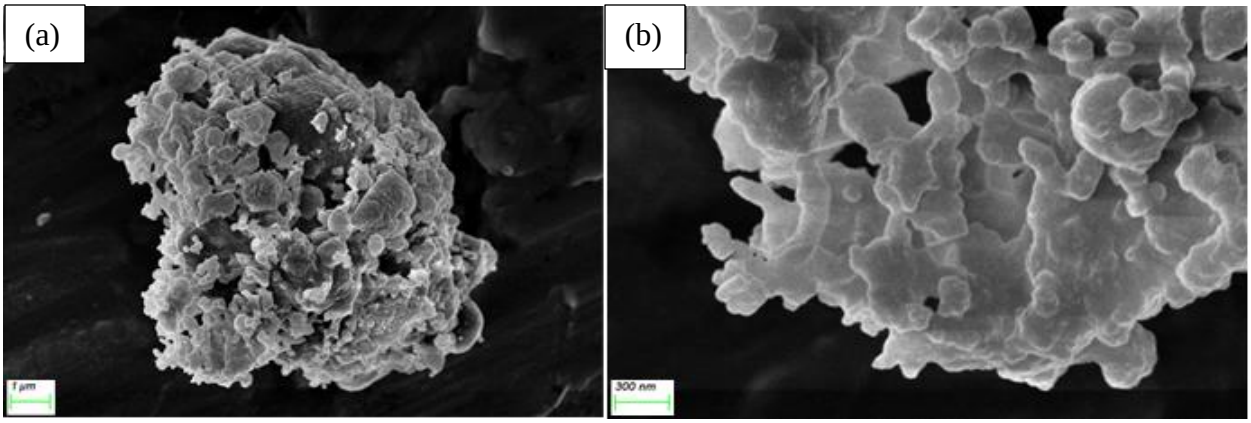


Figure 5.7: Products grown from Sasol fly ash at CO_2/Ar flow rate of 600.1/1202 sccm with a decreased pressure showing (a) a dried chunk of fly ash material and (b) a flat-like structure

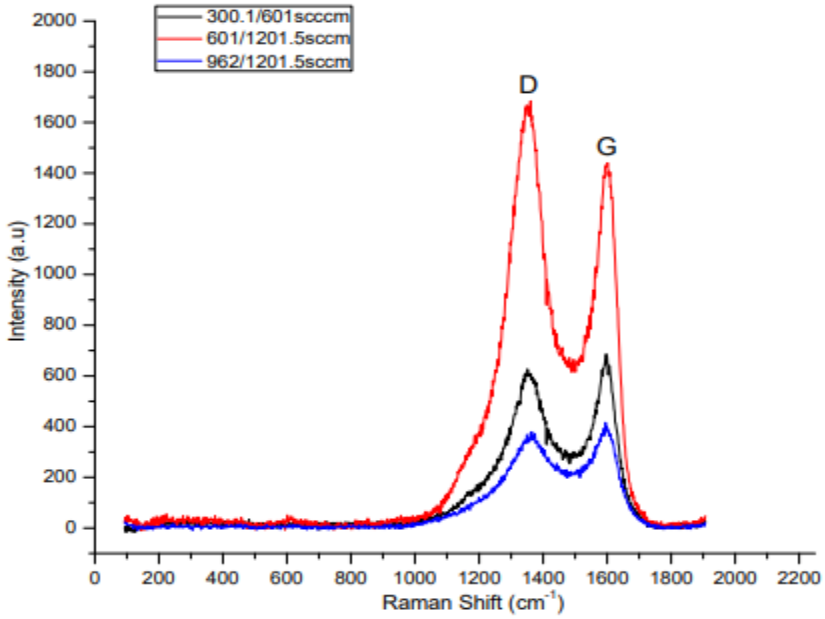


Figure 5.8: Raman Spectroscopy of carbonaceous products synthesized from Sasol fly ash at various CO_2 and argon flow

At CO_2/Ar flow rates of 962/1202 sccm (run 8), the growth of CNMs was favourable as seen in the TGA measurements (Figure 5.6a). It is the highest yield obtained in the investigated flow rates. At these high flow rates, there is enough carbon source gas reaching the reactor. More carbon atoms can dissolve and diffuse through the catalyst surface to precipitate CNMs as described in the growth mechanism. The result is an increase in the yield. The DTG curve at these flow rates is similar to the CO_2/Ar flow rates of 300.1/601 sccm, meaning the increase in flow rate had little effect on the crystallinity of the nanomaterials at the same pressure. The two peaks observed (broad and sharp) indicate that more than one product formed. This non-uniformity is attributable to the heterogeneous nature of fly ash and its wide diameter range resulting in CNMs with large diameters. At temperatures below 100 ℃ in the DTG, a small broad peak is seen. This occurs due to the oxidation of amorphous carbon.

The SEM micrographs of the CNMs at the increased flow rates (962/1202 ssccm) are shown in Figure 5.9. Nanotubes and nanofibers of short lengths were grown from the irregular fragments of fly ash, Figure 5.9a. These interconnected nanostructures show some branching and various diameters mixed with other fly ash fragments. In Figure 5.9b, the nanostructures grown are completely covering or wrapping the fly ash sphere and are longer and with larger diameters. Their large diameters indicate the formation of CNFs. They show a certain growing pattern and orientation on the sphere, which forms circles or hexagonal structures and wave-like patterns on the surface. They also appear to have a dusty texture that comes from the fly ash.

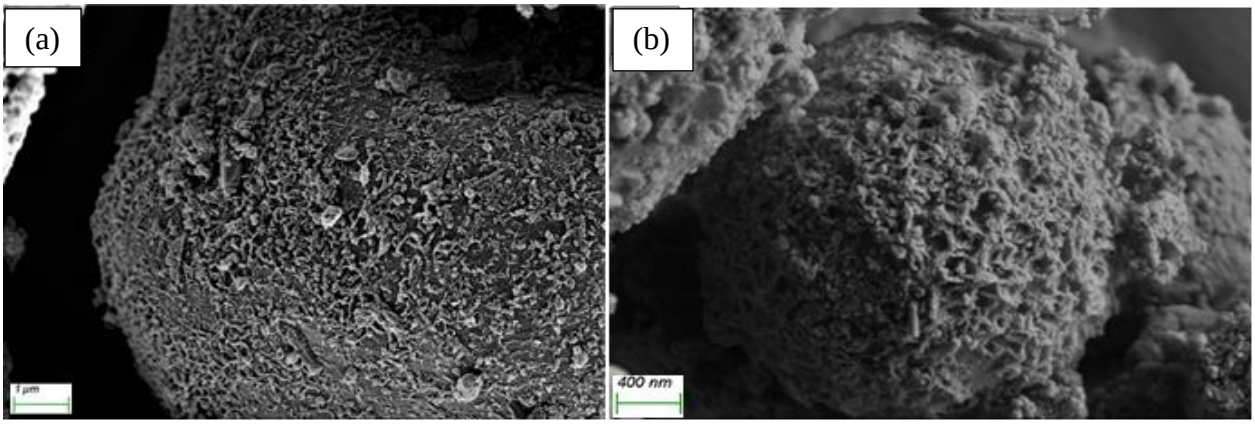


Figure 5.9: SEM micrographs of CNMs grown at CO_2/Ar flowrates of 962/1202 sccm showing (a) short-length CNMs mixed fly ash particles and (b) CNMs covering fly ash sphere

The I_D/I_G ratio from the Raman spectroscopy was 0.84, indicating a material with good crystallinity. Compared with the other flow rates, the crystallinity is similar to the CO_2/Ar flow rate of 300.1/901.5 sccm. However, they both are better than the flow rates of 601/1202 sccm where pressure was decreased. From this, it can be deduced that pressure has a greater influence on the yield and crystallinity than the flow rate. The flow rate has mostly influenced the yield and purity of the nanomaterials. In other studies that used CO_2 as a carbon source in the CVD, high flow rates were used to achieve CNTs growth [23], [24][41]. Simate et al. [25] found that the production of CNTs was low at high flow rates, contradicting the results found in this study and others. For fly ash as a catalyst, Salah [30] found that an acetylene flow rate of 30sccm showed a good formation of uniform CNTs.

Effect of catalyst mass

To examine the effect of catalyst mass on the production of CNMs, three different runs with catalyst mass of 600, 800, and 1000 mg were carried out. Other reaction parameters were held constant at 750 ℃ and CO_2/Ar flow rate of 962/1202 sccm for 60 minutes. From the TGA thermograms in Figure 5.10, increasing the mass of the catalyst increased the yield of CNMs.

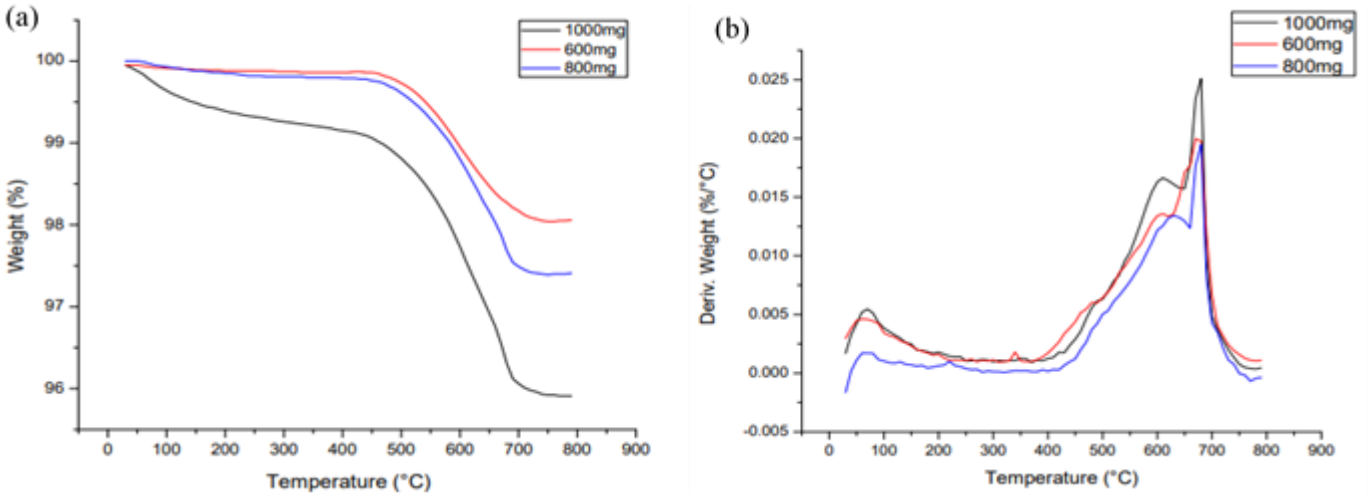


Figure 5.10: Effect of catalyst mass (S-FA) on the growth of CNMs determined using (a) TGA and (b) DTG

The highest yield was obtained with the mass of 1000 mg of fly ash and it also contained amorphous carbon which had an oxidation temperature of 70 ℃ in the DTG, Figure 5.10b. The

oxidation temperature of the carbon nanomaterials is relatively similar which indicates that their crystallinity is also similar as depicted in the DTG. The increase in the yield can be attributed to the increased catalyst particles that can grow CNMs in the fly ash.

The SEM images of the carbonaceous products are depicted in Figure 5.11. The images reveal a network of CNFs and CNTs grown on the surface of the catalyst having various morphologies and diameters. Large amounts of unreacted catalyst particles are seen, which agrees with low yields in the TGA measurements. In Figure 5.11a, CNMs laying flat on the fly ash surface are grown. The splashed-like orientation seen in Figure 5.4 is also observed for the CNMs grown from 800mg catalyst mass (Figure 5.11b). The smaller fly ash spheres have decomposed (melted) to form strands of CNFs and get attached on top of the larger sphere. At a mass of 1000 mg, unreacted fly ash particles and crystallized minerals are mixed with the grown products in Figure 5.11c. At this mass, short nanomaterials with some branching coming from the fly ash particle are seen.

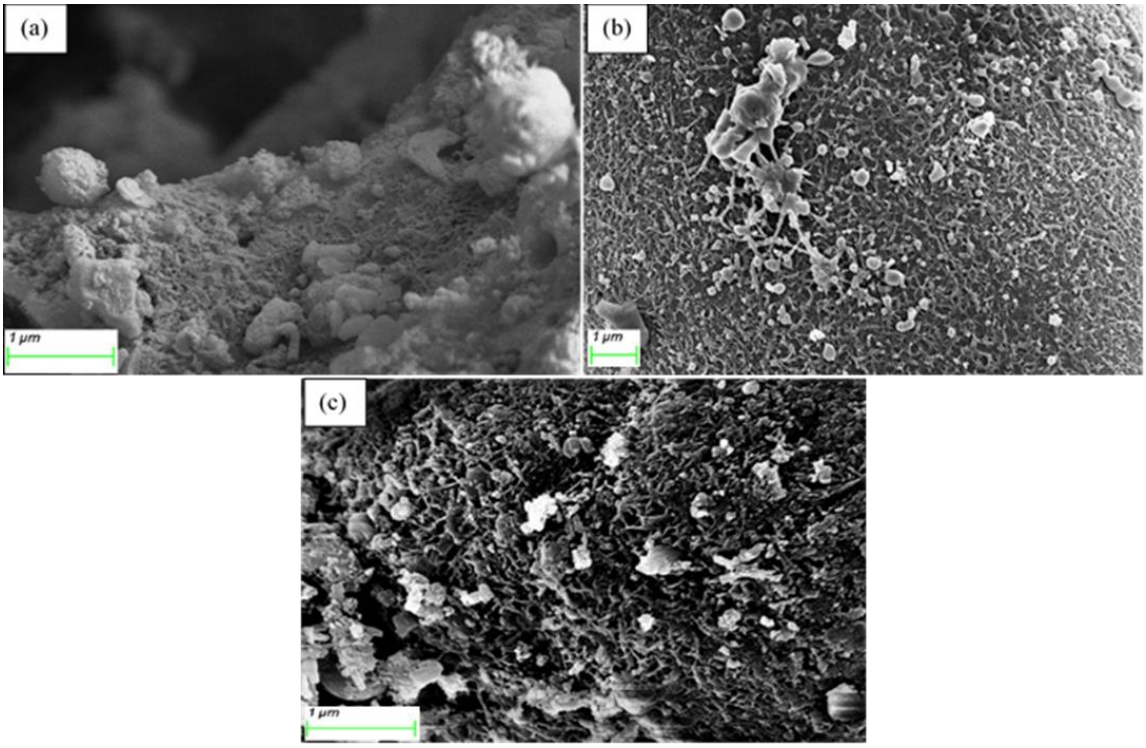


Figure 5.11: SEM micrographs showing CNMs grown from Sasol fly ash masses of (a) 600 mg, (b) 800 mg and (c) 1000 mg

Figure 5.12 exhibits the effect of the catalyst mass on crystallinity. The Raman spectra show that minor differences exist in the shifts of the peaks. This can be corroborated by the I_D/I_G ratio, which was found to be 0.95 for 600 mg, 0.98 for 800 mg, and 0.96 for 1000 mg, which shows the CNMs contain similar defects and degree of graphitization. The relative intensity ratios are coherent with the DTG measurements of the nanomaterials. Therefore, increasing the mass of the catalyst increases the yield of CNMs. However, the degree of graphitization of the synthesized CNMs remains unchanged.

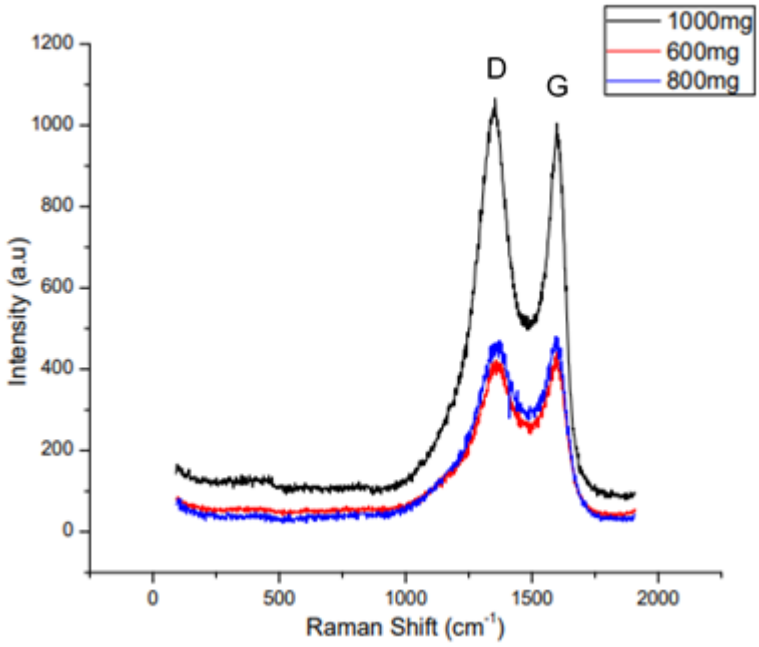


Figure 5.12: Raman spectra showing the effect of catalyst mass on the crystalinity of the CNMs

5.3.2 CNMs synthesis from Eskom fly ash

The effects of temperature, carbon source, and carrier gas flow rates, and catalyst mass were investigated using Eskom fly ash as a catalyst.

Effect of Temperature

The effect of temperature was investigated by using the same synthesis conditions used for Sasol fly ash in Table 5.1. The colour of the catalyst remained unchanged (light grey) when it was

removed from the furnace and was slightly dry and hard. This means that the yield, crystallinity, and purity of the CNMs from Eskom fly (E-FA) ash are extremely poor. Therefore, their TGA measurements are not shown. Instead, SEM images of the structures obtained post-synthesis are shown in Figure 5.13, Figure 5.14, and Figure 5.15. Crystallization of the mineral's phases in fly ash and their various shapes and morphologies was observed. The changes the catalyst underwent showed slight differences at their respective temperatures. CNMs are not visible possibly due to the low yields and the abundance of the fly ash catalyst. Several minerals occur from the same catalyst on the same synthesis run.

At temperatures of 750 ℃ in Figure 5.13a, the fly ash sphere shows small twigs and rod-like structures and no identifiable carbonaceous products. These twigs and rod-like structures are mullite crystals [43]. At the same temperature in Figure 5.13b, a sphere covered with hematite minerals [42] is shown.

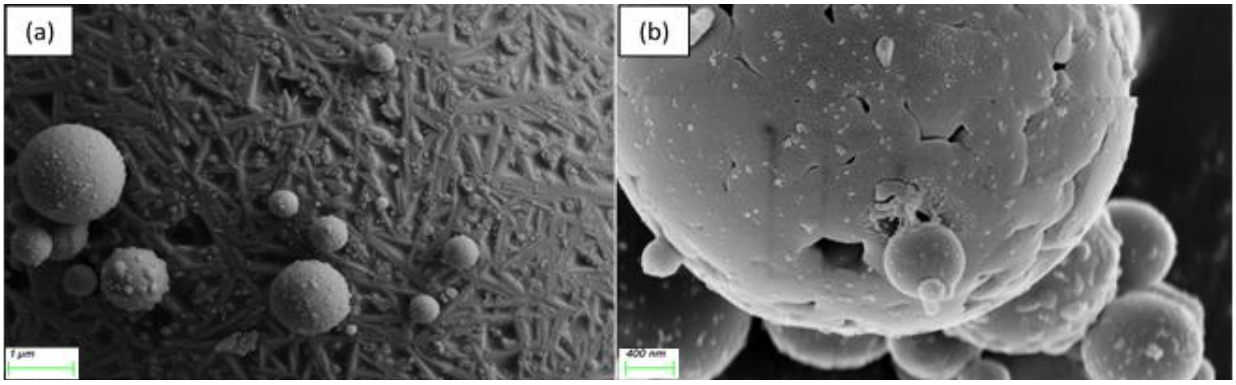


Figure 5.13: SEM micrographs of products obtained from Eskom fly ash at a temperature of 750℃ showing (a) small twigs or rod-like structures in the fly ash sphere (b) hematite minerals

The difference in these structures is attributable to the unequal distribution of minerals in each of the fly ash particles and its heterogenous composition. The mullite minerals in Figure 5.13a are also seen at temperatures of 850 ℃ (Figure 5.14b) and 950 ℃ (Figure 5.15b). These mullite minerals were also obtained by Song et al. [44] when they calcined amorphous silica-alumina particles at various temperatures (500-900 ℃) in air. Figure 5.14a & Figure 5.15a show the products obtained at temperatures of 850 ℃ and 950 ℃, respectively. The resulting minerals at 850 ℃ show pore with some fly ash spheres occupying them. These porous structures are thought to be lime [45]. At 950 ℃, a patterned formation of silica and magnetite is seen on the surface of

the sphere [46], [47]. The structures observed also indicate that the synthesis conditions were conducive for the crystallization of the minerals in the fly ash and can be extracted for other applications.

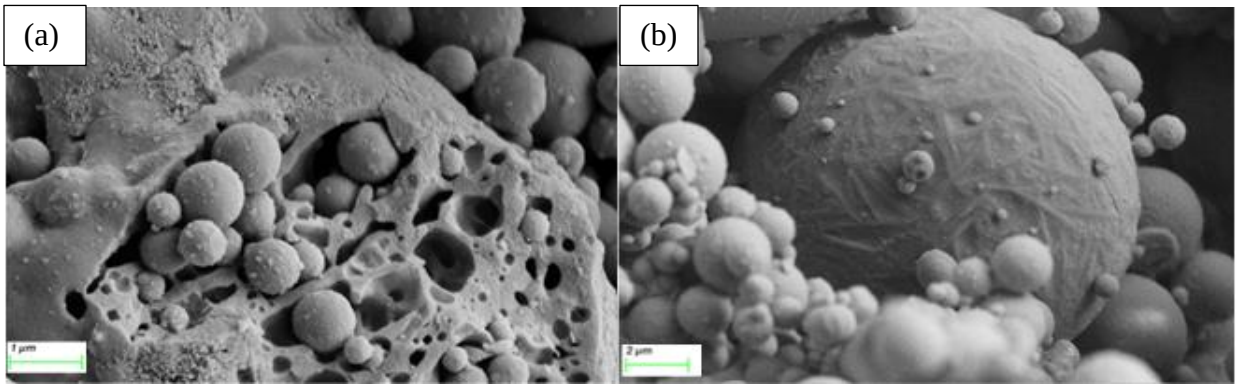


Figure 5.14: Products obtained from Eskom fly ash grown at 850℃ showing (a) pores in fly ash with spheres occupying them and (b) twigs and rod-like structures

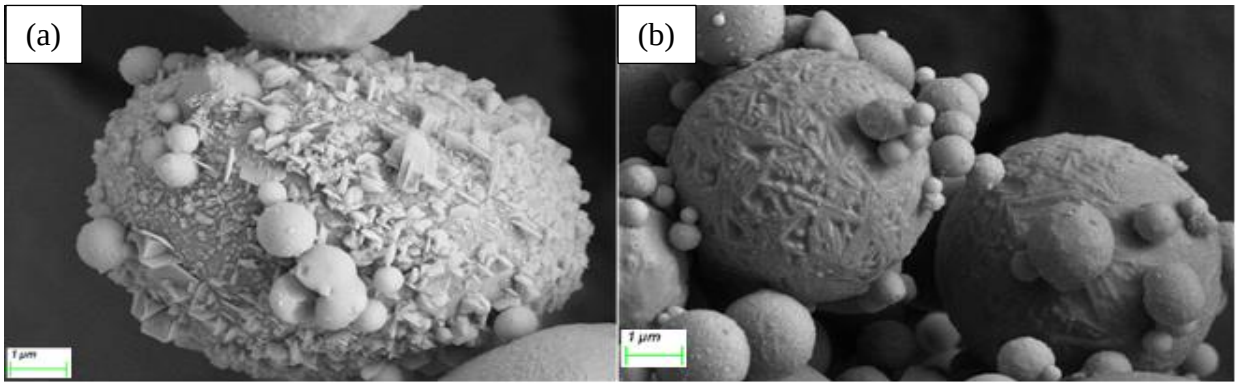


Figure 5.15: Products obtained at 950℃ during CNMs synthesis showing (a) a fly ash sphere covered with patterned and growth of magnetite and silica minerals and (b) twigs or rod-like structures of mullite

The Raman spectra of the very low yield of CNMs from E-FA are shown in Figure 5.16. The spectra obtained are coherent with the SEM results, showing nanomaterial of poor crystallinity at all temperatures since the D band is higher than the G band. The I_D/I_G ratios at 750, 850, and 950

℃ are 0.97, 1.16, and 1.12, respectively. This suggests that at low temperatures more crystalline carbonaceous products are formed from E-FA.

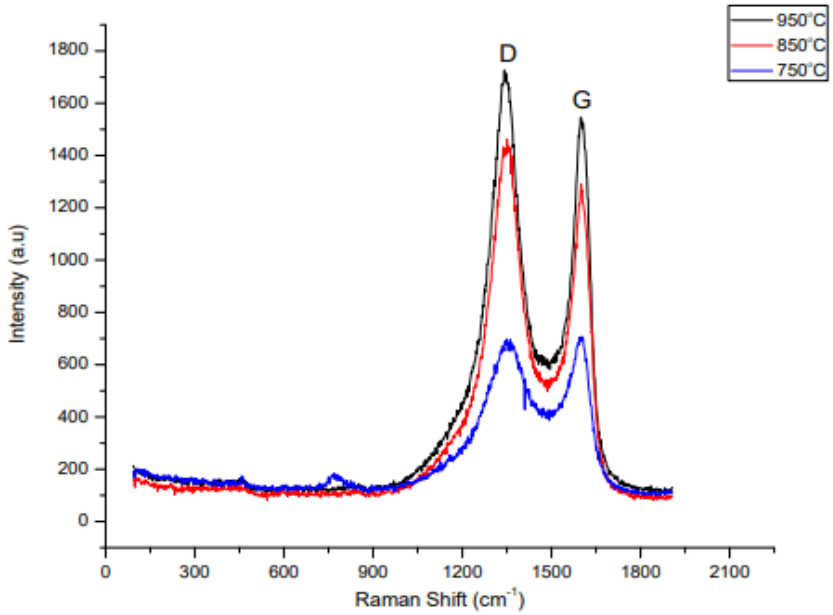


Figure 5.16: Raman Spectra of products synthesized from Eskom fly ash at temperatures of 750℃, 850℃, and 950℃

Effect of flow rate

The SEM micrographs obtained when the effect of flow rate was studied are shown in Figure 5.17. They show that the flow rate had a similar effect on the production of CNMs as temperature. Very low yields of CNMs were obtained. Alternatively, what is observed is the crystallization of the fly ash particles for the various flow rates investigated.

The Raman spectra of the synthesized products were obtained as depicted in Figure 5.18. The I_D/I_G ratios are 0.94, 1.02, and 1.00 for CO_2/Ar flow rates of 300.5/601, 600.1/1202, and 901.5/1202 sccm, respectively. These findings indicate that lower CO_2/Ar flow rates give CNMs better crystallinity and a low level of defects than at high flow rates. The low yields obtained from E-FA can be attributed to the low Fe content and loss on ignition (LOI), and lack of transition metal

catalyst active CNMs growth. This reduces the number of catalyst active sites available to catalyze the growth of CNMs.

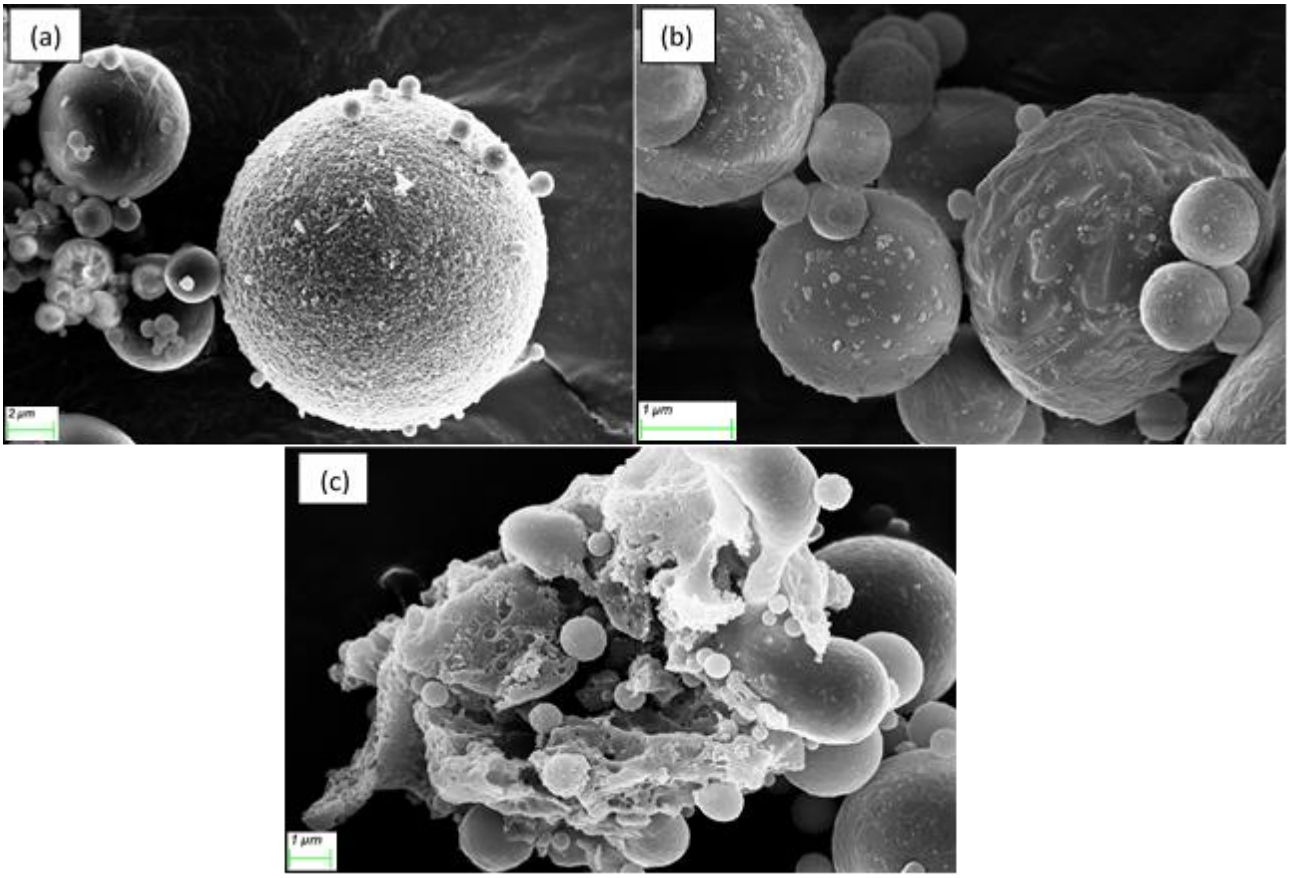


Figure 5.17: SEM images of products obtained from Eskom fly ash at CO_2/Ar flowrates of (a) 300.1/601 sccm, (b) 600.1/1202 sccm and (c) 901.5/1202 sccm

The low LOI reduces the ability of E-FA to act as a carbon source to provide extra carbon atoms and the low Fe content renders it an unfavourable catalyst for CNMs growth. While the high LOI and Fe content in S-FA enables it to act as both a better catalyst and carbon source, respectively. The different minerals observed when the effect of temperature and flow rate was investigated were not observed in the S-FA. Carbon nanomaterials could not be identified as seen in the previous parameters. It is due to this that the results of the influence of mass are not included and therefore not discussed.

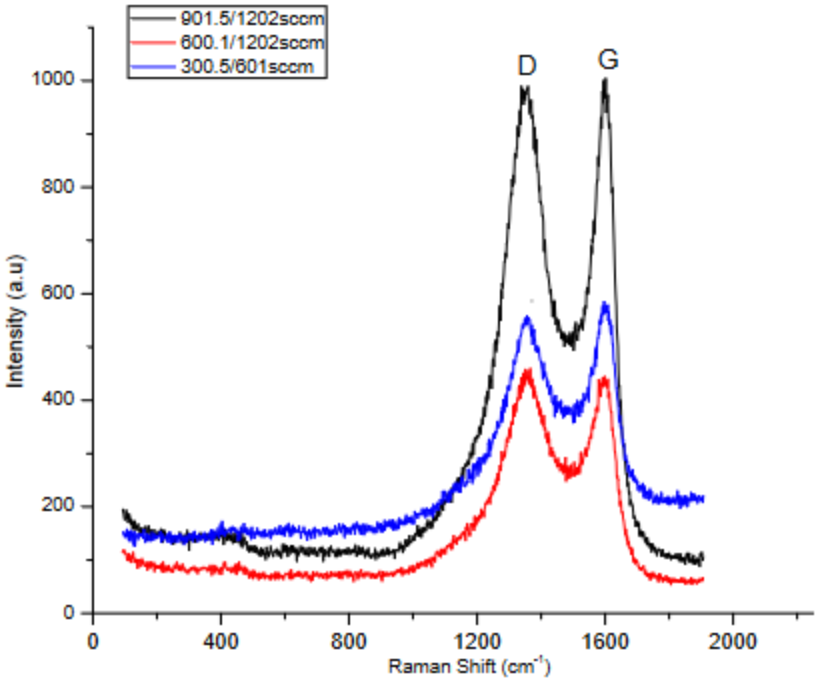


Figure 5.18: Raman Spectra of products synthesized from Eskom fly ash at CO_2/Ar flow rates of 300.5/601 sccm, 600.1/1202 sccm and 901.5/1202sccm

5.4 Conclusion

The synthesis of carbon nanomaterials from CO_2 as a carbon source and fly ash as both carbon source and catalyst was demonstrated. The catalytic activity of two South African fly ashes i.e., Sasol and Eskom, were compared under various temperatures, CO_2 and argon gas flow rates, and mass of catalyst. Overall, the yield obtained was poor in both fly ash catalysts. However, it was found that Sasol fly ash (S-FA) is a better catalyst for CNMs production than Eskom fly ash (E-FA). Better yields and crystallinity were obtained from S-FA compared to E-FA. The yield of CNMs from E-FA was extremely low and contained high amounts of unreacted catalysts. While the yield of CNMs from S-FA varied between 2-4% from the TGA. The E-FA fly ash products

visualized using SEM showed crystallization of the major minerals in fly ash. Whereas Sasol CNMs showed different morphologies and various diameter ranges from the investigated parameters. No crystallized minerals were observed in S-FA. The Raman spectra and DTG showed products of poor crystallinity under all the parameters and conditions from E-FA. For S-FA, good yields, and crystallinity CNMs were obtained at lower temperatures (750 °C), high CO_2 gas (962 sccm), and argon gas (1202 sccm) flow rates as well as bigger catalyst mass (1000 mg). The CNMs were mostly CNFs and CNTs.

5.5 References

[1] R. S. at al. Ruoff and D. C. Lorents, “Mechanical and thermal properties of carbon nanotubes,” *Carbon N. Y.*, vol. 33, no. 7, pp. 925–930, 1995.

[2] S. Frank, P. Poncharal, Z. L. Wang, and W. A. de Heer, “Carbon nanotube quantum resistors,” *Sci. (Washington, D. C.)*, vol. 280, no. 5370, pp. 1744–1746, 1998.

[3] S. Uemura *et al.*, “CARBON NANOTUBE EMITTERS FOR FIELD EMISSION DISPLAYS,” in *IEEE/CPMT/SEMI. 28th International Electronics Manufacturing Technology Symposium (Cat. No.03CH37479)*, 2003.

[4] M. S. D. Ado Jorio, Gene Dresselhaus, *Carbon Nanotubes Advanced Topics in the Synthesis, Structure, Properties and Applications*, vol. 111. 2007.

[5] K. Balasubramanian and M. Burghard, “Biosensors based on carbon nanotubes,” *Anal. Bioanal. Chem.*, vol. 385, no. 3, pp. 452–468, 2006.

[6] G. Mittal, V. Dhand, K. Y. Rhee, S. J. Park, and W. R. Lee, “A review on carbon nanotubes and graphene as fillers in reinforced polymer nanocomposites,” *J. Ind. Eng. Chem.*, vol. 21, pp. 11–25, 2015.

[7] J. Doh and J. Lee, “Prediction of the mechanical behavior of double walled-CNTs using a molecular mechanics-based finite element method: Effects of chirality,” *Comput. Struct.*, vol. 169, pp. 91–100, Jun. 2016.

[8] K. S. Karimov, F. A. Khalid, and M. T. S. Chani, “Carbon nanotubes based strain sensors,” *Meas. J. Int. Meas. Confed.*, vol. 45, no. 5, pp. 918–921, 2012.

[9] V. Jourdain and C. Bichara, “Current understanding of the growth of carbon nanotubes in catalytic chemical vapour deposition,” *Carbon*, vol. 58. Elsevier Ltd, pp. 2–39, 2013.

[10] M. Kumar and Y. Ando, “Chemical Vapor Deposition of Carbon Nanotubes: A Review on Growth Mechanism and Mass Production,” *J. Nanosci. Nanotechnol.*, vol. 10, no. 6, pp. 3739–3758, 2010.

[11] J. P. Tessonnier and D. S. Su, “Recent progress on the growth mechanism of carbon nanotubes: A review,” *ChemSusChem*, vol. 4, no. 7, pp. 824–847, 2011.

[12] G. D. Nessim, “Properties, synthesis, and growth mechanisms of carbon nanotubes with special focus on thermal chemical vapor deposition,” *Nanoscale*, vol. 2, no. 8, pp. 1306–1323, 2010.

[13] C. Journet *et al.*, “Large-scale production of single-walled carbon nanotubes by the electric-arc technique,” *Nature*, vol. 388, no. 6644, pp. 756–758, 1997.

[14] Y. Saito, R. Mizushima, S. I. Kondo, and M. Maida, “Field emission of electrons from graphitic nanofibers produced in a hydrogen arc discharge,” *Japanese J. Appl. Physics, Part 1 Regul. Pap. Short Notes Rev. Pap.*, vol. 39, no. 7 A, pp. 4168–4173, 2000.

[15] K. A. Shah and B. A. Tali, “Synthesis of carbon nanotubes by catalytic chemical vapour deposition: A review on carbon sources, catalysts and substrates,” *Materials Science in Semiconductor Processing*, vol. 41. Elsevier, pp. 67–82, 2016.

[16] S. A. Shokry, A. K. El Morsi, M. S. Sabaa, R. R. Mohamed, and H. E. El Sorogy, “Study of the productivity of MWCNT over Fe and Fe–Co catalysts supported on SiO2, Al2O3 and MgO,” *Egypt. J. Pet.*, vol. 23, pp. 183–189, 2014.

[17] E. D. Dikio, A. J. Kupeta, and F. T. Thema, “A comparative study of the effect of MgO and CaCO3 as support materials in the synthesis of carbon nanotubes with Fe/Co as catalyst,” *J. Chem.*, vol. 2014, 2014.

[18] D. Hardeman *et al.*, “The synergistic effect in the Fe-Co bimetallic catalyst system for the growth of carbon nanotube forests,” *J. Appl. Phys.*, vol. 117, no. 4, p. 044308, 2015.

[19] L. M. Hoyos-Palacio, A. G. García, J. F. Pérez-Robles, J. González, and H. V. Martínez-Tejada, “Catalytic effect of Fe, Ni, Co and Mo on the CNTs production,” in *IOP Conference Series: Materials Science and Engineering*, 2014, vol. 59, no. 1, p. 012005.

[20] “Effects | Facts – Climate Change: Vital Signs of the Planet.” [Online]. Available: https://climate.nasa.gov/effects/. [Accessed: 13-Oct-2020].

[21] A. Bradford and S. Pappas, “Effects of Global Warming | Live Science,” *Live Science*, 12-Aug-2017. [Online]. Available: https://www.livescience.com/37057-global-warming-effects.html. [Accessed: 13-Oct-2020].

[22] Hannah Ritchie and M. Roser, “CO2 and Greenhouse Gas Emissions,” *OurWorldInData.org*, 2020. [Online]. Available: https://ourworldindata.org/co2-and-other-greenhouse-gas-emissions#citation. [Accessed: 30-Mar-2021].

[23] X. j. Xu and S. ming Huang, “Carbon dioxide as a carbon source for synthesis of carbon nanotubes by chemical vapor deposition,” *Mater. Lett.*, vol. 61, no. 21, pp. 4235–4237, 2007.

[24] G. Allaedini, S. M. Tasirin, and P. Aminayi, “Synthesis of CNTs via chemical vapor deposition of carbon dioxide as a carbon source in the presence of NiMgO,” *J. Alloys Compd.*, vol. 647, pp. 809–814, 2015.

[25] G. S. Simate *et al.*, “Kinetic model of carbon nanotube production from carbon dioxide in a floating catalytic chemical vapour deposition reactor,” *RSC Adv.*, vol. 4, no. 19, pp. 9564–9572, 2014.

[26] N. Hintsho *et al.*, “Direct synthesis of carbon nanofibers from South African coal fly ash,” *Nanoscale Res. Lett.*, vol. 9, no. 387, 2014.

[27] O. M. Dunens, K. J. Mackenzie, and A. T. Harris, “Synthesis of Multiwalled Carbon Nanotubes on Fly Ash Derived Catalysts,” *Environ. Sci. Technol*, vol. 43, pp. 7889–7894, 2009.

[28] K. M. Rambau, N. M. Musyoka, N. Manyala, J. Ren, H. W. Langmi, and M. K. Mathe, “Preparation of carbon nanofibers/tubes using waste tyres pyrolysis oil and coal fly ash derived catalyst,” *J. Environ. Sci. Heal. - Part A Toxic/Hazardous Subst. Environ. Eng.*, vol. 53, no. 12, pp. 1115–1122, 2018.

[29] A. Yasui, Y. Kamiya, S. Sugiyama, S. Ono, H. Noda, and Y. Ichikawa, “Synthesis of carbon nanotubes on fly ashes by chemical vapor deposition processing,” *IEEJ Trans. Electr. Electron. Eng.*, vol. 4, no. 6, pp. 787–789, 2009.

[30] D. C. D. Nath and V. Sahajwalla, “Application of fly ash as a catalyst for synthesis of carbon nanotube ribbons,” *J. Hazard. Mater.*, vol. 192, pp. 691–697, 2011.

[31] N. Salah, A. A. Al-Ghamdi, A. Memic, S. S. Habib, and Z. H. Khan, “Formation of Carbon Nanotubes from Carbon-Rich Fly Ash: Growth Parameters and Mechanism,”

Mater. Manuf. Process., vol. 31, no. 2, pp. 146–156, 2016.

[32] M. S. Dresselhaus, G. Dresselhaus, R. Saito, and A. Jorio, "Raman spectroscopy of carbon nanotubes," *Physics Reports*, vol. 409. p. 47, 2005.

[33] C. Herrero-Latorre, J. Álvarez-Méndez, J. Barciela-García, S. García-Martín, and R. M. Peña-Crecente, "Characterization of carbon nanotubes and analytical methods for their determination in environmental and biological samples: A review," *Analytica Chimica Acta*, vol. 853, no. 1. pp. 77–94, 2015.

[34] T. Belin and F. Epron, "Characterization methods of carbon nanotubes: A review," *Materials Science and Engineering B: Solid-State Materials for Advanced Technology*, vol. 119, no. 2. pp. 105–118, 2005.

[35] A. Romero, A. Garrido, A. Nieto-Márquez, A. R. de la Osa, A. de Lucas, and J. L. Valverde, "The influence of operating conditions on the growth of carbon nanofibers on carbon nanofiber-supported nickel catalysts," *Applied Catalysis A: General*, vol. 319. pp. 246–258, 2007.

[36] Q. N. Pham *et al.*, "Effect of growth temperature on the synthesis of carbon nanotube arrays and amorphous carbon for thermal applications," *Phys. status solidi*, vol. 214, no. 7, p. 1600852, Jul. 2017.

[37] C. J. Lee, J. Park, Y. Huh, and J. Yong Lee, "Temperature effect on the growth of carbon nanotubes using thermal chemical vapor deposition," *Chem. Phys. Lett.*, vol. 343, no. 1–2, pp. 33–38, Jul. 2001.

[38] X. Z. Liao, A. Serquis, Q. X. Jia, D. E. Peterson, Y. T. Zhu, and H. F. Xu, "Effect of catalyst composition on carbon nanotube growth," *Appl. Phys. Lett.*, vol. 82, no. 16, pp. 2694–2696, 2003.

[39] A. C. Dupuis, "The catalyst in the CCVD of carbon nanotubes-a review," *Prog. Mater. Sci.*, vol. 50, no. 8, pp. 929–961, 2005.

[40] G. Allaedini, S. Masrinda Tasirin, P. Aminayi, Z. Yaakob, and M. Zainal MeorTalib, "Carbon nanotubes via different catalysts and the important factors that affect their production: A review on catalyst preferences," *Int. J. Nano Dimens*, vol. 7, no. 3, pp. 186–

185, 2016.

[41] M. H. Rümmeli *et al.*, “Catalyst size dependencies for carbon nanotube synthesis,” in *Physica Status Solidi (B) Basic Research*, 2007, vol. 244, no. 11, pp. 3911–3915.

[42] W. Z. Li, J. G. Wen, Y. Tu, and Z. F. Ren, “Effect of gas pressure on the growth and structure of carbon nanotubes by chemical vapor deposition,” *Appl. Phys. A Mater. Sci. Process.*, vol. 73, no. 2, pp. 259–264, 2001.

[43] G. Allaedini, S. M. Tasirin, and P. Aminayi, “Yield optimization of nanocarbons prepared via chemical vapor decomposition of carbon dioxide using response surface methodology,” *Diam. Relat. Mater.*, vol. 66, pp. 196–205, Jun. 2016.

[44] D. Valeev, A. Mikhailova, and A. Atmadzhidi, “Kinetics of iron extraction from coal fly ash by hydrochloric acid leaching,” *Metals (Basel).*, vol. 8, no. 7, p. 533, Jul. 2018.

[45] J. Li, X. Zhuang, X. Querol, O. Font, and N. Moreno, “A review on the applications of coal combustion products in China,” *International Geology Review*, vol. 60, no. 5–6. Taylor and Francis Inc., pp. 671–716, 26-Apr-2018.

[46] K. Song, W. Kim, C. Y. Suh, J. H. Bang, and J. W. Ahn, “Preparation of mullite-silica composites using silica-rich monophasic precursor obtained as a byproduct of mineral carbonation of blast-furnace slag,” *Minerals*, vol. 8, no. 5, 2018.

[47] Wu *et al.*, “Mineralogical and Environmental Geochemistry of Coal Combustion Products from Shenhuo and Yihua Power Plants in Xinjiang Autonomous Region, Northwest China,” *Minerals*, vol. 9, no. 8, p. 496, Aug. 2019.

[48] L. L. de Sousa, R. Salomão, and V. L. Arantes, “Development and characterization of porous moldable refractory structures of the alumina-mullite-quartz system,” *Ceram. Int.*, vol. 43, no. 1, pp. 1362–1370, Jan. 2017.

[49] Munasir *et al.*, “Structure Analysis of Fe3O4@SiO2 Core Shells Prepared from Amorphous and Crystalline SiO2 Particles,” in *IOP Conference Series: Materials Science and Engineering*, 2018, vol. 367, no. 1.

Chapter 6: Synthesis of CNMs from C_2H_2 using Sasol and Eskom Fly Ash

6.1 Introduction

Fly ash forms as a by-product of the combustion of fossil fuels such as coal in coal-fired power stations for electricity generation [1]. This solid amorphous and generally fine material contains glassy-spherical particles with an unequal size distribution that varies from a few to several microns [2]. It is largely composed of alumina-silicate minerals with minor amounts of lime and hematite and unburnt carbon. Metals in trace amounts are also found as constituents in fly ash. Their presence and some elements, as well as their disposal methods, raised serious environmental concerns which could result in air pollution or contaminate groundwater [3]–[5]. There are also costs involved in transporting the fly ash from the power station to the dumpsites since it is generated in huge amounts [6]. Additionally, to accommodate the large quantities generated, a vast amount of land needs to be available and maintained [7]. These challenges precipitated methods to find new ways of utilizing and recycling fly ash. It has been used in construction (cement and concrete) [8][7], agriculture[9][10], (supported) catalyst [11], [12] and adsorbents [13], [14]. Recently, there has been an increasing interest in using fly ash as a catalyst and co-precursor to synthesize carbon nanomaterials (CNMs). The advantages of fly ash in the application of CNMs are its affordability, readily available in large amounts, and can be used without any catalyst support and pre-treatments or preparation steps. South Africa is the 7th largest (277 million tons) producer of coal globally and 62 % of this coal is used for electricity generation [15]. This produces more than 50 million tons per annum (mta) of ash and only about 10% is utilized [16]. This shows that much work is still required to find possible ash utilization pathways. In the past couple of decades, nanocarbons have become one of the most researched fields of study. The interest in these materials can be attributed to their unique properties such as their extraordinary mechanical strength, remarkable thermal and electrical conductivity [17]. These nanostructures are grown using several techniques, namely arc discharge, laser ablation, and chemical vapour deposition (CVD). However, the CVD method has been used extensively since it is affordable, scalable, and allows for different forms of catalysts and carbon precursors to be tested [18]. A basic CVD method generally requires a catalyst, carbon source, carrier gas, and heat [19]. However, the transition metal catalysts (Fe, Ni, and Co) used are expensive and toxic. This calls for researchers

to find alternative catalysts that can be used with little to no pre-treatment, that are also affordable and less harmful. Such a material that has been explored as a catalyst and fits these criteria is fly ash.

Thus, in this study, we intend to use fly ash to produce CNMs from two South African major utilities, Sasol and Eskom. These two utilities produce fly ash in large amounts. Eskom is the largest electricity producer in Africa from coal, whereas Sasol converts it to liquids and also power generation [20]. Although both utilities use the pulverized coal combustion (PCC) method to burn the coal, different fly ash products with distinct quantities of unburnt carbon content and chemical composition are produced. Moreover, only fly ash from Eskom has been tested for carbon nanomaterial production and the literature surrounding fly ash utilization within the South African context is limited [21], [22]. Consequently, we compared the catalytic capability of fly ash from Eskom and Sasol to produce CNTs/Fs in good yield and crystallinity from acetylene. The yield, quality/crystallinity of the resulting carbon nanomaterial will be used to determine the catalytic ability of the fly ash to synthesize the carbon nanomaterials.

6.2 Experimental Method

The CVD method was used to synthesize CNMs with fly ash as a catalyst, acetylene as a carbon source, and argon as a carrier gas. Eskom fly ash (E-FA) was obtained from Lethabo power station through Lafarge (South Africa) and Sasol fly ash (S-FA) was obtained from Secunda, South Africa, and both were used as received. The catalyst (600 mg) was evenly spread on a quartz boat and placed at the centre of the reactor inside the horizontal tubular furnace. Then the catalyst was heated at a rate of 10 ℃/min for 70 minutes while purging with argon (500 sccm) and to also prevent oxidation of the CNMs. When the furnace reached a temperature of 800 ℃, acetylene was introduced into the reactor at a flow rate of 50 sccm. After a period of 1 hr had passed the acetylene flow was stopped, and the furnace was cooled down to room temperature under argon flow. The resulting black-powdery product was collected.

6.3 Results and Discussion

Thermogravimetric analysis (TGA) allows for the quantitative determination of impurities and the purity of CNMs. This is done by assessing the CNMs' mass loss with increasing temperature. It has been reported that the initial decomposition temperatures of amorphous carbon, single-wall carbon nanotubes (SWCNTs), and multi-walled carbon nanotubes (MWCNTs) occur at around

330-450 ℃, 500-600 ℃, and 700 ℃, respectively [32]–[35] CNFs synthesis produces little to no amorphous carbon and generally contains large diameters, making them likely to be resistant to oxidation [32].

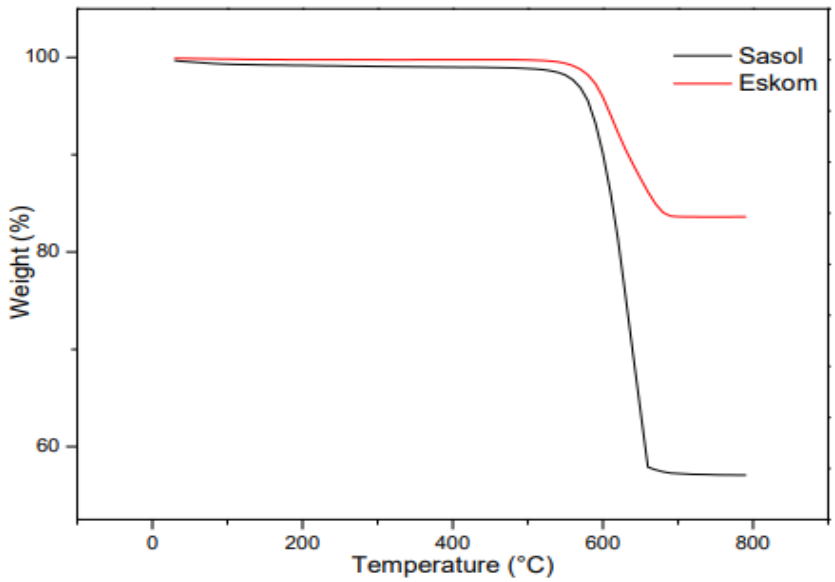


Figure 6.1: TGA data of CNMs synthesized from acetylene using raw Sasol and Eskom fly ash

Therefore, they would have higher decomposition and oxidative temperatures. The TGA was performed with 10 mg of each sample and heated at a rate of 20 ℃/min in air and nitrogen at 50 ml/min. The thermograms for the carbonaceous materials are shown in Figure 6.1. The presence of amorphous carbon was not detected. The product collected from the furnace was 1.15g from Sasol and 0.87 g from Eskom. The TGA data shows Sasol CNMs (S-CNMs) with a mass loss of 41 wt% and Eskom CNMs (E-CNMs) with 17wt%. By using these the yield is estimated to be: 0.47 g $(41\% \times 1.15\ g)$ for Sasol CNMs and for Eskom CNMs 0.15 g $(17\% \times 0.87\ g)$. The difference in the yield arises from the high amounts of iron and Loss on Ignition (LOI) and iron in S-FA as evidenced in chapter 4.

There are more catalyst sites where the Fe is high to catalyze CNMs. The high LOI in S-FA indicates that there is unburnt carbon which can provide extra carbon atoms for the growth of CNMs under the same conditions. Since TGA gives only the onset oxidation temperature, the derivative thermogravimetry (DTG) can be used to determine the oxidation temperature and

product distribution. A higher decomposition and oxidation temperature generally indicates a low level of impurities and a wider width peak indicates a wide size distribution of the materials. The DTG curves are given in Figure 6.2.

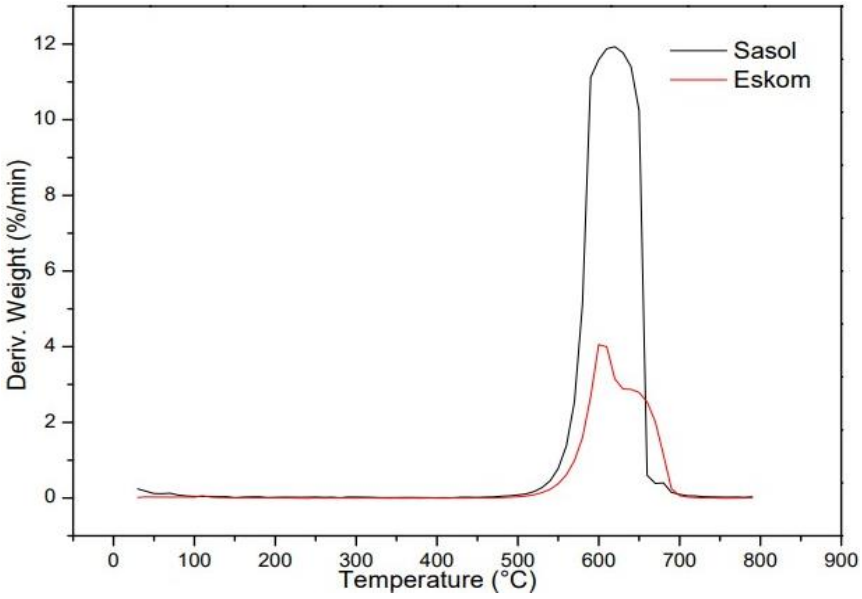


Figure 6.2: Derivative Weight curves of Sasol and Eskom carbon nanomaterials

The two peaks in E-CNMs indicate that two carbonaceous products were formed. The first peak is at 600 ℃ is nanofibers and the second peak occurs at 640 ℃ is attributed to carbon microspheres (CMSs). These two products are identified using TEM. S-CNMs show a strong and wide single peak at 620 ℃. Furthermore, the higher oxidation temperatures in the DTG thermogram suggested that products with good crystallinity were formed as explained previously. The high oxidation temperature of CNFs is also suspected to be from the large diameter of this material as mentioned by Dunens et al. [38]. A summary of the oxidation and decomposition temperatures from the derivative weight and TGA thermograms is given in Table 6.1.

Table 6.1: Summary of DTG and TGA temperature values of Eskom and Sasol CNMs

Products	Derivative Weight (℃)		TGA (℃)
	CMSs	CNFs/Ts	-
S-CNMs	-	620	550
E-CNMs	600	640	550

The products obtained from the decomposition of acetylene on fly ash catalysts from South African coals were visualized using SEM in Figure 6.3. The Eskom (Figure 6.3a) and Sasol fly ash (Figure 6.3b) surfaces were both covered in vast amounts of entangled CNFs and are distributed unequally on both catalysts. This is explained by the unequal distribution of Fe and carbon in fly ash where CNMs growth is favoured. The deposited CNMs contain longer nanofibers which are seen to be dividing or branching to form an enclosed shape (Figure 6.3c-d). CNFs with large diameters were formed during the synthesis due to the large sizes of the catalysts and varied significantly between the materials. S-CNFs had the largest diameter range, from 60-110 nm while E-CNFs ranged from 60-88 nm. The particle size distribution (chapter 4) also affirms this since S-FA contained a higher

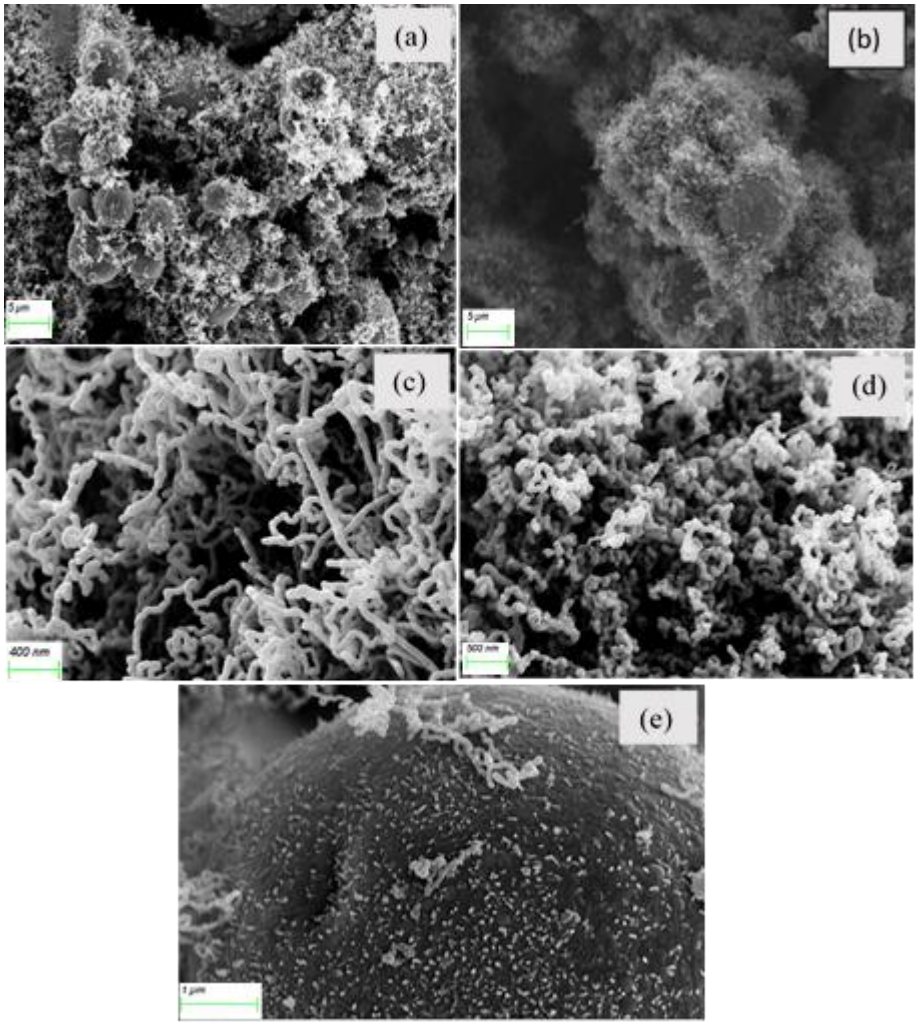


Figure 6.3: SEM images of CNMs grown on fly ash (a) Eskom CNMs (b) Sasol CNMs (c) morphology of E-CNMs (d) morphology of S-CNMs (e) small rod-like CNMs precipitating from E-FA

concentration of particles of the same size than E-FA. Similar results were obtained by Hintsho et al. [21] when E-FA was used as a catalyst for CNFs formation. Furthermore, it is well-established that the catalyst particle size has a direct influence on the diameter of CNT/Fs [19], [39]–[42]. The larger diameter of the products may also be influenced by the high temperature (800 ℃) used in this study, which coincides with the work of Miniach et al. [43]. In their study, CNFs were synthesized from methane on a hydroxyapatite-supported nickel catalyst at different temperatures. They observed that as the temperature increased, the diameter of the CNFs also increased. This was said to be from the ease at which the migration of the catalyst over the support surface occurs, which leads to their aggregation forming thicker CNFs [43]–[45].

On the surface of a spherical E-FA particle, small rod-like structures appear to be attempting to precipitate out of the sphere, while in some areas on the same sphere, strands of CNFs are observed (Figure 6.3c). This is due to the low LOI and Fe contents of E-FA which limits its ability to act as both carbon source and catalyst and would require a high rate of carbon supply to allow for complete precipitation. For S-FA, this carbon deficiency is compensated by the high LOI which enables it to also act as a co-precursor in addition to being a catalyst. Additionally, the high Fe content in S-FA gives it an advantage over E-FA such that the decomposition of the hydrocarbon is increased and provides more catalyst active sites for CNMs growth. The findings here are corroborated by differences in the yield. These findings are coherent with the work of Salah et al.[46] where high yields of CNTs were obtained from carbon-rich fly ash under various synthesis conditions. Therefore, CNMs growth was found to be favourable on S-FA compared to E-FA in terms of the yield.

The TEM images of the CNMs are depicted in Figure 6.4. Different types of CNF structures were obtained from the acetylene-treated fly ashes. A mixture of herringbone CNFs and CNTs is observed in Figure 6.4a from S-FA. The CNTs contain open ends. E-CNMs contain nanofiber structures with large and small diameters (Figure 6.4b). The E-CNFs have filled cores with closed ends, the dark centers and the circles along the strands observed in S-CNFs rarely occur. The ring-like and branching morphology of the nanocarbon products observed are consistent with the SEM images. This could The CNMs contain various diameters and lengths.

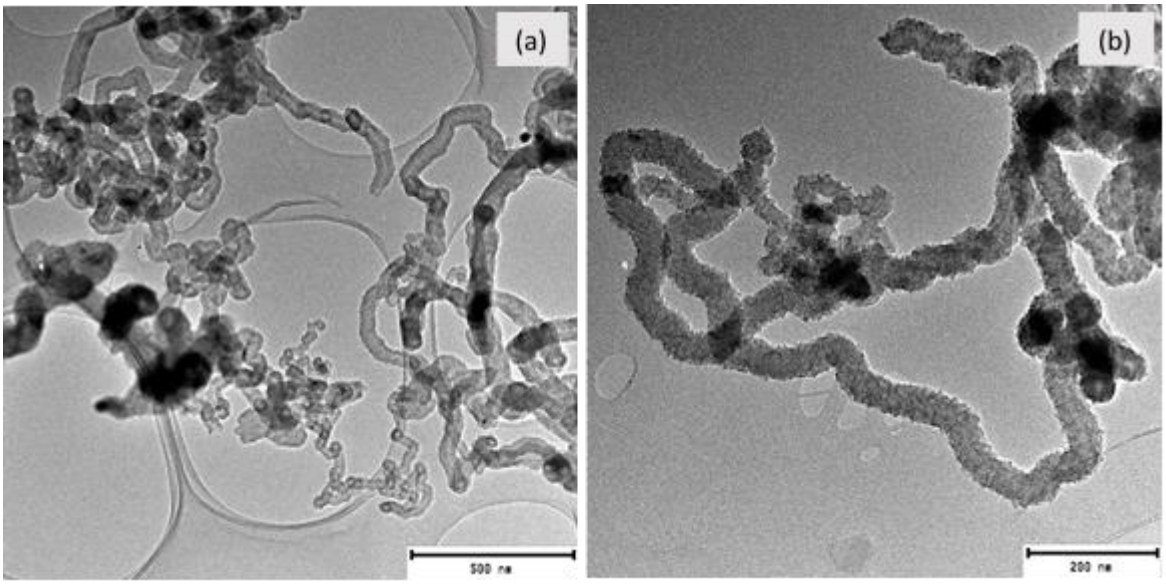


Figure 6.4: TEM micrographs showing morphology of (a) Sasol CNMs from S-FA and (b) Eskom CNMs from E-FA

This blend of structures could be attributed to the heterogeneity of the fly ash catalyst and the shape of the particles means that the CNFs growth occurs from a central point in the catalyst to different directions. The catalyst particles are visible in the center at the nanofibers and the tips, suggesting the tip-growth mechanism. The E-CNMs also contain microspheres (CMSs) shown in Figure 6.5 have a mixture of small and large spheres with smooth surfaces. Their growth took place due to the small amount of Fe found on E-FA since their growth generally occurs in the

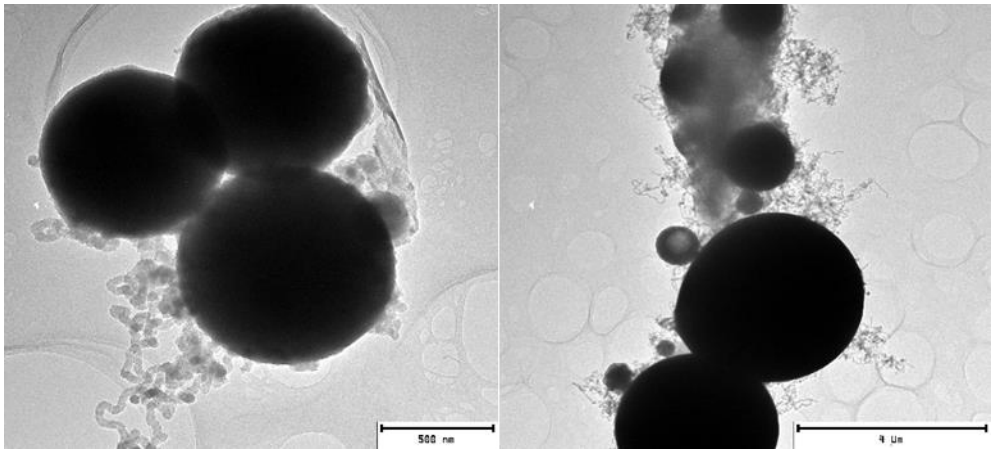


Figure 6.5: Carbon microspheres covered with amorphous material observed in Eskom carbon nanomaterials

absence of a catalyst [48]. The two carbonaceous products observed in the TEM of E-CNMs are the two peaks observed in the DTG (Figure 6.2)

The XRD patterns of the carbon nanomaterials were compared along with their respective fly ash catalysts to determine the changes in their crystalline phases and the presence of graphitic material. The XRD patterns of the catalysts and accompanying carbonaceous products are exhibited in Figure 6.6. The typical phases (mullite, quartz, calcite) are found in both catalysts Figure 6.6a. In the spectrum of Eskom fly ash, calcite was not detected whereas it was found in Sasol fly ash at low concentrations. A strong overlap of the graphitic and quartz/mullite phases is seen in the diffraction peaks of the CNMs Figure 6.6b. Peak broadening and widening were also observed in the narrow degree range ($2\theta = 20\text{-}32°$) of graphite peak which was not seen in the raw fly ash [49]. However, it is more pronounced in the S-CNMs (since its yield is higher) signifying changes in the structure.

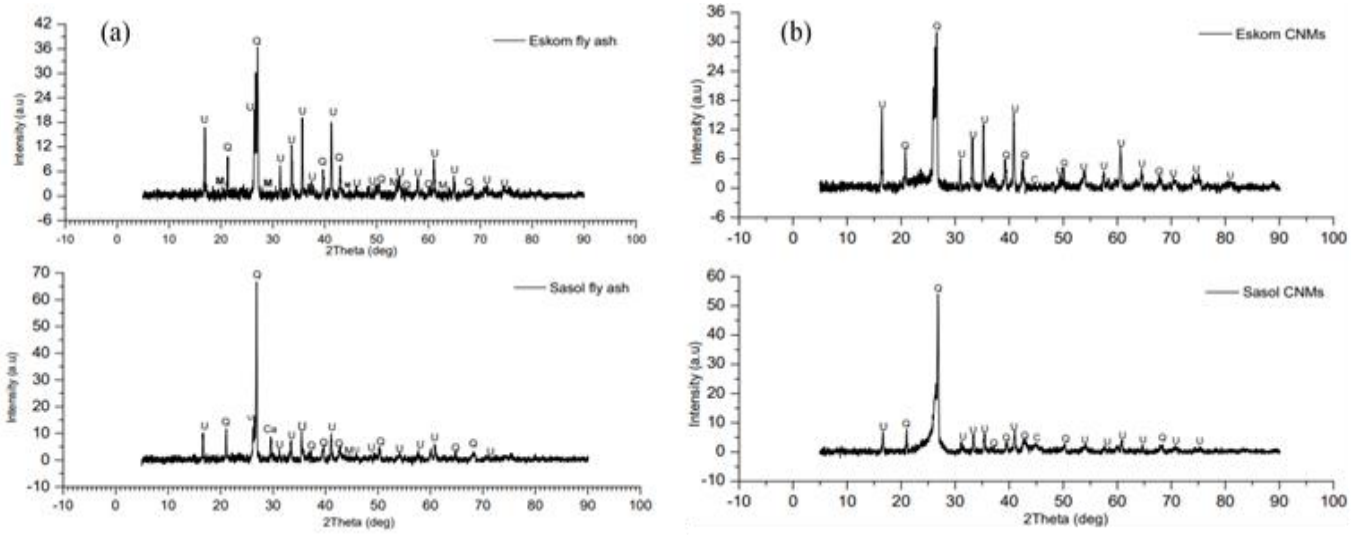


Figure 6.6: XRD patterns of (a) Raw Sasol and Eskom fly ashes and (b) synthesized CNMs from Sasol and Eskom. U-Mullite, Q-quartz, Ca-calcite, M-magnetite

Raman spectroscopy is used to determine the presence of defective carbon and the degree of graphitization of the nanocarbon structure [41]. The D band which is generally observed at ~1350 cm^{-1} results from the presence of defective carbon. While the G band ranges from 1400-1700 cm^{-1} gives the existence of graphitic carbon [42], [43]. The relative intensity ratio (I_D/I_G) of the D band

and the G-band gives the degree of graphitization and quality of the CNMs. A low I_D/I_G ratio is indicative of a CNM structure with good crystallinity and a low level of defects [44]. The Raman spectra obtained from the synthesis of CNMs from S-FA and E-FA catalysts are shown in Figure 6.7. Two strong peaks are observed for both CNMs. The D and G bands of S-CNMs are located at 1347 cm^{-1} and 1601 cm^{-1}, respectively. The intensity of the D peak is lower than the G peak which indicates more ordered carbon in the CNMs [45]. The I_D/I_G ratio of CNMs from S-FA was found to be 0.86. While in E-CNMs the D band is at a wavelength of 1342 cm^{-1} and the G band at 1598 cm^{-1}, and their I_D/I_G ratio was 0.84. Since intensity ratios of both materials are low and closely similar, this would suggest that their CNM structure has good crystallinity and quality with negligible differences.

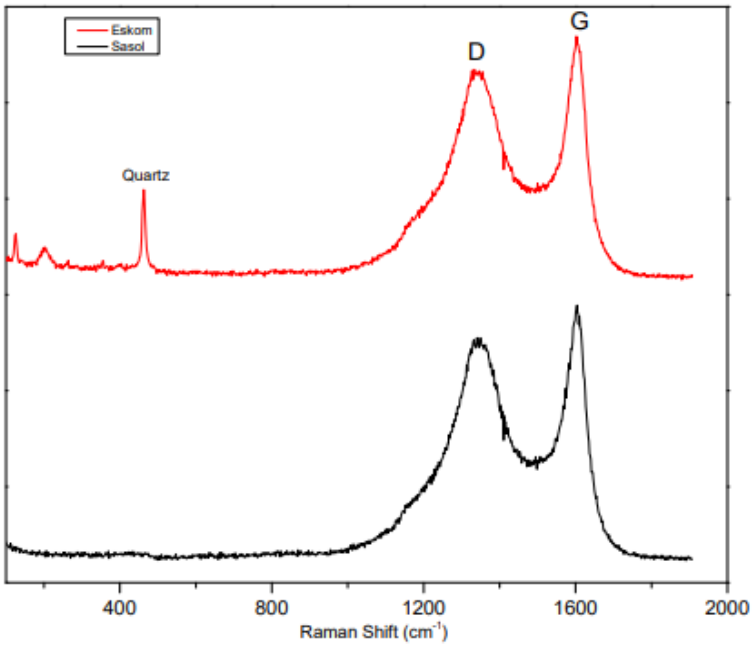


Figure 6.7: Raman Spectra of CNMs synthesized from Eskom and Sasol fly ash as catalyst

6.4 Conclusion

In this chapter, carbon nanomaterials which were comprised of carbon nanotubes, carbon nanofibers, and carbon microspheres were successfully synthesized from Eskom and Sasol fly ash. CNMs from E-FA were formed in lower yields compared to S-FA. An entangled network of CNFs with diameters ranging from 60 nm to 110 nm and unreacted fly ash particles were seen in the SEM images of Sasol CNMs. The large diameters were confirmed by the broad peak width in

DTG, while E-CNMs had a narrow contained two peaks indicating different forms of carbon. These were identified with TEM and were found to be CNFs and microspheres. Raman spectroscopy indicated that both materials had a high degree of crystallinity with E-CNMs showing peaks of quartz and SWCNTs at the lower region of the spectrum. The TGA results confirmed this with the high onset oxidation (550 ℃) and oxidation temperature and further showed that no amorphous carbon was present in both products. Although their crystallinity is relatively similar, the results obtained suggested that S-FA would be better suitable for CNMs synthesis than E-FA since it gave a higher yield.

6.5 References

[1] S. K. Ritter, “A New Life For Coal Ash| Chemical & Engineering News,” *American Chemical Society*, vol. 94, no. 7, pp. 10–14, 15-Feb-2016.

[2] R. Sett, “Flyash: Characteristics, Problems and Possible Utilization,” *Adv. Appl. Sci. Res.*, vol. 8, no. 3, pp. 32–50, 2017.

[3] R. K. Singh, N. C. Gupta, and B. K. Guha, “Fly Ash Disposal in Ash Ponds: A Threat to Ground Water Contamination,” *J. Inst. Eng. Ser. A*, vol. 97, no. 3, pp. 255–260, 2016.

[4] lubna A. A. Ibrahim, “Chemical characterization and mobility of metal species in fly ash–water system,” *Water Sci.*, vol. 29, no. 2, pp. 109–122, Oct. 2015.

[5] D. Paswan, S. M. A, M. Shaikh, A. Nadar, and S. D. Maniyar, “Heavy Metals in Fly Ash ; Its Impact on Human Health and Environment,” in *NICMAR 2nd International Conference On Construction, Real Estate, Infrastructure and Project (CRIP) Managemen*, 2017.

[6] Z. T. Yao *et al.*, “A comprehensive review on the applications of coal fly ash,” *Earth-Science Rev.*, vol. 141, pp. 105–121, 2015.

[7] N. Ghazali, K. Muthusamy, and S. Wan Ahmad, “Utilization of Fly Ash in Construction,” *IOP Conf. Ser. Mater. Sci. Eng.*, vol. 601, no. 1, 2019.

[8] G. Xu and X. Shi, “Characteristics and applications of fly ash as a sustainable construction material: A state-of-the-art review,” *Resour. Conserv. Recycl.*, vol. 136, pp. 95–109, 2018.

[9] M. R. Khan and M. W. Khan, “The effect of fly ash on plant growth and yield of tomato,” *Environ. Pollut.*, vol. 92, no. 2, pp. 105–111, Apr. 1996.

[10] D. C. Adriano, T. A. Woodford, and T. G. Ciravolo, “Growth and Elemental Composition of Corn and Bean Seedlings as Influenced by Soil Application of Coal Ash,” *J. Environ. Qual.*, vol. 7, no. 3, pp. 416–421, Jul. 1978.

[11] S. Wang, “Application of solid ash based catalysts in heterogeneous catalysis,” *Environ. Sci. Technol.*, vol. 42, no. 19, pp. 7055–7063, 2008.

[12] D. Jain, C. Khatri, and A. Rani, “Fly ash supported calcium oxide as recyclable solid base

catalyst for Knoevenagel condensation reaction," *Fuel Process. Technol.*, vol. 91, no. 9, pp. 1015–1021, Sep. 2010.

[13] Z. Aksu and J. Yener, "The usage of dried activated sludge and fly ash wastes in phenol biosorption/adsorption: Comparison with granular activated carbon," *J. Environ. Sci. Heal. - Part A Toxic/Hazardous Subst. Environ. Eng.*, vol. 34, no. 9, pp. 1777–1796, 1999.

[14] D. Mohan, K. P. Singh, G. Singh, and K. Kumar, "Removal of Dyes from Wastewater Using Flyash, a Low-Cost.pdf," *Ind. Eng. Chem. Res.*, vol. 41, no. 15, pp. 3688–3695, 2002.

[15] Eskom, "Coal Power." [Online]. Available: https://www.eskom.co.za/AboutElectricity/ElectricityTechnologies/Pages/Coal_Power.aspx. [Accessed: 19-Oct-2020].

[16] K. Reynolds-Clausen and N. Singh, "South Africa's power producer's revised Coal Ash Strategy and Implementation Progress," in *2017 World of Coal Ash Conference*, 2017, pp. 1–10.

[17] A. Eatemadi *et al.*, "Carbon nanotubes: Properties, synthesis, purification, and medical applications," *Nanoscale Res. Lett.*, vol. 9, pp. 1–13, 2014.

[18] N. M. Mubarak, E. C. Abdullah, N. S. Jayakumar, and J. N. Sahu, "An overview on methods for the production of carbon nanotubes," *Journal of Industrial and Engineering Chemistry*, vol. 20, no. 4. The Korean Society of Industrial and Engineering Chemistry, pp. 1186–1197, 2014.

[19] K. A. Shah and B. A. Tali, "Synthesis of carbon nanotubes by catalytic chemical vapour deposition: A review on carbon sources, catalysts and substrates," *Materials Science in Semiconductor Processing*, vol. 41. Elsevier, pp. 67–82, 2016.

[20] M. Steyn and R. C. A. Minnitt, "Thermal coal products in South Africa," *J. South. African Inst. Min. Metall.*, vol. 110, no. 10, pp. 593–599, 2010.

[21] N. Hintsho *et al.*, "Direct synthesis of carbon nanofibers from South African coal fly ash," *Nanoscale Res. Lett.*, vol. 9, no. 387, 2014.

[22] K. M. Rambau, N. M. Musyoka, N. Manyala, J. Ren, H. W. Langmi, and M. K. Mathe, "Preparation of carbon nanofibers/tubes using waste tyres pyrolysis oil and coal fly ash derived catalyst," *J. Environ. Sci. Heal. - Part A Toxic/Hazardous Subst. Environ. Eng.*, vol. 53, no. 12, pp. 1115–1122, 2018.

[23] A. G. Bannov, M. V. Popov, and P. B. Kurmashov, "Thermal analysis of carbon nanomaterials: advantages and problems of interpretation," *J. Therm. Anal. Calorim.*, vol. 142, no. 1, pp. 349–370, 2020.

[24] S. Santangelo, G. Messina, G. Faggio, M. Lanza, A. Pistone, and C. Milone, "Calibration of reaction parameters for the improvement of thermal stability and crystalline quality of multi-walled carbon nanotubes," *J. Mater. Sci.*, vol. 45, no. 3, pp. 783–792, 2010.

[25] J. H. Lehman, M. Terrones, E. Mansfield, K. E. Hurst, and V. Meunier, "Evaluating the characteristics of multiwall carbon nanotubes," *Carbon N. Y.*, vol. 49, no. 8, pp. 2581–2602, 2011.

[26] S. M. Toussi, A. Fakhru'L-Razi, A. L. Chuah, and A. R. Suraya, "Effect of synthesis condition on the growth of SWCNTs via catalytic chemical vapour deposition," *Sains Malaysiana*, vol. 40, no. 3, pp. 197–201, 2011.

[27] Y. Li *et al.*, "Mass production of high-quality multi-walled carbon nanotube bundles on a Ni/Mo/MgO catalyst," *Carbon N. Y.*, vol. 43, no. 2, pp. 295–301, 2005.

[28] E. MacCallini *et al.*, "A spectro-microscopic investigation of Fe-Co bimetallic catalysts supported on MgO for the production of thin carbon nanotubes," *Carbon N. Y.*, vol. 48, no. 12, pp. 3434–3445, 2010.

[29] O. M. Dunens, K. J. Mackenzie, and A. T. Harris, "Synthesis of Multiwalled Carbon Nanotubes on Fly Ash Derived Catalysts," *Environ. Sci. Technol*, vol. 43, pp. 7889–7894, 2009.

[30] C. L. Cheung, A. Kurtz, H. Park, and C. M. Lieber, "Diameter-controlled synthesis of carbon nanotubes," *J. Phys. Chem. B*, vol. 106, no. 10, pp. 2429–2433, 2002.

[31] A. Magrez, J. W. Seo, R. Smajda, M. Mionić, and L. Forró, "Catalytic CVD synthesis of carbon nanotubes: Towards high yield and low temperature growth," *Materials*, vol. 3, no.

11. pp. 4871–4891, 2010.

[32] F. Schäff *et al.*, “Tailoring the diameter, density and number of walls of carbon nanotubes through predefined catalyst particles,” *Phys. Status Solidi Appl. Mater. Sci.*, vol. 205, no. 6, pp. 1382–1385, Jun. 2008.

[33] M. H. Rümmeli *et al.*, “Catalyst size dependencies for carbon nanotube synthesis,” in *Physica Status Solidi (B) Basic Research*, 2007, vol. 244, no. 11, pp. 3911–3915.

[34] E. Miniach, A. Śliwak, A. Moyseowicz, and G. Gryglewicz, “Growth of carbon nanofibers from methane on a hydroxyapatite-supported nickel catalyst,” *J. Mater. Sci.*, vol. 51, no. 11, pp. 5367–5376, 2016.

[35] A. Romero, A. Garrido, A. Nieto-Márquez, A. R. de la Osa, A. de Lucas, and J. L. Valverde, “The influence of operating conditions on the growth of carbon nanofibers on carbon nanofiber-supported nickel catalysts,” *Applied Catalysis A: General*, vol. 319. pp. 246–258, 2007.

[36] G. D. Nessim, “Properties, synthesis, and growth mechanisms of carbon nanotubes with special focus on thermal chemical vapor deposition,” *Nanoscale*, vol. 2, no. 8, pp. 1306–1323, 2010.

[37] N. Salah, A. A. Al-Ghamdi, A. Memic, S. S. Habib, and Z. H. Khan, “Formation of Carbon Nanotubes from Carbon-Rich Fly Ash: Growth Parameters and Mechanism,” *Mater. Manuf. Process.*, vol. 31, no. 2, pp. 146–156, 2016.

[38] H. Terrones *et al.*, “Graphitic cones in palladium catalysed carbon nanofibres,” *Chem. Phys. Lett.*, vol. 343, no. 3–4, pp. 241–250, 2001.

[39] S. D. Mhlanga, K. C. Mondal, N. Naidoo, N. Kunjuzwa, M. J. Witcomb, and N. J. Coville, “Synthesis and study of carbon microspheres for use as catalyst support for cobalt,” *S. Afr. J. Sci.*, vol. 105, no. 7–8, pp. 304–308, 2009.

[40] U. Narkiewicz, M. Podsiadły, R. Jędrzejewski, and I. Pełech, “Catalytic decomposition of hydrocarbons on cobalt, nickel and iron catalysts to obtain carbon nanomaterials,” *Appl. Catal. A Gen.*, vol. 384, no. 1–2, pp. 27–35, 2010.

[41] M. S. Dresselhaus, G. Dresselhaus, R. Saito, and A. Jorio, “Raman spectroscopy of carbon nanotubes,” *Physics Reports*, vol. 409. p. 47, 2005.

[42] C. Herrero-Latorre, J. Álvarez-Méndez, J. Barciela-García, S. García-Martín, and R. M. Peña-Crecente, “Characterization of carbon nanotubes and analytical methods for their determination in environmental and biological samples: A review,” *Analytica Chimica Acta*, vol. 853, no. 1. pp. 77–94, 2015.

[43] T. Belin and F. Epron, “Characterization methods of carbon nanotubes: A review,” *Materials Science and Engineering B: Solid-State Materials for Advanced Technology*, vol. 119, no. 2. pp. 105–118, 2005.

[44] L. M. Hoyos-Palacio, A. G. García, J. F. Pérez-Robles, J. González, and H. V. Martínez-Tejada, “Catalytic effect of Fe, Ni, Co and Mo on the CNTs production,” in *IOP Conference Series: Materials Science and Engineering*, 2014, vol. 59, no. 1, p. 012005.

[45] D. C. D. Nath and V. Sahajwalla, “Application of fly ash as a catalyst for synthesis of carbon nanotube ribbons,” *J. Hazard. Mater.*, vol. 192, pp. 691–697, 2011.

[46] N. Hintsho, A. Shaikjee, P. K. Tripathi, P. Franklyn, and S. Durbach, “The effect of CO2 on the CVD synthesis of carbon nanomaterials using fly ash as a catalyst,” *RSC Adv.*, vol. 5, no. 66, pp. 53776–53781, 2015.

Chapter 7: Conclusion and Recommendations

Two South African fly ashes, pre-combustion (Sasol), and post-combustion fly (Eskom) were successfully compared and characterized. Although these materials are essentially produced by closely similar processes, some major differences have been demonstrated in their properties. This would ultimately affect their applications. A physical inspection of both catalysts could already show some differences. Eskom fly ash was physically brighter compared to Sasol fly ash. Their particle size distribution was found to be similar, however, high contents of small and large particles were found in Sasol's fly ash. This would affect the diameter of the CNMs The SEM images showed Eskom fly ash as having spherical particles with smooth surfaces, whereas in Sasol, the surface of the spheres was rough and chipped. Their chemical composition was found to be the most influential factor in determining yield. In the XRF data, Eskom fly ash had much higher weight percentages of SiO_2 (silica) and Al_2O_3 (alumina). Sasol contained higher percentages of unburnt carbon, iron, and calcite. This would make Sasol fly ash a favourable catalyst as demonstrated. The EDS was done to compare and locate particles where iron was dominant. It was seen from several particles that iron was higher in the spheres for Eskom and higher for irregular particles for Sasol fly ash. Therefore, growth higher growth would be expected in the particles. The mineral composition of each catalyst was similar. However, calcite was not detected in Eskom fly ash.

Only Sasol fly ash catalysts exhibited the growth of CNMs, albeit in small yields. The effect of temperature was found to be significant in both the yield and crystallinity. The yield of Sasol CNMs decreased with increasing temperature from TGA measurements. At low temperatures, amorphous was found. The DTG of nanomaterials showed multiple broad and sharp peaks, indicating the presence of multiple carbonaceous products. Raman spectroscopy showed nanomaterial of good crystallinity with a decrease in temperature. The pressure was found to be more influential than the flow rate to the quality and quantity. When it was decreased and flow rates increased, a dramatic decrease in yield and crystallinity was observed. The TGA showed an increase in yield when the pressure was increased to its initial value and the flow rate increased higher. The crystallinity was closely similar except for the low pressures. This shows how influential pressure is on yield and crystallinity. While the flow rate has minimal impact on the crystallinity. The last parameter investigated, the mass of catalyst, showed an increase in yield

when it was increased. However, the crystallinity was closely similar. From this parametric study of Sasol fly ash, the temperature was shown to have a significant influence on crystallinity. The yield of CNMs was extremely low for Eskom fly ash for all the parameters. Instead, crystallization of the catalyst took place and SEM images showed mullite, quartz, and calcite minerals. The Raman spectra showed nanomaterial of poor quality. Therefore, Sasol fly ash was found to be a better catalyst for the growth of CNMs.

When the carbon source was acetylene, an increase in the yield for both catalysts was observed. However, the percentage yield was still high in Sasol compared to Eskom fly ash. A mixture of nanomaterials was obtained from both catalysts. CNFs were formed with large diameters and CNTs of various lengths were formed in Sasol fly ash. A strong broad peak was obtained with TGA, proving that a product with a large diameter was formed. The SEM images showed rings in the middle of the tubes, implying the tip growth mechanism. Eskom fly ash formed CNFs and carbon microspheres. These were seen in TEM, supported by the derivative thermogravimetry (DTG), which showed two peaks in the decomposition region of CNTs and CNFs. The crystallinity of the nanomaterial was shown to be closely similar, with Sasol CNMs being higher. The unburnt carbon and Fe content were found to be key properties in the CNMs from the fly ashes, especially the yield. The catalysts were treated under the same conditions and yielded different products. However, CNFs were dominant and most common in both treated samples. Therefore, the growth of CNFs is more favoured from South African fly ash is the catalyst.

Recommendations

The following recommendations can be made based on the finding made in this study:

- A lot of unreacted fly ash particles were observed in the TGA and SEM, implying low yields. The yield of the CNMs can be increased by impregnating the fly ash with other catalysts such as ferrocene. It can also act both as a carbon source and catalyst to produce CNMs.
- The growth mechanism of fly ash from CO_2 and fly ash has not been ascertained. This also includes the growth of CNMs from other catalysts and carbon sources. Since fly ash was not supported by any catalysts supports, the mechanism would allow tailoring and directing the growth to high yields and crystallinity.

- Many CVD methods such as microwave and water-assisted CVD have been developed and shown to be effective for the growth of CNMs. Testing the modified CVD might improve the yield and quality.
- The unburnt carbon and iron can be leached and be tested for nanomaterials growth